

GRAPHENE BASED ANODE MATERIALS FOR LITHIUM-ION BATTERIES

A thesis submitted in partial fulfillment
of the requirements for the degree of
Master of Science in Engineering

By

SREE LAKSHMI CHEEKATI
B.E., Andhra University, 2005

2011
Wright State University

WRIGHT STATE UNIVERSITY
SCHOOL OF GRADUATE STUDIES

March 24,2011

I HEREBY RECOMMEND THAT THE THESIS PREPARED UNDER MY SUPERVISION BY Sree Lakshmi Cheekati ENTITLED Graphene Based Anode Materials For Lithium Ion Batteries BE ACCEPTED IN PARTIAL FULFILLMENT OF THE REQUIREMENTS FOR THE DEGREE OF Master of Science in Engineering

Hong Huang, Ph.D.

Thesis Director

George Huang, Ph.D., Chair

Department of Mechanical and Materials Engineering

College of Engineering and Computer Science

Committee on Final Examination

Dr. Dan Young, Ph.D.

Dr. Kuan-lun Chu, Ph.D.

Andrew Hsu, Ph.D.
Dean, School of Graduate Studies

ABSTRACT

Cheekati, Sree Lakshmi. M.S.Egr, Department of Mechanical and Materials Engineering, Wright State University, 2011

Graphene Based Anode Materials for Lithium-Ion Batteries

Improvements of the anode performances in Li-ions batteries are in demand to satisfy applications in transportation. In comparison with graphitic carbons, transition metal oxides as well as graphene can store over twice amount of lithium per gram. Recently, graphene-based anodes for Li-ion batteries are under extensive development. In this research, lithium storage characteristics in graphene oxide (GO), GO/Manganese acetate (GO/MnAc), GO/manganese oxide (GO/MnO_x) composites and Nano Graphene Platelets (NGP) were studied. The prepared GO delivered reversible capacities of 706mAh/g with an average columbic efficiency of 87%. Reversible capacities of 533 mAh/g were observed for GO/MnAc composite. GO/MnO_x nanocomposite thermal annealed at 400°C in inert atmosphere exhibited high reversible charge capacity of 798 mAh/g with an average columbic efficiency of 95 % and capacity fade per cycle of 1.8 %. The EIS spectra of discharge and charge profiles of GO and GO/MnO_x composites were analyzed to investigate the kinetics evolution of electrode process at different stages of lithium storage.

TABLE OF CONTENTS

1.	Introduction	1
1.1	Electrochemical Energy Conversion Systems.....	1
1.2	A Battery System	4
1.3	Types of Batteries.....	6
1.3.1	Lead-Acid Batteries	7
1.3.2	Nickel-Cadmium Batteries.....	8
1.3.3	Nickel Metal Hydride Batteries	9
1.3.4	Lithium Ion Batteries	10
1.4	Lithium Ion Batteries –Materials Development and Status	13
1.4.1	Anode Materials.....	15
1.4.2	Cathode Materials	23
1.4.3	Electrolytes	25
1.5	Objective and Scope of this Research	27
2.	Research Status of Graphene-base Anodes	29
2.1	Graphene	29
2.2	Graphene-Alloy Composites	33
2.3	Graphene Metal Oxide Composites	37
2.4	Summary	40

3.	Experimental Apparatus and Procedure	41
3.1	Apparatus	41
3.1.1	Swagelok-type Cell.....	41
3.1.2	Glove Box	42
3.1.3	Electrochemical Working Station.....	43
3.1.4	Electrochemical Measurement System-Gamry Instruments.....	44
3.1.5	Box Furnace	46
3.1.6	Tube Furnace	47
3.1.7	Vacuum Oven	48
3.2	Preparation and Testing of Working Electrode.....	49
3.3	Electrochemical Data Presentation Graphs	53
3.3.1	Voltage Capacity Graphs	53
3.3.2	Capacity Cycle Graphs	54
3.3.3	Electrochemical Impedance Graphs	55
4.	Synthesis and Li Storage Characteristics of GO.....	58
4.1	Chemical Synthesis of Graphene Oxide and Graphene	58
4.1.1	Chemical Synthesis of Graphene Oxide	58
4.1.2	Chemical Synthesis of Reduced Graphene oxide	59
4.2	Graphene Oxide – Electrochemical Characteristics.....	60

4.2.1	GO250.....	60
4.2.2	Reduction	62
4.2.3	GO400.....	64
4.2.4	NGP.....	66
4.3	Summary	70
5.	Synthesis and Li Storage Characteristics of GO/MnAc	73
5.1	Chemical Synthesis of GO/MnAc Composites.....	73
5.2	Effect of Heat Treatment on Charge Capacities.....	74
5.3	Effect of Mixing Methods on Charge Capacities.....	78
5.4	Effect of GO and MnO _x Composition Ratio on Charge Capacities.....	81
5.5	Summary	84
6.	Synthesis and Li Storage Characteristics of GO/MnO _x	88
6.1	Chemical Synthesis of GO/MnO _x - Nano Composites	88
6.2	GO/MnO _x Nano Composite vs. GO/MnAc Composite	89
6.3	Effect of Heat Treatment on Charge Capacities.....	95
6.3.1	At Different Temperatures	95
6.3.2	Thermal Treatment Environment.....	100
6.4	Summary	105
7.	Electrochemical Impedance Results.....	110

7.1	Graphene Oxide.....	110
7.2	GO/MnO _x Nano Composite	113
7.3	GO/MnO _x Nano Composite – HT in Air at 400°C	117
7.4	GO/MnO _x Nano Composite – HT in Inert Atmosphere at 400°C	120
7.5	Summary	123
8.	Conclusion and Future Work	125
8.1	Conclusion.....	125
8.2	Future Work	128
	REFERENCES	130

LIST OF FIGURES

Figure	Page
1.1 Ragone plot of the energy storage domains for various electrochemical energy conversion systems.....	3
1.2 Basic elements of a battery system	4
1.3 Three dimensional structure of graphite	19
2.1 Atomic model of LiC_3 graphene. Top: top view; bottom: side view.....	31
2.2 Sn/graphene nanocomposite with a 3D architecture.....	34
3.1 A) Swagelock Cell B) Various parts in the assembly of swagelock cell.....	42
3.2 Glove Box (Vacuum Atmospheres Company).	43
3.3 Battery Testing Station (Land CT2001A).....	44
3.4 Gamry Potentiostat.....	46
3.5 Box Furnace (Carbolite)	47
3.6 Tube Furnace (Carbolite).....	48
3.7 Vacuum Oven (Cascade Tek)	49
3.8 Program used to test working electrode on electrochemical working station	51
3.9 Sample voltage capacity graph of an anode electrode	54

3.10 Sample capacity cycle graph of an anode electrode	55
3.11 Typical impedance spectra of an intercalation material	56
4.1 Discharge - charge profiles of Graphene Oxide synthesized at 250°C (GO250)	61
4.2 Cycle performance of Graphene Oxide synthesized at 250°C (GO250)	62
4.3 Discharge - charge profiles of reduced graphene oxide (RGO)	63
4.4 Cycle performance of reduced Graphene Oxide (RGO) and GO250	64
4.5 Discharge - charge profiles of GO thermally treated at 400°C (GO400)	65
4.6 Cycle performance of Graphene Oxide synthesized at 400°C (GO400) and 250°C (GO250).....	66
4.7 AFM image of the specimen NGP	67
4.8 Discharge - charge profiles of Nano Graphene Platelets (NGP)	68
4.9 Capacity cycle performances of NGP and GO250	69
4.10 Combined discharge charge profiles of graphene oxide samples (GO250, RGO, GO400 and NGP).....	71
4.11 Combined charge capacity cycle performances of graphene oxide samples (GO250, RGO, GO400 and NGP)	72
5.1 Discharge - charge profiles of GO and MnAc composite anode synthesized at room temperature through simple method (GO/MnAc).....	76

5.2 Discharge - charge profiles of GO and MnAc composite synthesized at 400°C temperature through simple method (GO/MnAc-400).....	76
5.3 Capacity cycle performances of GO/MnAc and GO/MnAc-400	77
5.4 Discharge - charge profiles of GO/MnAc-SM composite synthesized at 400°C through simple method.....	79
5.5 Discharge - charge profiles of GO/MnAc-LM composite synthesized at 400°C through liquid method	79
5.6 Capacity cycle performances of GO/MnAc-SM and GO/MnAc-LM	80
5.7 Discharge - charge profiles of GO/MnO _x -5050 composite synthesized at 500°C through solid method.....	81
5.8 Discharge - charge profiles of GO/MnO _x -7525 composite synthesized at 500°C through solid method.....	82
5.9 Capacity cycle performances of GO/MnO _x -5050 and GO/MnO _x -7525.....	82
5.10 Combined discharge charge profiles of graphene oxide and manganese acetate composite samples (GO/MnAc, GO/MnAc-400, GO/MnAc-SM, GO/MnAc-LM, GO/MnO _x --5050 and GO/MnO _x --7525).....	87
5.11 Combined charge capacity cycle performances of graphene oxide and manganese acetate composite samples (GO/MnAc, GO/MnAc-400, GO/MnAc-SM, GO/MnAc-LM, GO/MnO _x -5050 and GO/MnO _x -7525)	87

6.1 Discharge - charge profiles of GO/MnO _x	89
6.2 Schematic diagram of the synthesis of the Graphene oxide/MnO _x nanocomposite with a 3D architecture	91
6.3 Discharge - charge profiles of GO/MnAc composite synthesized at room temperature	93
6.4 Capacity cycle performance of GO/MnO _x nano composite and GO/MnAc composite	95
6.5 Discharge – charge profiles of GO/ MnO _x nano composite synthesized at 250°C (GO/ MnO _x -250)	97
6.6 Discharge - charge profiles of GO/ Mn ₃ O ₄ nano composite synthesized at 400°C (GO/ MnO _x -400)	98
6.7 Capacity cycle performance of GO/ MnO _x -250 and GO/ Mn ₃ O ₄ -400 in air	100
6.8 Discharge - charge profiles of GO/ MnO _x -Inert nano composite synthesized at 400°C in inert atmosphere	102
6.9 Discharge - charge profiles of GO/ MnO _x -Air nano composite synthesized at 400°C in air	103
6.10 Capacity cycle performance of GO/ MnO _x -Air and GO/ Mn ₃ O ₄ -Inert samples	105

6.11 Combined discharge charge profiles of graphene oxide and manganese oxide nano composite samples (GO/MnO _x , GO/MnO _x -250, GO/MnO _x -400, GO/MnO _x -Air, GO/MnO _x -Inert and GO/MnAc)	109
6.12 Combined charge capacity cycle performances of graphene oxide and manganese oxide nano composite samples (GO/MnO _x , GO/MnO _x -250, GO/MnO _x -400, GO/MnO _x -Air, GO/MnO _x -Inert and GO/MnAc)	109
7.1 a) Nyquist plots of GO at different discharge stages b) R _{electrolyte} and R _{electrode} plots at different discharge stages c) Nyquist plots of GO at different charge stages d) R _{electrolyte} and R _{electrode} plots at different charge stages e) Discharge charge profile with different voltage points.....	112
7.2 a) Nyquist plots of GO/MnO _x at different discharge stages b) R _{electrolyte} and R _{electrode} plots at different discharge stages c) Nyquist plots of GO/MnO _x at different charge stages d) R _{electrolyte} and R _{electrode} plots at different charge stages e) Discharge charge profile with different voltage points.	115
7.3 a) Nyquist plots of GO/MnO _x -Air heat treated at 400°C at different discharge stages b) R _{electrolyte} and R _{electrode} plots at different discharge stages c) Nyquist plots of GO/MnO _x -Air heat treated at 400°C in air at different charge stages d) R _{electrolyte} and R _{electrode} plots at different charge stages e) Discharge charge profile with different voltage points.....	119
7.4 a) Nyquist plots of GO/MnO _x -Inert heat treated at 400°C in inert atmosphere at different discharge stages b) R _{electrolyte} and R _{electrode} plots at different discharge stages	

c) Nyquist plots of GO/MnO_x-Inert heat treated at 400°C in inert atmosphere at different charge stages d) R_{electrolyte} and R_{electrode} plots at different charge stages e) Discharge charge profile with different voltage points. 122

LIST OF TABLES

Table	Page
1.1 Range of Applications Which Use Batteries Together with Battery Capacities	5
1.2 Major Types of Batteries	7
1.3 Different Types of Anode Materials	16
2.1 Summary of Current Research of Graphene Based Anode Materials	40
3.1 List of Chemicals Used in Electrode Preparation	50
3.2 Initial Settings Used in Gamry EIS.....	52
4.1 Graphene Oxide Anode Samples	58
4.2 Summary of Graphene Oxide Results.....	71
5.1 Graphene Oxide and Manganese Acetate Composite Anode Samples	74
5.2 Summary of Graphene Oxide and Manganese Acetate Composite Results	86
6.1 Graphene Oxide and Manganese Acetate Composite Anode Samples	88
6.2 Summary of Graphene Oxide and Manganese Oxide Nano Composite Results.....	108

ACKNOWLEDGMENTS

I would like to express my heartfelt gratitude and sincere thanks to my research advisor Dr. Hong Huang, Assistant Professor of Materials Science, Department of Mechanical and Materials Engineering at Wright State University. Without her guidance, constant supervision, and valuable suggestions throughout the entire period of the work, it would have been impossible to complete the research work.

I am very grateful to the faculty and staff of the Department of Mechanical and Materials Engineering at Wright State University for providing me with the opportunity to pursue higher studies.

1. Introduction

1.1 *Electrochemical Energy Conversion Systems*

High energy consumption and the dwindling fossil energy supplies is projected to have a severe future impact on world economics and ecology. Electrochemical energy production is under serious consideration as an alternative energy/power source, as long as this energy consumption is designed to be more sustainable and more environmentally friendly. Electrochemical energy storage and conversion systems include batteries, fuel cells, and electrochemical capacitors. Although the energy storage and conversion mechanisms are different, there are electrochemical similarities of these three systems. Common features are that the energy-providing processes take place at the phase boundary of the electrode/electrolyte interface and that electron and ion transport are separated. Batteries, fuel cells, and super capacitors all consist of two electrodes in contact with an electrolyte solution. In batteries and fuel cells, electrical energy is generated by conversion of chemical energy via redox reactions at the anode and cathode. Redox stands for reduction-oxidation, and are electrochemical processes involving electron transfer to or from a molecule or ion changing its oxidation state. This reaction can occur through the application of an external voltage or through the release of chemical energy. Electrochemical cells have two conductive electrodes (the anode and the cathode). The anode is defined as the electrode where oxidation occurs and the cathode is the electrode where the reduction takes place. As reactions at the anode usually take place at lower electrode potentials than at of the cathode, the terms negative and

positive electrode (indicated as minus and plus poles) are used. The more negative electrode is designated as the anode, whereas the cathode is the more positive one.

The difference between batteries and fuel cells is related to the locations of energy storage and conversion. Batteries are closed systems, with the anode and cathode being the charge-transfer medium and taking an active role in the redox reaction as active masses. In other words, energy storage and conversion occur in the same compartment. Fuel cells are open systems where the anode and cathode are just charge-transfer media and the active masses undergoing the redox reaction are delivered from outside the cell, either from the environment, for example, oxygen from air, or from a tank, for example, fuels such as hydrogen and hydrocarbons. Energy storage (in the tank) and energy conversion (in the fuel cell) are thus locally separated. In electrochemical capacitors (or super capacitors), energy may not be delivered via redox reactions and, thus the use of the terms anode and cathode may not be appropriate but are in common usage.

The terms specific energy expressed in watt-hours per kilogram (Wh/kg) and energy density in watt-hours per liter (Wh/L) are used to compare the energy contents of a system, whereas the rate capability is expressed as specific power in W/kg and power density in W/L. To compare the power and energy capabilities, a representation known as the Ragone plot or diagram has been developed. A simplified Ragone plot as shown in Figure 1.1 discloses that fuel cells can be considered to be high-energy systems, whereas supercapacitors are considered to be high-power systems. Batteries have intermediate power and energy characteristics. There is some overlap in energy and power of supercapacitors, or fuel cells, with batteries. Indeed, batteries with thin film electrodes

exhibit power characteristics similar to those of supercapacitors. No single electrochemical power source can match the characteristics of the internal combustion engine which have high power and high energy. High power and high energy can best be achieved when the available electrochemical power systems are combined. In such hybrid electrochemical power schemes, batteries and/ or supercapacitors would provide high power and the fuel cells would deliver high energy [1]. Batteries have found by far the most application markets and have an established market position in comparison to super capacitors and fuel cells. Supercapacitors are mostly considered for pulse power applications and fuel cells are recently introduced commercially to provide power supply to certain large institutions.

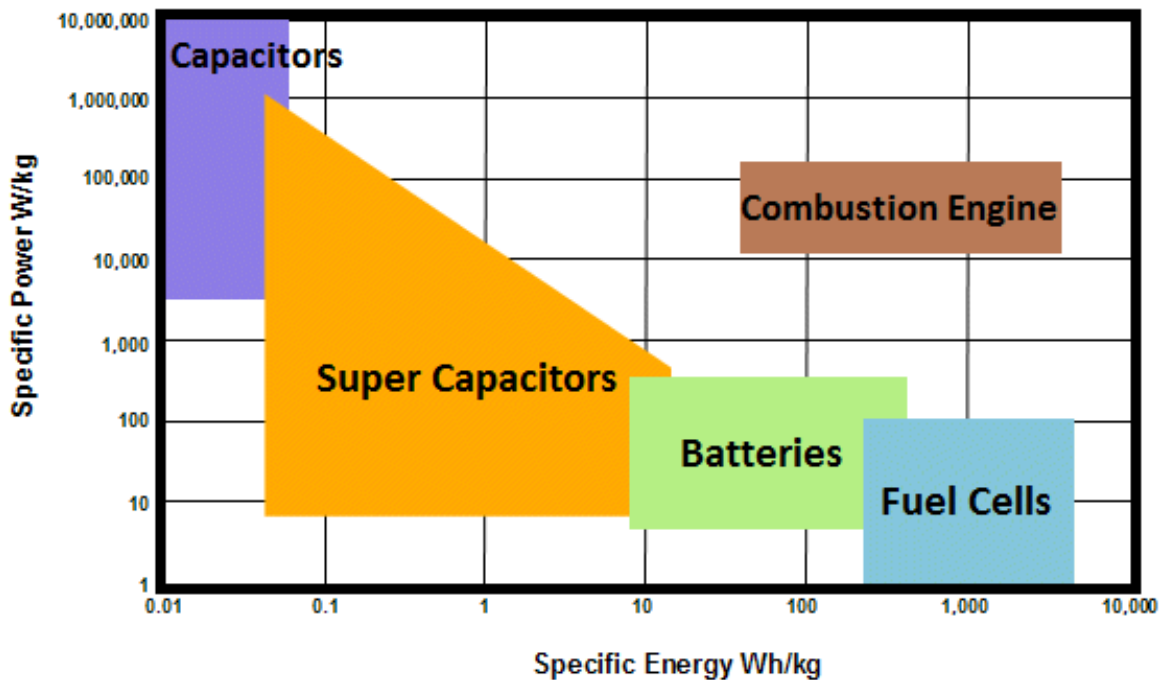


Figure 1.1 Ragone plot of the energy storage domains for various electrochemical energy conversion systems.

1.2 A Battery System

A battery is an electrochemical that produces an electric current from energy released by a spontaneous redox reaction. Electrodes in battery system can be made from any sufficiently conductive materials, such as metals, semiconductors, graphite, and even conductive polymers. In between these electrodes is the electrolyte which is a pure ionic conductor that physically separates the anode from the cathode to prevent any direct contact. Should the anode and cathode physically touch, the battery will be shorted and its full energy released as heat inside the battery. The Figure 1.2 depicts the basic elements of a battery. The negative electrode is a good reducing agent (electron donor) such as lithium, zinc, or lead. The positive electrode is an electron acceptor such as lithium cobalt oxide, manganese dioxide, or lead oxide.

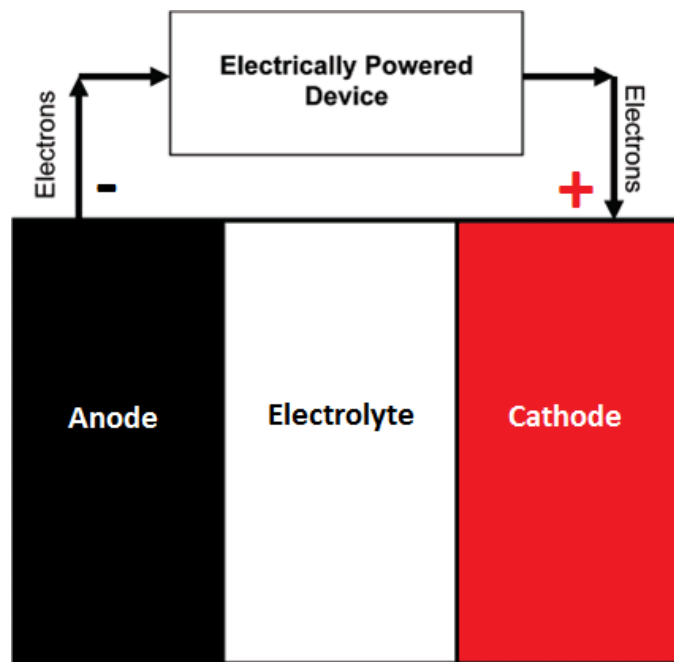


Figure 1.2 Basic elements of a battery system

Advantages

- Batteries operate over a wide temperature range
- Choice of chemical system and voltage can be decided for a battery
- Batteries operate in any orientation unlike fuel cells
- Batteries do not require pumps, filters, etc. unlike fuel cells
- Batteries are available in varied sizes
- Batteries are available in certain standard sizes throughout the world.
- Batteries can generate can high current pulses
- User has the option to choose best battery for a specific purpose (portable, mobile, and stationary applications)

Disadvantages

- Energy density of a battery is very low when compared to gasoline and other fuels
- Batteries are expensive when compared to coal and gasoline

Applications

The Table 1.1 shows the range of applications which use batteries together with typical battery capacities required by the application.

Table 1.1 Range of Applications Which Use Batteries Together with Battery Capacities [2-4]

Type	Energy	Applications
Miniature Batteries	100mWh- 2Wh	Electric watches, calculators, implanted medical devices (Mostly primary cells)
Batteries for Portable Equipment	2Wh-100Wh	Flashlights, toys, power tools, portable radio and TV, mobile phones, camcorders,

		lap-top computers, memory refreshing, instruments, cordless devices, wireless peripherals, emergency beacons (Mostly secondary cells)
SLI Batteries (Starting Lighting & Ignition)	100-600Wh	Cars, trucks, buses, lawn mowers, wheel chairs, robots (Mostly Lead Acid batteries)
Vehicle Traction Batteries	20-630kWh	EVs, HEVs, PHEVs, fork lift trucks, milk floats, locomotives (NiMH and Lithium)
Stationary Batteries	250Wh-5MWh	Emergency power, local energy storage, remote relay stations, communication base stations, uninterruptible power supplies (UPS).
Military & Aerospace	Wide range	Satellites, munitions, robots, emergency power, communications
Special purpose	3MWh	Submarines
Load Leveling Batteries	5-100MWh	Spinning reserve, peak shaving, load leveling (Various Lead Acid and Lithium plus Alternatives)

1.3 Types of Batteries

There are several types of batteries which are commonly divided into three general classes: primary batteries that are discharged once and discarded; secondary, rechargeable batteries that can be discharged and then restored to their original condition by reversing the current flow through the cell; and specialty batteries that are designed to fulfill a specific purpose. The latter are mainly military and medical batteries that do not find wide commercial use for various reasons of cost, environmental issues, and limited market application.

The development of electrochemical cells is crucial to the scientific study and industrial applications of electricity. There were successive improvements in battery technology which permitted the rise of major electrical advances. Listed in Table 1.2 are the major types of batteries developed in chronological order.

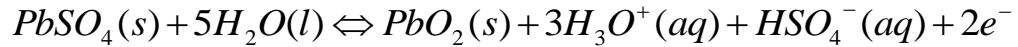
Table 1.2 Major Types of Batteries

Battery	Anode	Cathode	Electrolyte	Voltage (V)	Capacity (Ah/kg)
Lead-acid	Lead	Lead Oxide	Sulphuric acid	2.1V	120
NiCd	Cadmium	Nickel Oxide	Potassium Hydroxide	1.2V	181
NiMH	Intermetallic compound	Nickel Oxide	Potassium Hydroxide	1.2V	178
Li-Ion	Li_xC_6	Lithium Cobalt Oxide	LiPF_6 dissolved in organic solvent	4.1V	100

1.3.1 Lead-Acid Batteries

Lead-acid batteries, invented in 1859 by French physicist Gaston Planté, is the first ever battery that could be recharged by passing a reverse current through it [5]. A lead acid cell consists of a lead anode and a lead dioxide cathode immersed in sulphuric acid. Both electrodes react with the acid to produce lead sulfate, but the reaction at the lead anode releases electrons whilst the reaction at the lead dioxide consumes them, thus producing a current. These chemical reactions can be reversed by passing a reverse current through the battery, thereby recharging it. The chemical reactions occurring during discharge are

Anode (oxidation):



Cathode (reduction):



Despite having a very low energy-to-weight ratio and a low energy-to-volume ratio, their ability to supply high surge currents means that the cells maintain a relatively large power-to-weight ratio. These features, along with their low cost, make them attractive for use in motor vehicles to provide the high current required by automobile starter motors. It also has very low internal resistance, meaning a single battery could be used to power multiple circuits. The lead-acid battery is still used today in automobiles and other applications where weight isn't a big factor. The basic principle has not changed since 1859, though in the 1970s a variant was developed that used a gel electrolyte instead of a liquid (commonly known as a "gel cell"), allowing the battery to be used in different positions without failure or leakage. The lead-acid cell was the first "secondary" cell.

1.3.2 Nickel-Cadmium Batteries

Nickel-Cadmium battery, invented in 1899 by a Swedish scientist named Waldmar Jungner, a rechargeable battery that had nickel and cadmium electrodes in a potassium hydroxide solution; the first battery to use an alkaline electrolyte [6]. NiCd battery had significantly better energy density than lead-acid batteries, but was much

more expensive. NiCd batteries typically last longer, in terms of number of charge/discharge cycles, than other rechargeable batteries such as lead/acid batteries. The capacity of a nickel cadmium battery is not significantly affected by very high discharge currents. Even with discharge rates as high as 50C, a nickel cadmium will provide very nearly its rated capacity. By contrast, a lead acid battery will only provide approximately half its rated capacity when discharged at a relatively modest 1.5 C. As this battery contains cadmium, a toxic material, it should always be recycled or disposed of properly. NiCd batteries suffer from what's called the memory effect. Memory Effect means that if a battery is repeatedly only partially discharged before recharging, the battery will forget that it can further discharge.

1.3.3 Nickel Metal Hydride Batteries

A nickel-metal hydride battery is a type of rechargeable battery similar to the nickel-cadmium cell. The NiMH battery uses a hydrogen-absorbing alloy for the negative electrode instead of cadmium. As in NiCd cells, the positive electrode is nickel oxyhydroxide (NiOOH) [7]. A NiMH battery can have two to three times the capacity of an equivalent size nickel-cadmium battery. Nickel Metal Hydride batteries are the cadmium-free replacement for NiCd. They are less affected by the memory effect than NiCd and thus require less maintenance and conditioning. However, they have problems at very high or low room temperatures. And even though they use less hazardous materials (i.e., they do not contain heavy metals), they cannot be fully recycled yet. Another main difference between NiCd and NiMH is that NiMH battery offers higher energy density than NiCd. In other words, the capacity of a NiMH is approximately twice

the capacity of its NiCd counterpart. What this means is increased run-time from the battery with no additional bulk or weight.

1.3.4 Lithium Ion Batteries

Lithium-ion (Li-ion) cells are now the most widely used secondary battery systems for portable electronic devices [2]. Lithium is the metal with lowest density and has the greatest electrochemical potential and energy-to-weight ratio, so in theory it would be an ideal material with which to make batteries. This battery primarily consists of graphite as negative electrode and LiCoO_2 as a positive electrode separated by a lithium ion conducting electrolyte. Compared to conventional aqueous rechargeable cells, such as nickel–cadmium and nickel metal hydride, Li-ion cells have higher energy density, higher operating voltages, lower self discharge, and lower maintenance requirements than any of the other battery types. These properties have made Li-ion cells the highest-performing available secondary battery chemistry.

Advantages

- Li-Ion batteries are much lighter than other energy-equivalent secondary batteries.
- High open circuit voltage in comparison to aqueous batteries (such as lead acid, nickel-metal hydride and nickel-cadmium). This is beneficial because it increases the amount of power that can be transferred at a lower current.
- Li-Ion batteries can be manufactured in wide variety of shapes and sizes efficiently fitting the devices they power.

- Li-Ion batteries do not suffer significantly from the memory effect unlike their NiMH and Ni-Cd counterparts.
- Li-Ion batteries has self-discharge rate of approximately 5-10% per month, compared to over 30% per month in common nickel metal hydride batteries, approximately 1.25% per month for Low Self-Discharge NiMH batteries and 10% per month in nickel-cadmium batteries.
- Li-Ion batteries are environmentally safe as there is no free lithium metal.

Disadvantages

- Charging of a battery forms deposits inside the electrolyte that inhibit ion transport. Over time, the cell's capacity diminishes. The increase in internal resistance reduces the cell's ability to deliver current. Also high charge levels and elevated temperatures hasten capacity loss.
- The internal resistance of standard lithium-ion batteries is high compared to both other rechargeable chemistries such as nickel-metal hydride and nickel-cadmium batteries. Internal resistance increases with both cycling and age. Rising internal resistance causes the voltage at the terminals to drop under load, which reduces the maximum current draw. Eventually increasing resistance means that the battery can no longer operate for an adequate period.
- If overheated or overcharged Li-ion batteries may suffer thermal runaway and cell rupture. In extreme cases this can lead to combustion. To reduce these risks, Lithium-ion battery packs contain fail-safe circuitry that shuts down the battery when its voltage is outside the safe range of 3–4.2 V per cell.

- These safety features increase costs compared to nickel metal hydride batteries.

Applications

- Small lithium ion batteries are very commonly used in small, portable electronic devices, such as PDAs, cell phones, iPods and calculators, as batteries in computers, laptops and communication equipment. They are available in many shapes and sizes. The heavy electrical demands of many of these devices make lithium ion batteries a particularly attractive option.
- Recently all major car manufacturers are developing hybrid vehicles that are powered by lithium ion batteries and additionally supported by a small internal combustion engine. Li-ion batteries pack a more powerful punch and store more energy in smaller spaces than the more traditional lead-acid and nickel-metal-hydride ones. Lithium has the most energy density and electrochemical potential of all metals, which is what gives it that stamina. The nickel-metal-hydride batteries in hybrids on the road are also heavy, limiting their potential, whereas Li-ion batteries can amp the speed without weighing the car down.

The commercialized rechargeable lithium battery was first announced by Sony in the early 1990. Although these batteries are commercially successful, we are reaching limits in the performance with the current materials. In order to use in the hybrid and electric vehicles, further breakthroughs in materials are essential.

In 1996, the lithium ion polymer battery was released. These batteries hold their electrolyte in a solid polymer composite instead of a liquid solvent, and the electrodes and separators are laminated to each other. The latter difference allows the battery to be encased in a flexible wrapping instead of a rigid metal casing, which means such batteries can be specifically shaped to fit a particular device. They also have a higher energy density than normal lithium ion batteries. These advantages have made it a choice battery for portable electronics such as mobile phones and PDAs, as they allow for more flexible and compact design.

1.4 Lithium Ion Batteries –Materials Development and Status

A lithium-ion battery consists of a lithium-ion intercalation negative electrode (generally graphite), and a lithium-ion intercalation positive electrode (generally the lithium metal oxide, LiCoO_2), these being separated by a lithium-ion conducting electrolyte, for example a solution of LiPF_6 in ethylene carbonate-diethyl carbonate. However, due to miniaturization and other advances presently occurring in the portable device industry, and to use their advantages for aerospace, military, and automobile applications, their mass capacities (Wh/kg), and energy densities (Wh/l) require a further increase. The energy density and performance of lithium-ion batteries largely depend on the physical and chemical properties of the cathode and anode materials. The possibilities for the improvement of cathode materials are quite limited due to the stringent requirements such as high potential, structural stability, and inclusion of lithium in the structure. Nevertheless, there is considerable room for exploring new anode materials, owing to many materials having reversible lithium storage capability.

One approach to improve the energy density of lithium ion batteries is to substitute the carbon anode for a new material. The theoretical lithium insertion capacity of graphite is 372mAh/g, which is only about one-tenth of Li. Unfortunately, the use of lithium metal as the anode in the electrolyte solution was difficult, because of the dendrite formation on the lithium anode surface. In recent years, there is considerable interest in using graphene as anode materials owing to its 2D structure resulting in twice the capacities when compared to graphite. Recently, the development of new high-capacity anode materials such as alloys, metal oxides with carbon-based composites has attracted significant interest.

Also there are several advantages associated with the usage of nano size materials for electrode preparation in lithium ion batteries. Advantages include better accommodation of the strain of lithium insertion/removal and thereby improving cycle life, new reactions are not possible with bulk materials, higher electrode/electrolyte contact area leads to higher charge/discharge rates, short path lengths for electronic transport (permitting operation with low electronic conductivity or at higher power), short path lengths for Li^+ transport (permitting operation with low Li^+ conductivity or higher power). However there are certain disadvantages of using nano size materials for electrode preparation like increase in undesirable electrode/electrolyte reactions due to high surface area, leading to self-discharge, poor cycling and calendar life, inferior packing of particles leading to lower volumetric energy densities unless special compaction methods are developed. With these advantages and disadvantages in mind, efforts have been devoted to exploring negative and, more recently, positive nanoelectrodes.

1.4.1 Anode Materials

The choice of the anode material is based on properties that require fast and large insertion kinetics of lithium, and a redox potential vs. Li which is less than that of the cathode to provide a sufficiently large cell voltage. Also the anode material should maintain its structural stability without any loss of electrical contact even after repeated charge discharge cycles [3].

Most improvements in anodes actually implemented over the last decade have involved carbonaceous materials. This is partly based on the fact that graphite and graphitic carbons forms intercalation compounds with lithium. The reason that lie behind the commercial success of carbon-based negative electrodes include the relatively low inherent cost of carbon, its excellent reversibility for lithium insertion, and its formation of positive surface film with many electrolyte solutions. Recently the most common among anode materials are carbon and lithium-alloying metals. The host element in the graphite intercalation compound/alloy ‘shields’ the inserted lithium, making the alloy less reactive towards electrolytes. As a result, the chemical potential of lithium in the lithiated material is less than that in metallic lithium. This translates into a safety advantage, which, however, comes with a penalty in cell voltage and, therefore, also in energy and power density. Besides, the charge–discharge performance of these alternative anode materials also depends on the rate of diffusion of lithium in the host matrix.

Metals that store lithium are among the most appealing and competitive candidates for new types of anodes (negative electrodes) in lithium-ion batteries. Indeed, a number of metals and semiconductors, for example aluminum, tin and silicon, react

with lithium to form alloys by electrochemical processes that are partially reversible and of low voltage (relative to lithium), involve a large number of atoms per formula unit, and in particular provide a specific capacity much larger than that offered by conventional graphite. Unfortunately, the accommodation of so much lithium is accompanied by enormous volume changes in the host metal plus phase transitions. The mechanical strain generated during the alloying/de-alloying processes leads to cracking and crumbling of the metal electrode and a marked loss of capacity to store charge, in the course of a few cycles. Although these structural changes are common to alloying reactions, there have been attempts to limit their side effects on the electrode integrity. Among them, the active/inactive nanocomposite concept represents one attractive route. This involves intimately mixing two materials, one reacting with lithium where as the other acts as an inactive confining buffer. Within this composite, the use of nano-size metallic clusters as lithium hosts considerably suppresses the associated strains, and therefore improves the reversibility of the alloying reaction. Table 1.3 lists the different types of anode materials.

Table 1.3 Different Types of Anode Materials

Material	Theoretical Capacity (mAh/g)	Practical Capacity (mAh/g)	Problems
Graphite	372	250	Low charge capacities
Silicon	4200	2158	Large volume expansion and high capacity fade per cycle
Tin	994	400	Large volume expansion and high capacity fade per cycle

Metal Oxide Composites (Co, Mn, Fe)	880	700	Large volume expansion
Graphene	744	350	Large voltage hysteresis between charge discharge profiles
Graphene Alloy Composites (Si)	2500	1168	

The various anode materials for lithium ion batteries can be classified as follows

Graphite: Carbon is a prime anode material in lithium-ion batteries because of favorable electrochemical properties, less cost and easy availability. The theoretical lithium-intercalation capacity of graphitic carbon is a poor 372 mAh/g (for a stoichiometry of LiC_6) compared to 3862 mAh/g, the charge density of lithium. The chemical diffusion coefficient for lithium in carbon is of the order of 10^{-9} sq.cm/s. Carbon based anode material forms a protective surface film with many electrolyte solutions. This film which is often called SEI (Solid Electrolyte Interface) effectively passivates the graphite surface and prevents further co-interaction decomposition of solvent molecules, allowing only Li ion migration. The term “intercalation” implies the restricting condition that a layered host takes up guests within its interlayer gaps (“galleries”), which may result in volume change perpendicular to layers, but which cause no other structural changes. Even graphite would be not a pure intercalation host, as during Li accommodation the stacking changes by sliding of the graphene layers.

The various structural properties of graphite are as detailed below. Figure 1.3 shows the 3D structure of graphite which is comprised of number of graphene layers stacked on each other.

- Graphite is a layered compound. In each layer, the carbon atoms are arranged in a hexagonal lattice with separation of 0.142 nm, and the distance between planes is 0.335 nm as shown in Figure 1.3.
- Graphitic carbons basically comprise of SP²-hybridized carbon atoms which are arranged in a planar “honeycomb-like” network, i.e., a “graphene” layer is formed. Vander waals forces provide a weak cohesion of the graphene layers leading to layered graphite structure.
- Graphite can conduct electricity due to the vast electron delocalization within the carbon layers. These valence electrons are free to move, so are able to conduct electricity. However, the electricity is only conducted within the plane of the layers.
- The quality and quantity of sites which are capable of reversible lithium accommodation and the type and extent of interaction with the electrolyte depend in a complex manner on the crystallinity, texture, microstructure, micro morphology of the carbonaceous host material.
- Graphite powder has a surface area of 8.5 m²/g.
- Graphite has a theoretical capacity of 372 mAh/g through the formation of LiC₆.
- Graphite forms a protective surface film with many electrolyte solutions.
- Graphite has a bulk density between 1.3 and 1.95 g/cm³

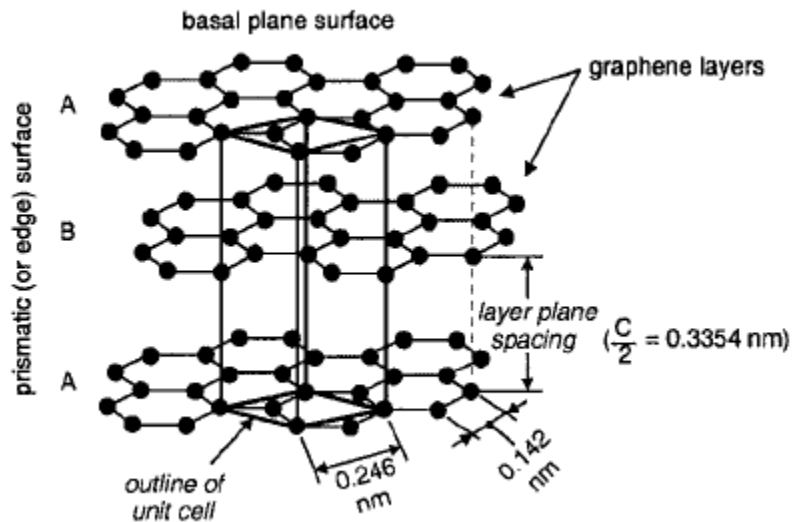


Figure 1.3 Three dimensional structure of graphite

The energy density of lithium-ion batteries based on carbon has been increasing by about 10% annually. This has been facilitated largely by successive improvements in the charge–discharge efficiency and discharge capacity of carbonaceous anodes by a combination of structural and surface modifications. However, to combat the onslaught from competing anode materials, further improvements are required

Carbon Nanotubes: Carbon nanotubes (CNTs) are particularly attractive as high-capacity anodes for lithium storage. They provide a variety of lithium accommodation sites, namely, spacing between the graphite layers, local disorders arising from their highly defective structures, and the central core. In fact, studies have shown lithium intake of more than 1400 mAh/g in CNTs. Their irreversible capacities, however, are too large to merit practical applicability.

Nano Graphene Platelets: Nano Graphene Platelets(NGPs) collectively refer to platelets, sheets, or ribbons of mono layered and/or multiple layered graphene from “pristine graphene” (containing insignificant amount of oxygen) to “graphene-oxide” (containing substantial oxygen contents).NGPs, usually with x and y dimensions less than hundreds of nanometers and z dimension less than ten of nanometers, have exhibited similar outstanding properties to the pristine monolayer graphene sheets as well as carbon nanotubes (CNT). Distinguished from graphene and CNTs, NGPs can be achieved via exfoliation from graphite at significantly low cost [7, 8,64].

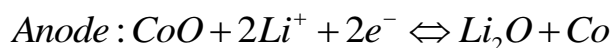
Silicon: Silicon is an attractive anode material for lithium batteries because it has a low discharge potential and the lithium– silicon alloy in its fully lithiated composition, $\text{Li}_{4.4}\text{Si}$ has a theoretical specific capacity of 4,200 mAh/g compared with 3,600 mAh/g for metallic lithium and 372 mAh/g for graphite [9, 44]. Although this is more than ten times higher than existing graphite anodes and much larger than various nitride and oxide materials, silicon anodes have limited applications because silicon's volume changes by 400% upon insertion and extraction of lithium which results in pulverization and capacity fading. Several approaches can be considered to enhance the capacity retention, such as reducing the Si particle size to the nanoscale or dispersing the electro active particles in a carbon matrix. It is believed that carbon-based materials buffer the volume changes and improve the electronic and ionic conductivities.

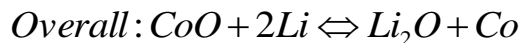
Tin: Sn and Sn based compounds have also been extensively investigated as high capacity anode materials for lithium-ion batteries. Theoretical lithium insertion capacity of Sn is 994mAh/g, based on the mass of Sn, which is 2.67 times that of graphite [10].

The main disadvantage of using tin as an anode material is Sn atoms tend to aggregate during repeated cycling, inducing rapid loss of capacity of the electrode.

Metal oxide: Electrodes made of nanoparticles of transition metal oxides (MO, where M is Co, Mn and Fe) demonstrates electrochemical capacities of 700mAh/g, with 100% capacity retention for up to 100 cycles and high recharging rates have been reported. Problems with metal oxides are large changes of volume and electronic properties during the formation and decomposition of Li_2O [12]. This problem can be overcome by using nano size particles of metal, thereby increasing the reactivity which will enable the decomposition of Li_2O during charge process.

The mechanism of Li reactivity differs from the classical Li insertion/de-insertion or Li-alloying processes, and involves the formation and decomposition of Li_2O , accompanying the reduction and oxidation of metal nanoparticles (in the range 1 ± 5 nm) respectively. The advantages of such MO-based lithium-ion cells over commercial LiCoO_2/C cells are due to the fact that MO has about twice the capacity of carbon per unit mass, and three times its density; MO therefore has about 6 times the capacity of carbon per unit volume [12, 22-24]. These materials (CoO for instance) crystallize in a rock-salt structure that does not contain any available empty sites for Li ions, and also that none of the 3d metals considered forms alloys with Li. It appears that the reversible electrochemical reaction mechanism of Li with the transition-metal oxides, such as CoO, entails for the most part a displacive redox reaction, as follows.





This implies the reversible formation and decomposition of Li_2O . Formation reaction is thermodynamically feasible and thereby expected. In contrast, the ability to drive decomposition reaction electrochemically is surprising. Indeed, Li_2O has always been reported to be electrochemically inactive. However, when dealing with nano-sized materials, chemical and physical phenomena are strongly affected. The electrochemically driven size confinement of the metal particles is thus believed to enhance their electrochemical activity towards the formation/decomposition of Li_2O . With decreasing particle size, an increasing proportion of the total number of atoms lies near or on the surface making the electrochemical reactivity of the particles more and more important. Such considerations can explain why the cycling performances of such materials should be extremely sensitive to their degree of division or aggregation.

Graphene: Graphene has become the material of choice for anode in the present generation of lithium ion cells. Graphene is a single sheet of graphitic carbon, offers great advantages owing to its high surface area, good conductivity, and good mechanical properties. The lightweight and low electrochemical potential lying close to that of metallic lithium have made graphene an attractive anode. It has a theoretical capacity of 744 mAh/g, which corresponds to insertion of one lithium per 3 carbon atoms [11]. A number of technologies have been developed for fabrication of graphene. Graphene with superior electrical conductivities, high surface areas of over $2600\text{m}^2/\text{g}$, excellent thermal

property and mechanical property, has attracted much attention in the field of materials science [45-48].

Graphene alloy/oxide composite anodes: Electrodes made of nanoparticles of metals such as Sn, Si and graphene which can accommodate the large strains of lithium insertion and de-insertion and provide good electronic contact owing to the good mechanical properties and high conductivity provided by graphene. Therefore, the cycling stability can be greatly enhanced. The 3D nanoarchitecture gives the Sn/graphene nanocomposite electrode an enhanced electrochemical performance [13]. Electrochemical tests show that the Si/graphene composite maintains a capacity of 1168 mAh/g and an average columbic efficiency of 93% up to 30 cycles [14]. This strategy can be extended to prepare anode and cathode materials for advanced energy storage and conversion devices such as lithium ion batteries. Additionally graphene can be utilized to act as conducting agent and also buffer large volume changes during reduction and oxidation of metal oxide giving good cycle life.

1.4.2 Cathode Materials

The various cathode materials for lithium ion batteries can be classified as follows.

Layered Lithium Metal Oxides: Lithium-based layered transition metal oxides such as LiMO_2 (where M is a 3d transition metal such as Ni, Co, Mn, Al and V) have attracted great interest world-wide [3]. Their specific properties such as high energy density, long cycle life, good safety features, stable discharge properties and wide range of operating temperatures have made them excellent candidates for active compounds as high capacity

cathode materials in rechargeable lithium batteries. The general structure of these materials is similar to the sodium chloride lattice with the cations filling the octahedral interspaces and oxygen atoms in close-packed sites. In most of the cases in LiMO_2 oxides, the cations are arranged in an ordered tunnel structure that permits lithium ions reversible intercalation during the electrochemical process. Among the above-mentioned compounds, LiCoO_2 is the most widely used material for commercial lithium batteries due to its excellent electrochemical cycling stability. It is a result of the structural stability of the material, in which the layered cation ordering is extremely well preserved even after a repeated process of insertion and extraction of Li^+ ions. Even though the technology is rather expensive and the material is highly toxic, lithium cobaltate is still the most widely used cathode material in lithium-ion batteries.

Lithium Manganese Spinels: With increasing concerns about the cost and toxicity of cobalt-based cathode (LiCoO_2), and difficulty in synthesizing phase-pure LiNiO_2 , the cubic spinel LiMn_2O_4 is expected to supplant the popular LiCoO_2 cathode in commercial cells [3]. Apart from low cost, LiMn_2O_4 offers other advantages such as high thermal threshold, excellent rate capability, and minimal health and environmental impacts.

Lithium Iron/Manganese Phosphate (Olivines): LiFePO_4 is non-toxic and exhibits very low capacity fade, although its performance is sensitive to impurities, especially Fe^{3+} . It has an exceptionally flat discharge plateau at 3.4 V and a moderate capacity 77 of 150–160 mAh/g [3]. The compound exhibits smaller volume changes and charge–discharge heat flow compared to other cathode materials. It gives optimum output at 50°C and above, restricting its use with conventional liquid electrolytes. LiFePO_4 also

offers significant safety advantages over LiCoO_2 and could hence prove critical in batteries designed for high-power applications. However, its room temperature conductivity is poor, of the order of 10^{-9} S/cm, and capacities close to its theoretical value may be realized only at low current densities or at elevated temperatures. The charging voltage of cells with LiFePO_4 is less than 4 V, which makes it less taxing on the electrolyte.

1.4.3 Electrolytes

Electrolytes used in lithium ion batteries can be classified as follows

Liquid Electrolytes: Liquid electrolytes in lithium-ion batteries consist of lithium salts, such as LiPF_6 , LiBF_4 or LiClO_4 in an organic solvent, such as ethylene carbonate, dimethyl carbonate, and diethyl carbonate [15]. A liquid electrolyte conducts lithium ions, acting as a carrier between the cathode and the anode when a battery passes an electric current through an external circuit. Typical conductivities of liquid electrolyte at room temperature (20°C (68°F)) are in the range of 1 S/m, increasing by approximately 30–40% at 40°C (104°F) and decreasing by a slightly smaller amount at 0°C (32°F). Unfortunately, organic solvents easily decompose on anodes during charging. However, when appropriate organic solvents are used as the electrolyte, the solvent decomposes on initial charging and forms a solid layer called the solid electrolyte interphase (SEI), which is electrically insulating yet provides sufficient ionic conductivity. The interphase prevents decomposition of the electrolyte after the second charge. For example, ethylene carbonate is decomposed at a relatively high voltage, 0.7 V vs. lithium, and forms a dense and stable interface.

Polymer Electrolytes: Ionically conducting polymers were first discovered about 20 years ago and were subsequently used as electrolytes in solid-state batteries. Ion-conducting polymers are solutions of salts in polymers in which a macroscopically solid state is achieved by entanglement or cross-linking [3]. Microscopically they behave as liquids. The polymer electrolytes are generally composites of a polyethylene oxide and a salt such as LiPF_6 , LiClO_4 , LiAsF_6 , or LiCF_3SO_3 . The common polymer electrolyte solution is LiPF_6 which is not only flammable but also has electrochemical stability up to only about 4.5 V. The poor thermal stability of LiPF_6 limits its use in polymer electrolytes that work between 50 and 80°C. Composite polymer electrolytes based on nanoparticles of ceramics exhibit higher conductivity and are apparently resistive towards high-voltage oxidation. Improved electrical and mechanical properties have been realized with polymer-silicate nanocomposites in which nanoscale clay particles are molecularly dispersed within a polymeric matrix.

Non-flammable Electrolytes: Solvents used in lithium-ion batteries are typically low boiling and have flash points around 30°C. Therefore, a major danger lurks from a cell that vents or explodes due to the flammability of the spewing hot electrolyte vapors. Present-day electrolyte formulations contain additives to retard the flammability that also affects the cell performance. The fall in cell performance is due either to electrochemical instability that leads to capacity fade or increased viscosity of the additive, which leads to reduced ionic transport and hence to lower capacity utilization and power[3]. Since performance cannot be sacrificed, studies mostly focus on flame-retardants used as additives or co-solvents in known electrolyte formulations. Fluorinated compounds and

organo-phosphorus compounds are among the most investigated co-solvents to mitigate flammability.

1.5 Objective and Scope of this Research

Lithium-ion batteries currently are ubiquitous power sources for portable electronics. But more advanced lithium-ion batteries with high energy and high power density still need to be achieved for the projected era of hybrid electric vehicles. The energy density and performance of lithium-ion batteries largely depend on the physical and chemical properties of the cathode and anode materials. In this research, several anode materials are explored having reversible lithium storage capability. Initially, current research on anode materials is reviewed in chapter 2. The various experimental apparatus, cell preparation and battery testing procedures are described in chapter 3

At first, the electrochemical behavior of anode materials graphene oxide and and graphene nano platelets (NGP's) are studied. Graphene oxide was synthesized in large quantities using modified hummers method. Electrochemical behavior of Graphene oxide and Reduced Graphene oxide is compared. Also the effect of heat treatment on the reversible capacities of graphene oxide is studied. Finally the graphene oxide is compared with commercially available Nano Graphene Platelets for their capacities and cycle life. The results are discussed in the chapter 4.

Second, graphene oxide and manganese acetate composite was synthesized using a chemical approach. Effect of heat treatment on electrochemical capacities of graphene oxide and manganese acetate anode material is studied. Effect of mixing methods and

composition ratio of graphene oxide and manganese oxide anode material on electrochemical charge capacities and cycle life are studied in chapter 5.

Third, new approach of chemical synthesis of graphene oxide and manganese oxide nano composite has been devised. Graphene oxide manganese acetate composite anode and graphene oxide manganese oxide nano composite are compared for their electrochemical performances. The results are discussed in chapter 6.

Fourth, Electrochemical Impedance results of graphene oxide and graphene oxide/manganese oxide composite anode materials are discussed in chapter 7.

Finally the conclusion of the thesis work and future scope of work is discussed in the chapter 8.

2. Research Status of Graphene-base Anodes

Research to develop alternative electrode materials with high energy densities in Li-ion batteries has been actively pursued to satisfy the power demands for electronic devices and hybrid electric vehicles. In this chapter, the current research on the anode materials graphene, graphene-alloy composites and graphene-metal oxide composites is reviewed.

2.1 Graphene

Graphene, a single layer of carbon (carbon atoms in a two-dimensional (2D) honeycomb lattice), was found to exist as a free-standing form and exhibits many unusual and intriguing physical, chemical and mechanical properties [35-37]. Due to the high quality of the sp^2 carbon lattice, electrons were found to move ballistically in graphene layer even at ambient temperature. Graphene powders are used as anode materials for reversible lithium storage in lithium-ion batteries. During the intercalation process, lithium transfers its 2s electrons to the carbon host and is situated between the carbon sheets. High capacity carbon materials have also been reported [16-18]. This could be mainly ascribed to

- Lithium insertion within the ‘cavities’ in the material,
- Lithium absorbed on each side of the carbon sheet,
- Lithium binding on the so called ‘covalent’ site, and
- Lithium binding on hydrogen terminated edges of graphene fragments in carbon materials.

Owing to its large surface-to-volume ratio and highly conductive nature, graphene may have properties that make it suitable for reversible lithium storage in lithium-ion batteries. This is because the lithium ions can be adsorbed on both sides of the graphene sheet that arranged like a “house of cards” in hard carbons, leading to two layers of lithium for each graphene sheet, with a theoretical capacity of 744 mAh/g through the formation of Li_2C_6 . On the other hand, nano-cavities between graphene nanosheets due to scrolling and crumpling could also contribute to the lithium storage. Due to the large surface to volume ratio and the formation of nano cavities, graphene nano sheets depict enhanced Lithium storage capacity and very good cyclic performance. Therefore, it is expected that graphene could overtake its 3D counterpart (graphite) for enhanced lithium storage in lithium-ion batteries; whereas maximum specific lithium insertion capacity for graphite (3D network of graphene) is only 372 mAh/g, corresponding to the formation of LiC_6 – first stage graphite intercalation compounds.

Structure and Properties

The various structural properties of graphene are as detailed below. Figure 2.1 shows the 2 dimensional layered structure of graphene.

- Nanosheets are naturally crumpled and curved.
- Graphene nanosheets depict graphitic crystalline structure.
- Graphene has large surface area of $492.5 \text{ m}^2/\text{g}$ when compared with the graphite powder which has about $8.5 \text{ m}^2/\text{g}$
- Graphene has a theoretical capacity of 744 mAh/g through the formation of Li_2C_6 .

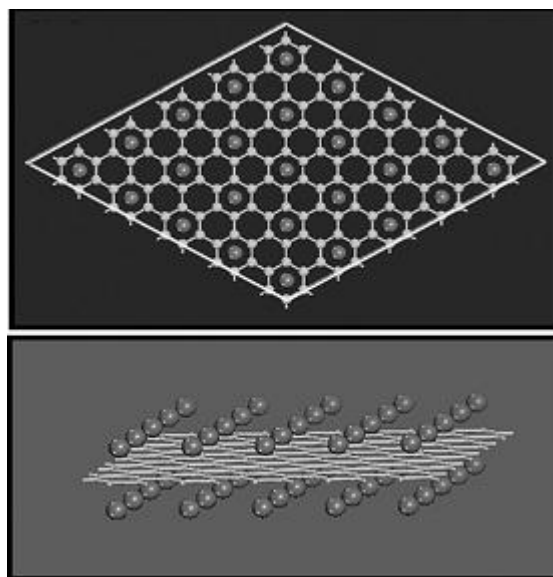


Figure 2.1 Atomic model of LiC_3 graphene. Top: top view; bottom: side view [13]

Graphene materials can be prepared in many ways. The most popular way is to prepare graphene oxide (GO) first and then obtain graphene sheets by chemical reduction or thermal reduction [16, 29]. Another economic way to get largescale graphene-based materials is to thermally expand the expandable graphite at a very high heating rate to about 1000°C [49, 50]. Usually, the time for preparation must be short enough to avoid aggregation and graphitization under so high temperature. In addition, the graphene sheets also could be obtained by exfoliating graphite directly via mechanical or electrochemical routes [51-52], or via bottom-up routes, e.g. epitaxial growth [53-55], chemical vapor deposition and solvothermal method [56-58]. The properties of graphene sheets usually depend on the route for their preparation. As a novel anode material for the lithium-ion batteries, graphene sheets mostly exhibit a higher reversible capacity than graphite [29,59,60].

Wang et al. [16] synthesized graphene nano sheets in large quantities using a modified hummer's method. Graphene nanosheets delivered a specific capacity of 945 mAh/g and a reversible capacity of 650 mAh/g in the first cycle. After 100 cycles the graphene anode still maintained a specific capacity of 460 mAh/g which is better than that of graphite anodes. The nano sheets exhibited an enhanced lithium storage capacity as anodes in lithium-ion cells with good cyclic performance.

Peichao Lian et al. [29] prepared high quality graphene sheets from graphite powder through oxidation followed by rapid thermal expansion in nitrogen atmosphere. It is found that the graphene sheets possesses a curled morphology consisting of a thin wrinkled paper-like structure, fewer layers (4 layers) and large specific surface area (492.5 m²/g). The first discharge and charge capacities of graphene sheets were as high as 2035 mAh/g and 1264 mAh/g, respectively. Obviously, the reversible capacity of graphene sheets with fewer layers is much higher than that of previously reported graphene nanosheets (540 mAh/g). The possible reason is that the larger surface area and curled morphology of graphene sheets with fewer layers can provide more lithium insertion active sites, such as edge-type sites, nanopores [30]. It's well known that the disordered carbons can yield higher capacity values than graphite [31–33], and the graphene can be considered as a very disordered carbon. The first reversible specific capacity of the prepared graphene sheets was as high as 1264 mAh/g at a current density of 100 mA/g. Even at a high current density of 500 mA/g, the reversible specific capacity remained at 718 mAh/g. The high rate discharge/charge properties are likely to originate in the shortened diffusion distance of lithium ions into the host position of the graphene

sheets with fewer layers and porous structure. After 40 cycles, the reversible capacity was still at 848 mAh/g at the current density of 100 mA/g. These results indicate that the prepared high quality graphene sheets with fewer layers have an intensive potential as a candidate of anode materials with high reversible capacity, good cycle performance and high rate discharge/charge capability.

2.2 Graphene-Alloy Composites

Composite anode materials made of nanoparticles of metals (Sn, Si) and graphene have large insertion capacity and can accommodate the large strains of lithium insertion and de-insertion to provide good electronic contact owing to the good mechanical properties and high conductivity provided by graphene. Therefore, the cycling stability of the electrodes can be greatly enhanced.

Graphene-Sn Alloy Composite Anode Materials

Wang et al designed a synthetic approach to prepare Sn/graphene nanocomposite with 3D architecture, in which Sn nanoparticles act as a spacer to effectively separate graphene nanosheets [13] as shown in Figure 2.2. First cycle discharge capacity of 1250 mAh/g and charge capacity of 810 mAh/g have been reported. The large irreversible capacity is ascribed to the formation of the solid electrolyte interphase (SEI) layers on the surface of the electrode. From the second cycle, the reversibility of the electrode was gradually improved on cycling, with an average columbic efficiency of 96.5% up to 100 cycles. The electrode maintained a capacity of 508 mAh/g after 100 cycles. Graphene nanosheets were crumpled to a curly and wavy shape, resembling flower pedals. Tiny Sn nanoparticles are homogeneously distributed on the curly graphene nanosheets. Due to

the corrugated nature of the graphene nanosheets, substantial voids exist between individual nanosheets. The deposited Sn nanoparticles could act as a spacer to prevent the re-stacking of individual graphene nanosheets[19]. Such a nanocomposite could deliver an enhanced electrochemical performance as an anode material in lithium ion batteries.

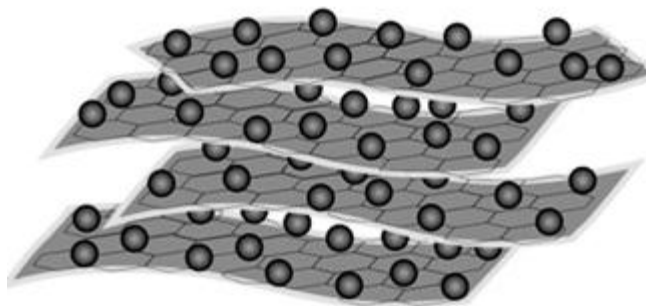


Figure 2.2 Sn/graphene nanocomposite with a 3D architecture

There have been a few reports about the preparation of SnO₂/graphene composite [10, 38–40]. Xuyang Wang et al. [34] designed a simple solution-based synthesis route, based on an oxidation–reduction reaction between graphene oxide and SnCl₂•2H₂O, has been developed to produce a SnO₂/graphene composite. In the prepared composite, crystalline SnO₂ nanoparticles with sizes of 3–5 nm uniformly clung to the graphene matrix. When used as an electrode material for lithium ion batteries, the composite presented excellent rate performance and high cyclic stability. The effect of SnO₂/graphene ratio on electrochemical performance has been investigated. It was found that the optimum molar ratio of SnO₂/graphene was about 3.2:1, corresponding to 2.4 wt.% of graphene. The SnO₂/graphene hybrid electrode materials delivered an initial discharge capacity of 1700 mAh/g and charge capacity of 978 mAh/g with a coulombic efficiency of 58% at the first cycle at a current density of 67mA/g, charge capacity

remained about 840 mAh/g with capacity retention of 86% up to the 30th cycle. And the hybrid composite could retain a charge capacity of about 590 and 270 mAh/g after 50 cycles at the current density of 400 and 1000 mA/g, respectively. The formation of SnO₂ nanoparticles on the surfaces of the nanosheets can be attributed to the functional groups, such as hydroxyl and epoxy groups, which are attached to both sides of the graphene oxide nanosheets [41-42]. In the SnO₂/graphene composite, the graphene nanosheets might virtually work as a barrier to avoid the aggregation of SnO₂ nanoparticles and also a buffer to prevent the electrode material from a large volume change during Li⁺ insertion/extraction resulting in an enhanced cycling performance.

Graphene-Si Alloy Composite Anode Materials

Si/graphene composite anode materials have become of particular interest recently because of large lithium insertion capacity of silicon and graphene acting as a buffering agent to accommodate the large volume changes during lithium insertion and de-insertion. The enhanced cycling stability is attributed to the fact that the Si/graphene composite can accommodate large volume change of Si and maintain good electronic contact. The graphene due to its sheet structure can provide better separation to prevent the agglomeration of silicon nanoparticles than carbon black, carbon nanotubes, or graphite[20].

Si/graphene composite was prepared by simply mixing of commercially available nanosize Si and graphene. Electrochemical tests on Si/graphene composite reported by Shu-Lei Chou et al [21] showed an initial discharge capacity and coulombic efficiency is 2158 mAh/g and 73%, respectively have been reported. After 30 cycles, the Si/graphene composite electrode retains a discharge capacity of 1168 mAh/g and an average

coulombic efficiency of 93%. It can be seen that the capacity retention and initial coulombic efficiency of the Si/graphene composite represent a significant improvement over that of the nanosize Si. EIS indicate that the Si/graphene composite electrode has less than 50% of the charge-transfer resistance compared with nanosize Si electrode, evidencing the enhanced ionic conductivity of Si/graphene composite. The enhanced cycling stability is attributed to the fact that the Si/graphene composite can accommodate large volume change of Si and maintain good electronic contact.

Similarly, Hongfa Xiang et al. [43] prepared graphene/nanosized silicon composites and used for lithium battery anodes. Two types of graphene samples were used and their composites with nanosized silicon were prepared in different ways. In the first method, the graphene sample was prepared by fast heat treatment of expandable graphite at 1050°C and the graphene/nanosized silicon composites were then prepared by mechanical blending. In the second method, graphene oxide (GO) and nanosized silicon particles were homogeneously mixed in aqueous solution and then the dry samples were annealed at 500°C to give thermally reduced GO and nanosized silicon composites. In both cases, homogeneous composites were formed and the presence of graphene in the composites has been proved to effectively enhance the cycling stability of silicon anode in the lithium-ion batteries. The significant enhancement on cycling stability could be ascribed to the high conductivity of the graphene materials and absorption of volume changes of silicon by graphene sheets during the lithiation/delithiation process[38]. The composites using thermally expanded graphite delivered discharge and reversible charge capacities of 3442mAh/g and 2753mAh/g respectively with an initial coulombic efficiency of 80%. After 30 cycles the capacity retention of the electrode is about 2136mAh/g. In

particular, the composites using thermally expanded graphite exhibited not only more excellent cycling performance, but also higher specific capacities because the graphene sheets prepared by this method have fewer structural defects than thermally reduced GO.

2.3 Graphene Metal Oxide Composites

The current research status on the lithium storage characteristics and cycle performance of graphene/metal oxides is discussed. Initially, Haegyem Kim et al [25] reported a Co_3O_4 /graphene hybrid material fabricated using a simple in-situ reduction process and demonstrated as a highly reversible anode for lithium rechargeable batteries. The hybrid is composed of 5 nm size Co_3O_4 particles uniformly dispersed on graphene. The Co_3O_4 /graphene anode can deliver a capacity of more than 800 mAh/g reversibly at a 200 mA/g rate in the voltage range between 3.0 and 0.001 V. The anode can retain a reversible capacity of 778 mAh/g with coulombic efficiency of 97% after 42 cycles. The high reversible capacity is retained at elevated current densities. At a current rate as high as 1000 mA/g, the Co_3O_4 /graphene anode can deliver more than 550 mAh/g, which is significantly higher than the capacity of current commercial graphite anodes. The shape of the charge discharge profiles is not significantly altered during 13 cycles, indicating the stability of the hybrid as anode. In discharge, plateau at 1.3 and 1.0 V corresponds to the formation of Li_2O accompanying the reduction of metal nanoparticles. In addition, the capacity below 1.0 V can be attributed to lithiation of graphene and/or a reversible polymerization of the electrolyte. In charging state, the reactions are reversed. The superior electrochemical performance of the Co_3O_4 /graphene is attributed to its unique

nanostructure, which intimately combines the conductive graphene network with uniformly dispersed nano Co_3O_4 particles.

Till now, there have been a very few reports about the preparation of CuO/graphene composite. Y.J. Mai et al. [61] synthesized CuO/graphene composite from CuO and graphene oxide sheets and reduced by hydrazine vapor. As the electrode material for lithium-ion batteries, CuO nanoparticles with sizes of about 30nm homogeneously locate on graphene sheets, and act as spacers to effectively prevent the agglomeration of graphene sheets, keeping their high active surface. In turn, the graphene sheets with good electrical conductivity server as a conducting network for fast electron transfer between the active materials and charge collector, as well as buffered spaces to accommodate the volume expansion/contraction during discharge/charge process. CuO/graphene electrode delivered an initial discharge capacity and reversible charge capacity of 752.4 and 583.5mAh/g respectively which are larger than their theoretical capacities (670mAh/g for CuO and 754mAh/g for graphene). The extra capacity compared with the theoretic capacity usually is ascribed to formation of SEI during the first discharge process, the reduction of the adsorbed impurities on active material surfaces, the initial formation of lithium oxide as well as possibly interfacial lithium storage. The introducing of graphene shows a strong synergistic effect in the composite for improving the reversible capacity of CuO/graphene composite, such as improved initial coulombic efficiency (68.7%) and reversible capacity of 583.5mAh/g with 75.5% retention of the reversible capacity after 50 cycles.

Peichao Lian et al [62]. prepared Fe_3O_4 -Graphene nanocomposite by a gas/liquid interface reaction. Electrochemical tests show that the Fe_3O_4 -22.7 wt.% graphene

nanocomposite exhibits much higher capacity retention with a large reversible specific capacity of 1048mA/g (99% of the initial reversible specific capacity) at the 90th cycle in comparison with that of the bare Fe₃O₄ nanoparticles (only 226mAhg⁻¹ at the 34th cycle). The theoretical specific capacity of the Fe₃O₄-22.7 wt.% graphene nanocomposite is 968mAh/g calculated based on the theoretical specific capacity of Fe₃O₄ (924mAh/g) and graphene sheets (1116mAh/g)[29]. Fe₃O₄-Graphene nanocomposite electrode delivered an initial discharge capacity and reversible charge capacity of 1360 and 1060mAh/g respectively, which is slightly higher than the theoretical specific capacity. The extra capacity may be attributed to the synergistic effect between the Fe₃O₄ nanoparticles and graphene sheets in the nanocomposite, such as the formed secondary pores could store some lithium. The initial coulombic efficiency of the Fe₃O₄-22.7 wt.% graphene nanocomposite is 78%, which is slightly lower than 82% of the Fe₃O₄ nanoparticles, indicating an increase of the irreversible capacity loss due to the increase of specific surface area. The irreversible capacity loss in the first cycle can be attributed to electrolyte decomposition and formation of solid electrolyte interface (SEI) film[63]. Nevertheless, after two cycles the coulombic efficiency of the Fe₃O₄-22.7 wt.% graphene nanocomposite increases to above 93% in the subsequent cycles. The enhanced cycling performance can be attributed to the facts that the graphene sheets distributed between the Fe₃O₄ nanoparticles can prevent the aggregation of the Fe₃O₄ nanoparticles, and the Fe₃O₄-graphene nanocomposite can provide buffering spaces against the volume changes of Fe₃O₄ nanoparticles during electrochemical cycling.

2.4 Summary

Table 2.1 summarizes the current research status on various graphene based anode materials.

Table 2.1 Summary of Current Research of Graphene Based Anode Materials

Anode Sample	Initial Discharge Capacity(mAh/g)	Initial Reversible Charge Capacity (mAh/g)	1st Cycle Columbic Efficiency 1st charge/discharge)	Capacity Fade Per Cycle	nth Cycle Charge Capacity	No of Cycles
Graphene	945	650	68%	0.29%	460	100
Fewer layers (4) of Graphene	2035	1264	63%	0.83%	848	40
Graphene-Sn	1250	810	64%	0.37%	508	100
Graphene-SnO₂	1700	978	58%	0.47%	840	30
Graphene-Si	2158	1575	73%	0.86%	1168	30
Thermally Reduced GO-Si	3442	2753	80%	0.74%	2136	30
Graphene-Co₃O₄	1450	850	58%	0.22%	772	42
Graphene-CuO	753	584	69%	0.48%	441	50
Graphene-Fe₃O₄	1360	1060	78%	0.01%	1048	90

3. Experimental Apparatus and Procedure

3.1 Apparatus

This chapter describes the apparatus throughout this research to conduct the electrochemical experiments on various anode materials. The various apparatus used are Swagelok-type cell, Glove box, Box furnace, Tube furnace and Gamry electrochemical work station. The procedure involved in cell preparation and testing is described. The experimental data is represented as voltage capacity graphs, capacity cycle graphs and impedance graphs to do the analysis.

3.1.1 Swagelok-type Cell

In electrochemistry, Swagelok-type cell is a prototype battery as shown in Figure 3.1 A, is to determine the capacity of an anode material in a lithium ion battery using electrochemistry work station. The Swagelok-type cell looks like a small cylinder with irregular diameter from top to bottom and it consists of the following parts: the bottom cap, the cathode electrode, the separator, the Teflon cylinder, the anode electrode, the liquid electrolyte, the spacer, the closing cap. All the experiments are carried using Swagelok-type cell to assemble the prototype battery for testing.

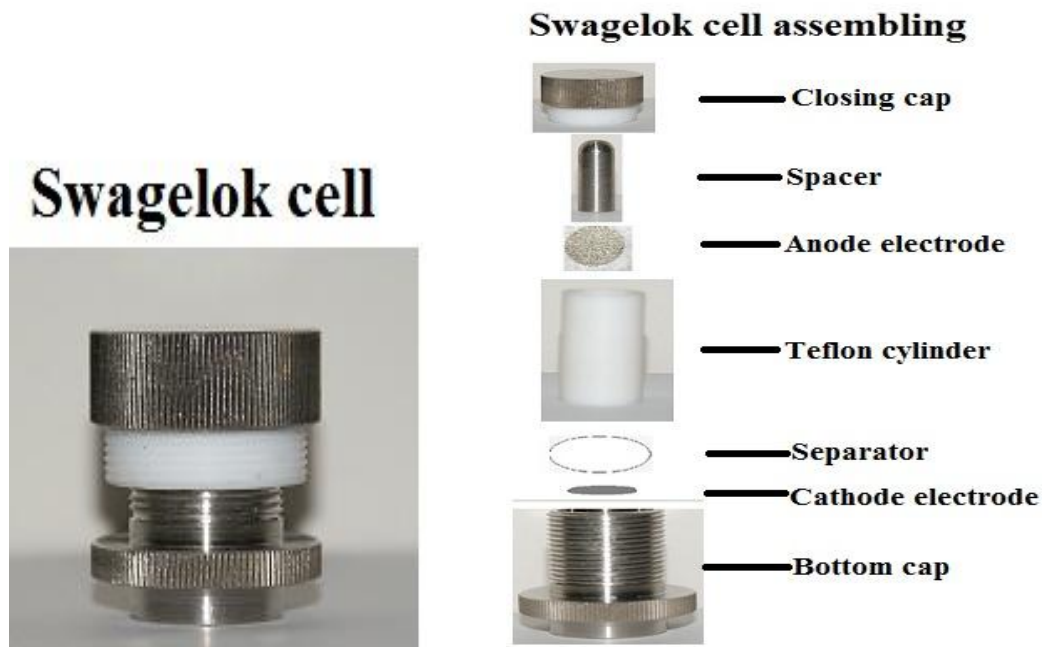


Figure 3.1 A) Swagelok Cell B) Various parts in the assembly of swagelok cell

Figure 3.1 B shows various parts in the assembly of Swagelok cell from top to bottom. First, the cathode electrode is placed inside the bottom cap and the separators are placed on top of the cathode. The teflon cylinder is inserted tightly onto the bottom cap and the anode electrode is placed inside the cylinder. The liquid electrolyte is poured into the cylinder and the cell is tightly packed using spacer with screw cap. All this assembly is done under inert atmosphere to avoid any traces of moisture. During testing negative terminal of the voltmeter is connected to the anode and the positive terminal to the cathode to measure the voltage and charge capacities.

3.1.2 Glove Box

The glove box is a sealed container as shown in Figure 3.2, is manufactured by Vacuum Atmospheres Company. Glove box is used to assemble the prototype battery

under inert atmosphere. Built into the sides of the glove box are gloves arranged in such a way that the user can place his hands into the gloves and perform tasks of building the prototype battery. Part or the entire box is usually transparent to allow the user to see what is being manipulated. Argon gas is pumped into the glove box to maintain the inert atmosphere.



Figure 3.2 Glove Box (Vacuum Atmospheres Company).

3.1.3 Electrochemical Working Station

Electrochemical working station is a battery testing instrument with the capability of testing multiple battery cells. The working station is fully automated programmable multiple channel turnkey system and can test the battery cells integrated into a single unit. The electrochemical working station used to conduct the battery tests for the current research is Land CT2001A model (as shown in Figure 3.3). This is a portable, 8-channel

instrument with potentiostat/galvanostat circuitry, -2V to 10V, $\pm 2A$ output and having 3 current ranges, every channel allows precision and flexibility to carry out the performance studies for materials, electrodes, cells, batteries, and battery packs. It also provides for optional second voltage, temperature, and pressure auxiliaries, as well as pulse testing capability. It provides for a voltage clamp to protect from over or under-charge/discharge. This instrument can be integrated with the onsite computers running on windows operating system and uses windows based software to capture the battery test output data from the working station. The working station is provided with a universal battery holder for easy material handling.

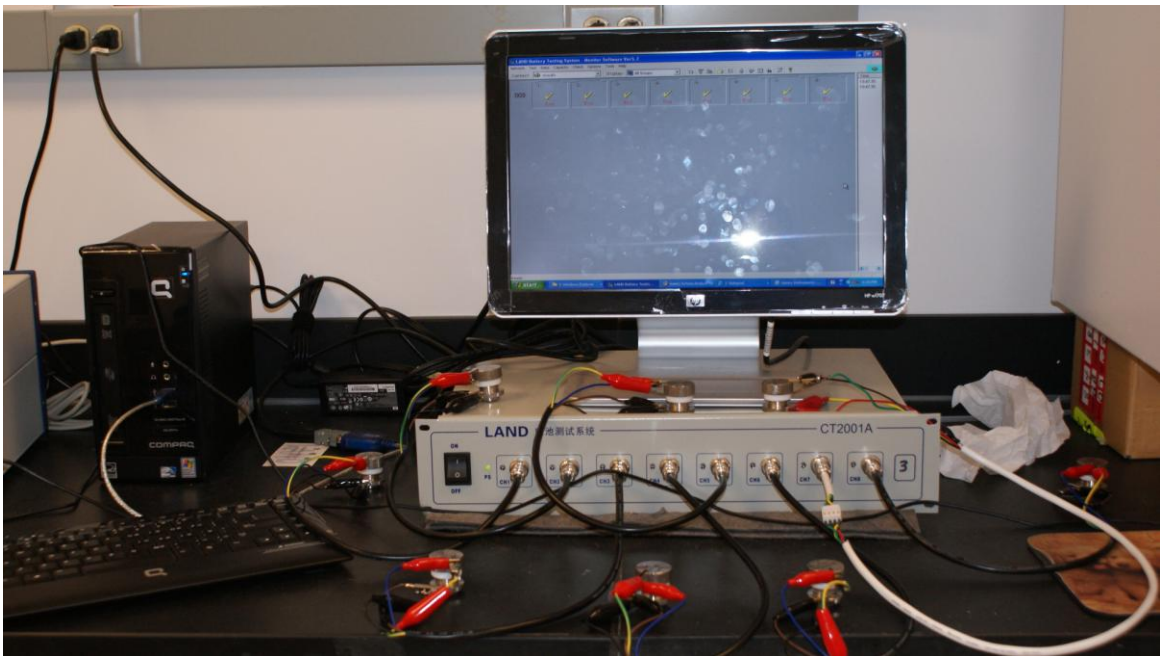


Figure 3.3 Battery Testing Station (Land CT2001A)

3.1.4 Electrochemical Measurement System-Gamry Instruments

Gamry Potentiostat (Figure 3.4) is used to conduct electrochemical Impedance Spectroscopy analysis. The electrochemical cell is maintained under potentiostatic

control in either two or three electrode configurations. The various setup parameters AC voltage, DC offset voltage, starting and ending frequencies, Estimated Initial Z, Conditioning Time & Potential, Initial Delay Time & Drift Rate, Data Filename, Notes and number of data points measured per decade frequency can be operator controlled using EIS600 software system. The EIS600 electrochemical impedance spectroscopy software measures impedances spanning 15 orders of magnitude over a frequency range of 10 μ Hz to 1 MHz. Impedance Error is less than 0.5% and applied signal amplitude can be from 2.75 μ V to 1425 mV rms.

The EIS600 system, along with Gamry Potentiostat, is configured and integrated into a desktop computer. Real time spectrum is shown in either Bode or Nyquist format. Nyquist, Bode (linear and log immitance), and Real and Imaginary Immitance versus Frequency graphs can be obtained. Immitance plotted as either impedance or as admittance. All curves represented are auto scaled. Pause/Continue, Skip and Abort controls can be used where appropriate. Model fitting is based on Non-linear Least Square or a Simplex fit. Model entry via a graphical schematic (click-and-drag) capture and automatic compilation features are available to improve the ease of use.



Figure 3.4 Gamry Potentiostat

3.1.5 Box Furnace

Box furnace manufactured by Carbolite as shown in Figure 3.5, is an electric heating device used for heat treating various anode samples at different temperatures. The heat treatment is carried out in normal atmosphere and the samples are oxidized. Carbolite's box furnaces The furnace have maximum temperatures of 1200°C.



Figure 3.5 Box Furnace (Carbolite)

3.1.6 Tube Furnace

Tube furnace manufactured by Carbolite as shown in Figure 3.6, is used for heat treating the various anode samples at different temperatures under inert atmosphere. Carbolite's tube furnaces utilize resistive wire heating elements, which is wound around the outside of a ceramic worktube making it an integral part of the tube furnace's heating element. Temperature is controlled via feedback from a thermocouple. The thermocouple is located in a protected position outside of the worktube and the heating element, allowing the full worktube diameter to be used and protects the thermocouple from mechanical damage. The carbolite tube furnace has a length of 900mm and tube diameter of 100mm. The tube furnaces have maximum temperature of 1200°C.

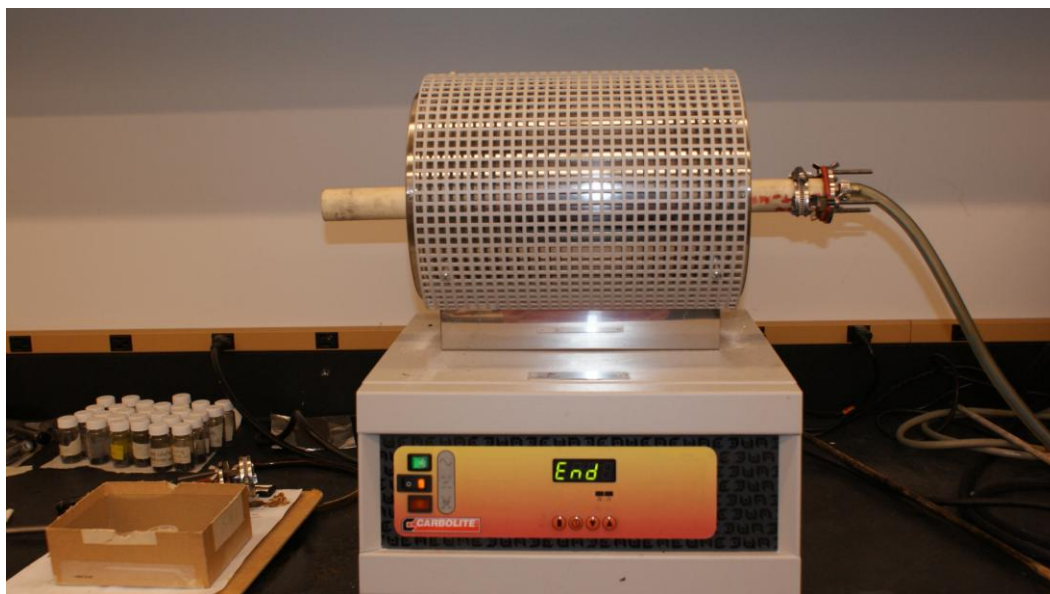


Figure 3.6 Tube Furnace (Carbolite)

3.1.7 Vacuum Oven

Vacuum Oven manufactured by Cascade Tek as shown in Figure 3.7, is used to dry the anode samples at 120°C. The vacuum oven has a capacity of 1.7 cubic feet and with an interior size of 12”Wx20”Dx12”H. The vacuum oven has an ambient temperature range of 5°C to 230°C.



Figure 3.7 Vacuum Oven (Cascade Tek)

3.2 Preparation and Testing of Working Electrode

Below are the steps involved in preparation of Swagelok-type battery cells used for testing in electrochemical work station.

- Each of the composition of anode material is taken and multiple samples are prepared in the following manner.
- The powders were mixed with a binder polyvinylidene fluoride (PVDF) in the weight ratios of 90:10 in N-Methyl-Pyrrolidone (NMP) solvent to form slurry.
- Then the resultant slurries were uniformly pasted on Cu foil with a blade.
- These prepared electrode sheets were dried at 120°C in a vacuum oven for 1h and pressed under a pressure of approximately 200 kg/cm².
- Coin cells were assembled in a glove box for electrochemical characterization.

- The electrolyte used was 1 M LiPF₆ in a 1:1 mixture of ethylene carbonate and dimethyl carbonate.
- Lithium metal foil was used as the counter and reference electrode.
- The cells were galvanostatically charged and discharged at a current density of 50 μA within the range of 0.01–3.0 V.

Electrode weight is the total weight including the weight of copper foil, PVDF binder and anode sample. The radius of the copper foil used for each electrode specimen is 3/8 inches. The weight of the copper foil used for each electrode specimen is 16.2 mg. Actual weight of the sample is the electrode weight minus the weight of copper foil and PVDF binder. The actual weight is used for calculating the specific capacity of the anode sample. Table 3.1 lists the chemicals used in electrode preparation. Flow chart shown in Figure 3.8 depicts the program followed in testing the working electrode on electrochemical working station.

Table 3.1 List of Chemicals Used in Electrode Preparation

Chemicals	Vendor
1-Methyl 2 Pyrrolidone (NMP)	Aldrich
Polyvinylidene fluoride (PVDF)	Aldrich
Copper foil	Aldrich
Lithium Metal foil	Aldrich
LiPF ₆	Aldrich
Ethylene Carbonate	Aldrich
Di-methyl Carbonate	Aldrich

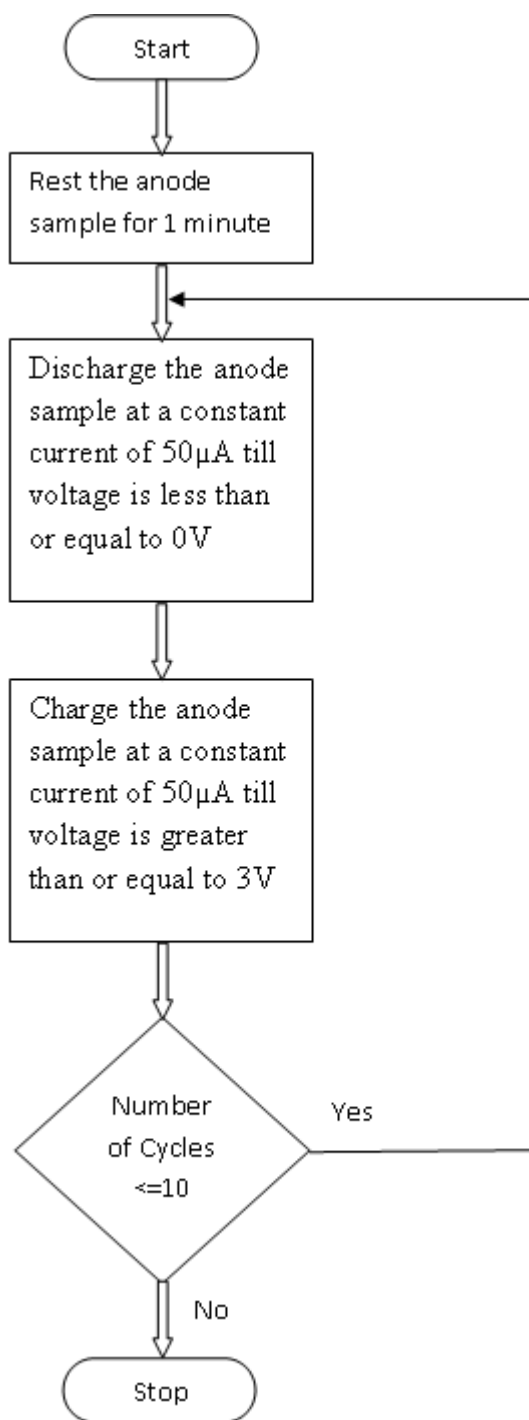


Figure 3.8 Program used to test working electrode on electrochemical working station

Table 3.2 shows the initial setting and its values used in the Gamry Potentiostat used for EIS analysis

Table 3.2 Initial Settings Used in Gamry EIS

Test Identifier	Potentiostatic EIS
Initial frequency	1MHz
Final frequency	0.1Hz
Points/decade	20
Estimated Z_{ohms}	1000
AC Volts(mv rms)	10
DC volts (V)	0
VS EOS	Yes

The following is the procedure to plot the Nyquist plot using the Gamry potentiostat which is integrated with Gamry EIS600 software system running on the desktop machine.

- First the Gamry instrument is switched on and the Gamry EIS600 software system running on the desktop is launched.
- In the electrochemical impedance option, select the potentiostat EIS to run. Set the initial setting and its values as specified in Table 3.1.
- Select the Nyquist plot as the type of graph to be plotted in a dropdown box.
- Press F2 to save the Nyquist plots to a specified folder on the file system.

3.3 Electrochemical Data Presentation Graphs

3.3.1 Voltage Capacity Graphs

Voltage versus capacity graphs are plotted with voltage on Y-axis and capacity on X-axis. Potential plateaus are observed for in the graphs which indicate cell discharge at constant voltage. The plateau formation indicates the formation of lithium intercalation compounds. The Swagelok cells were galvanostatically charged and discharged at a current density of $50\mu\text{A}$ within the range of 0.01–3.0 V for 10 cycles on an electrochemical working station. Total charge and discharge capacities (mAh) along voltage data is exported to a computer system in excel format. The capacity data is divided by the active weight of electrode sample in order to obtain the specific capacity in terms of mAh/g. Specific capacity (mAh/g) Vs Voltage (V) data are plotted using Origin data analysis and graphic software. Figure 3.9 shows the sample voltage capacity graph of an anode electrode. As can be seen from the graph, the discharge profile is carried till the voltage reaches 0V and the charge profile is carried till the voltage reaches 3V.

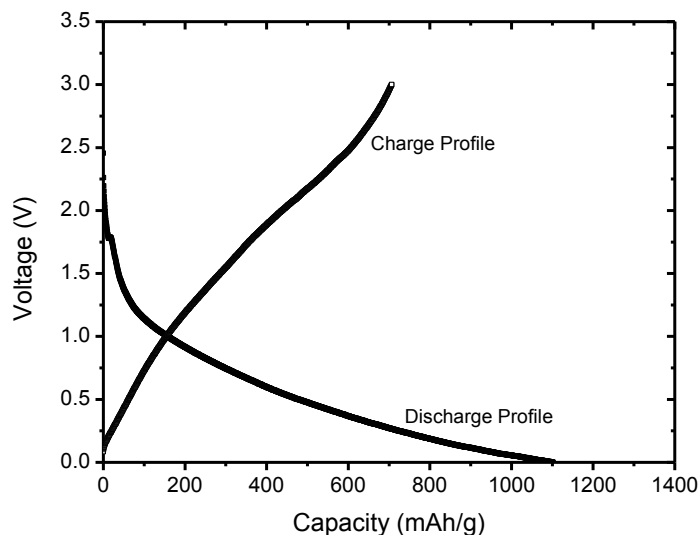


Figure 3.9 Sample voltage capacity graph of an anode electrode

3.3.2 Capacity Cycle Graphs

Capacity cycle graphs are plotted with capacity on the Y-axis and number of cycles on the X-axis. Capacity cycle graphs show the cycle life of battery samples. The cycling stability can be greatly enhanced, if the structural stability of the anode material is maintained by accommodating the large strains of lithium insertion and de-insertion and provide good electronic contact. The Swagelok cell is charged and discharged for 10 cycles in the electrochemical working station. Specific capacities are calculated after the data is exported to computer system in excel format. The discharge and charge capacities (mAh/g) for each cycle are plotted using Origin data analysis and graphic software. Figure 3.10 shows the sample capacity cycle graph of an anode electrode. As can be seen from the graph, with increase in number of cycles, the charge and discharge capacities

start fading. Also there is a large irreversible discharge capacity observed after the first cycle, this is due the solid electrolyte interface formation at the electrode surface.

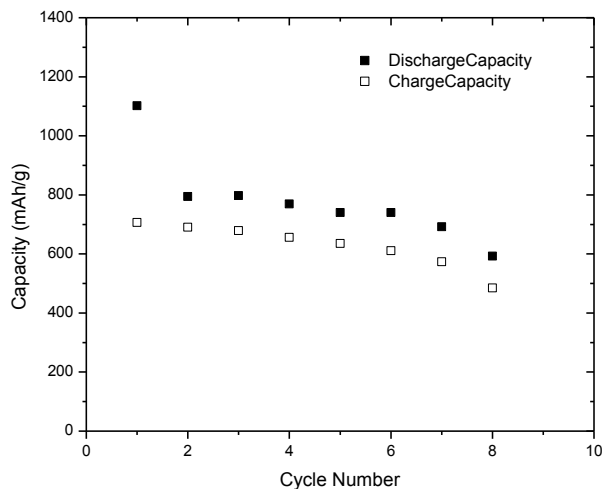


Figure 3.10 Sample capacity cycle graph of an anode electrode

3.3.3 Electrochemical Impedance Graphs

The basic design of all types of batteries shares several common elements. All batteries have electrodes consisting of particles of energy-storing material and conductive additive, held together by polymeric binder. They also include electrolyte and a separator, preventing electric contact between opposite electrodes. The general approach to study the battery kinetics can be based on analyzing the impedance of the above common components, namely electrode and electrolyte. This not only allows creating a working kinetic model of the battery as a whole but also allows the evaluation of the effect of each component on material power capability.

The kinetic steps in a lithium ion battery are shown in Figure 3.11. These include electronic conduction through the particles and ionic conduction through the electrolyte in cavities between particles. On the surface of each particle, charge transfer involves the resistance of an insulating layer and activated electron transfer resistance on the electronic/ionic conduction boundary. Further, ions have to diffuse into the bulk of particles via solid-state diffusion. Other subsequent processes, such as the formation of new crystalline structures, can also become limiting kinetic steps at frequencies below 1 mHz. Not indicated in the figure 3.11 are conduction through the electrolyte and porous separator, and conduction through wires, which both dominate high-frequency behavior above 10 kHz[2, 28].

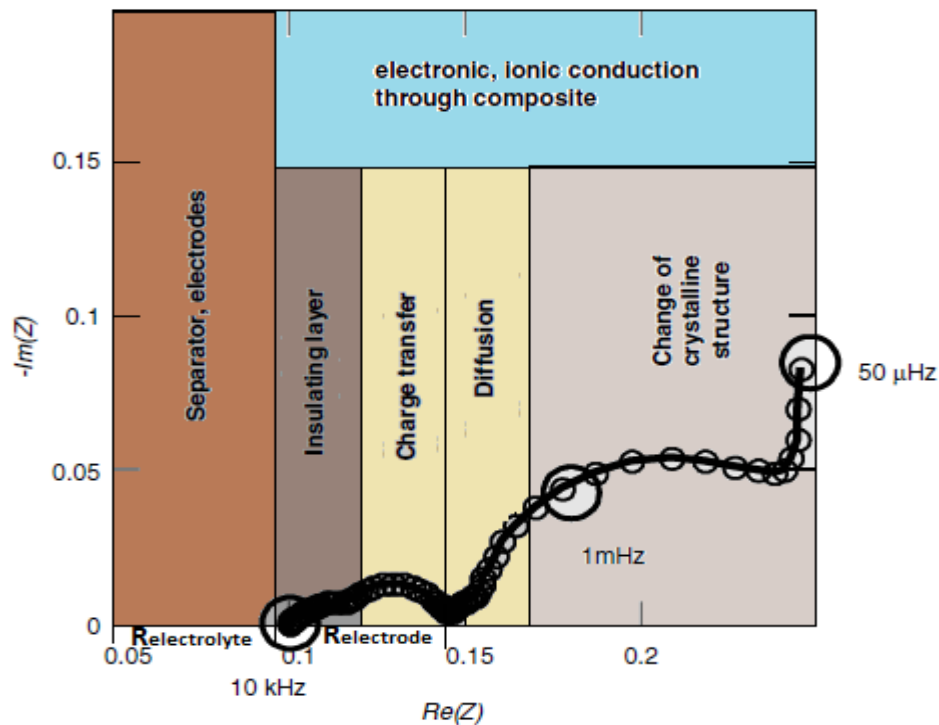


Figure 3.11 Typical impedance spectra of an intercalation material

To investigate the kinetics evolution of electrode process, electrochemical impedance spectroscopy is used to analyze the electrode impedance at different stages of lithium storage. The series of EIS spectra are analyzed by using the Z-plot software based on complex nonlinear least squares fitting. Impedance is represented as a complex quantity Z . In Cartesian form, $Z = R + jX$ where the real part of impedance is the resistance R and the imaginary part is the reactance X . The Nyquist plot (Z-plot) is used to encompass the processes including ion conductance in the electrolyte, electrochemical charge transfer, formation of double layer, diffusion inside the bulk and/or in the surface of active materials. At low frequency, the plot shows a well-developed diagonal line at an angle of 45° , indicative of Warburg impedance (Z_w). Nyquist complex plots representing impedance real (Z_{Real}) and imaginary ($Z_{\text{Imaginary}}$) are plotted at a capacity and a voltage representing a stage of lithium storage. Also resistance of electrode ($R_{\text{electrode}}$) and resistance of electrolyte ($R_{\text{electrolyte}}$) are plotted as a function of discharge capacity at each stage of lithium storage. The variation of electrolyte and electrode resistance is studied at each stage of lithium storage. $R_{\text{electrode}}$ point shown in the Figure 3.11 is considered approximate.

4. Synthesis and Li Storage Characteristics of GO

4.1 Chemical Synthesis of Graphene Oxide and Graphene

Graphene oxide and reduced graphene oxide (graphene) are chemically synthesized and tested as anode materials in lithium ion batteries. Various electrochemical studies are conducted on different anode samples to find the effect of temperature on the charge capacities and comparisons are made with the commercially available nano graphene platelets. The different graphene oxide anode samples with acronyms and description are provided in the Table 4.1.

Table 4.1 Graphene Oxide Anode Samples

S.No	Acronym	Anode sample
1	GO250	Graphene oxide heat treated at 250°C
2	RGO	Reduced graphene oxide
3	GO400	Graphene oxide heat treated at 400°C
4	NGP	Nano Graphene Platelets – Commercial Product

4.1.1 Chemical Synthesis of Graphene Oxide

Natural graphite powders (HPM 850) are oxidized to graphene oxide using a modified Hummers method. Graphene oxide is prepared in several batches and tested as anode materials in Lithium Ion batteries.

Below are the steps followed for chemical synthesis of graphene oxide using modified Hummer's method.

- One gram graphite powder and 0.5 g Sodium Nitrate is poured into 70 ml concentrated H_2SO_4 .
- Then 3 grams of potassium permanganate (KMnO_4) is gradually added.
- The mixture is thoroughly stirred for 5h and diluted with water.
- After 30 minutes, hydrogen peroxide (H_2O_2) is added to the solution until the color of the mixture changed to brilliant yellow.
- The obtained exfoliated graphite is placed on hot plate and heated at 150°C until it gets dried.
- The dried sample is heat treated at 250°C for 6 hours in air.
- Then the sample is washed thoroughly till the PH value of the solution turns to base.
- The sample is dried on a hot plate till the left over water is completely evaporated.
- The dried sample is again heat treated at 250°C for 6hrs in air.
- The heat treated sample is used for testing as anode material in lithium ion batteries.

4.1.2 Chemical Synthesis of Reduced Graphene oxide

Below are the steps followed in chemical synthesis of reduced graphene oxide using hydrazine reduction.

- 2 ml of hydrazine is added to 100 mg of graphene oxide obtained earlier and mixed homogeneously.
- The solution is heat treated at 100°C for 2 hours in the furnace.
- The heat treated sample is used for testing as anode material in lithium ion batteries.

4.2 Graphene Oxide – Electrochemical Characteristics

4.2.1 GO250

Figure 4.1 showed the charge-discharge profiles of electrodes prepared from graphene oxide heat treated at 250°C (GO250). The short plateau and slope observed in the vicinity of 1.0 V during the first discharge is associated to the electrolyte interaction of the functional groups on graphene sheets and the formation of solid electrolyte interface (SEI) film at the electrode/electrolyte interface[18]. Afterwards, in the GO250 charge/discharge curves, no distinguishable reversible plateaus are observed which can be attributed to the smaller crystal structure, high specific surface area and disorganized graphene stack, characteristic of non-graphitic carbons. The GO250 electrode exhibited a broad electrochemical window (0-3 V) as a function of lithium storage capacity and the large voltage hysteresis. The first discharge and charge capacities of GO250 are 1100 mAh/g and 706 mAh/g, respectively at an affordable charge/discharge efficiency of 72.5%. In the following ten cycles, an average columbic efficiency is over 95%.

Cycle performance of graphene oxide heat treated at 250°C at the current density of 50 $\mu\text{A}/\text{cm}^2$ is shown in Figure 4.2. The high irreversible capacity during first cycle

could be explained due to the formation of SEI layer in the nano cavities/defects. After 8 cycles the reversible capacity still maintains a 485 mAh/g for graphene oxide, which could be ascribed to the lithium storage on the both sides of the graphene surface and in the abundant micro pores and/or defects of graphene oxide. It can be suggested that graphene oxide possess the intensive potential as a candidate of anode materials with high reversible capacity and good cycle performance.

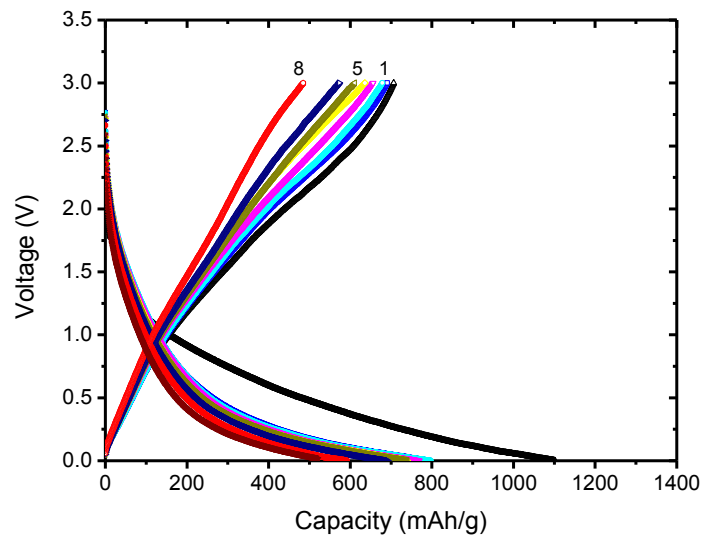


Figure 4.1 Discharge - charge profiles of Graphene Oxide synthesized at 250°C (GO250)

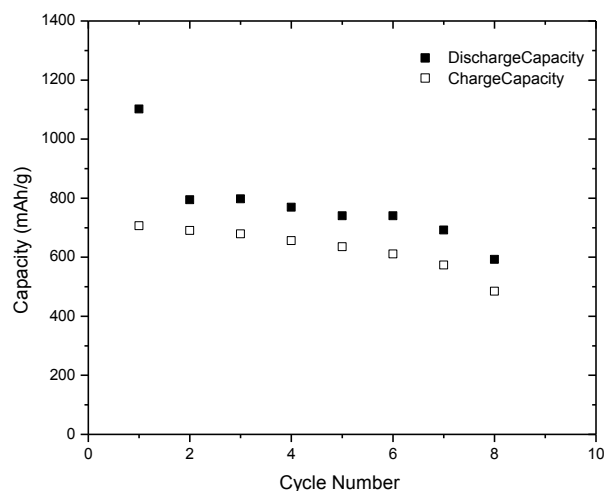


Figure 4.2 Cycle performance of Graphene Oxide synthesized at 250°C (GO250)

4.2.2 Reduction

Electrochemical studies conducted on reduced graphene oxide showed a distinguishable potential plateau in the first discharge curve at 1 V as shown in Figure 4.3. Plateau observed at 1 V can be attributed to the electrolyte decomposition and the formation of solid electrolyte interface (SEI) film at the electrode/electrolyte interface[18]. The first discharge and charge capacities of reduced graphene oxide are 708 mAh/g and 397 mAh/g respectively and showed an average columbic efficiency of 85% up to 10cycles. The capacity fade per cycle is 3.2% for 10 cycles. From the second cycle, no distinguishable plateaus are observed in charge/discharge curves similar to graphene oxide. The reduced graphene oxide electrode exhibit a broad electrochemical window (0-3 V) as a function of lithium capacity and the large voltage hysteresis, similar to non graphitic carbons is observed.

Figure 4.4 shows the capacity cycle graph of graphene oxide and reduced graphene oxide. It can be observed that the charge and discharge capacities of graphene oxide are much larger than those of reduced graphene oxide. This could be due to absence of oxygen containing functional groups in reduced graphene oxide. Lithium is absorbed on each side of the reduced graphene oxide sheet but not in the cavities and hydrogen terminated edges of the graphene fragments. This resulted in reduced capacities of the reduced graphene oxide when compared to the graphene oxide.

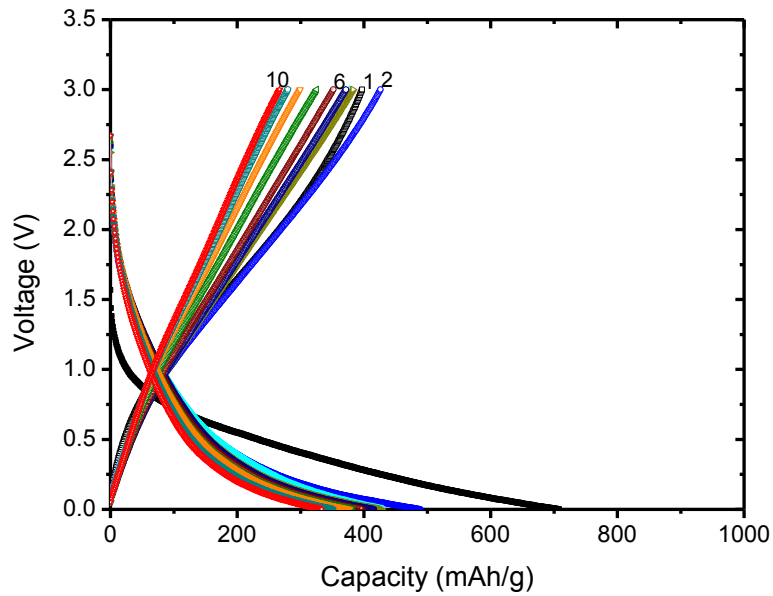


Figure 4.3 Discharge - charge profiles of reduced graphene oxide (RGO)

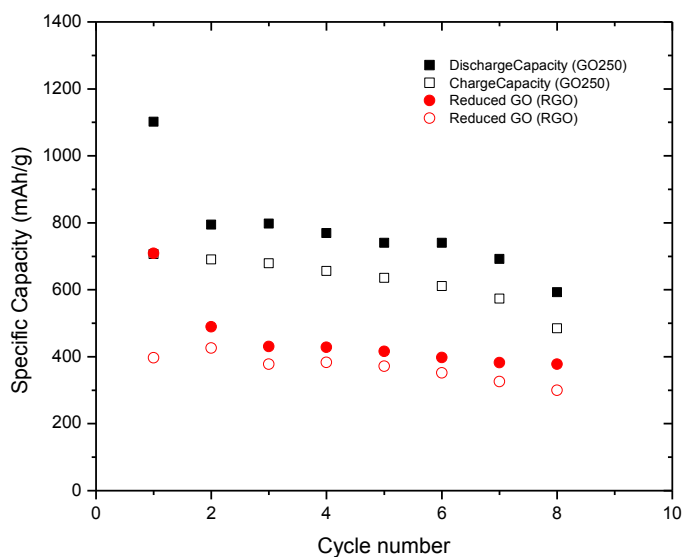


Figure 4.4 Cycle performance of reduced Graphene Oxide (RGO) and GO250

4.2.3 GO400

The charge-discharge profiles of graphene oxide heat treated at 400°C (GO400), were presented in Figure 4.5. Distinguished from GO250, populous lithium was stored in and removed from GO400 in the potential windows of 0.01 - 0.3V, characteristics of 3D stacked carbons. GO400 electrode delivered only capacity of 232 mAh/g in the first discharge and 200mAh/g in the second discharge. The low discharge capacities of GO400 is believed to be associated with the graphene layers stacked on top of each other into 3D structure as a consequence of heat treatment at 400°C. It is hypothesized that during the heating process at 400°C, the functional groups on the graphene sheets will interact and pin the sheets in three-dimension in random style, resulting in the so-called turbostratic misalignment structure. Consequently, the surface area decreased significantly. However, the thermal energy at this low temperature is far from sufficiency

to rotate of the pinning graphene sheets into the registered graphite stacking arrangement, desired for lithium intercalation/de-intercalation, caused the low lithium storage capacity. The above observation suggested that heat treatment of graphene oxide at elevated temperatures is inappropriate in the pursuit of high lithium storage capacity.

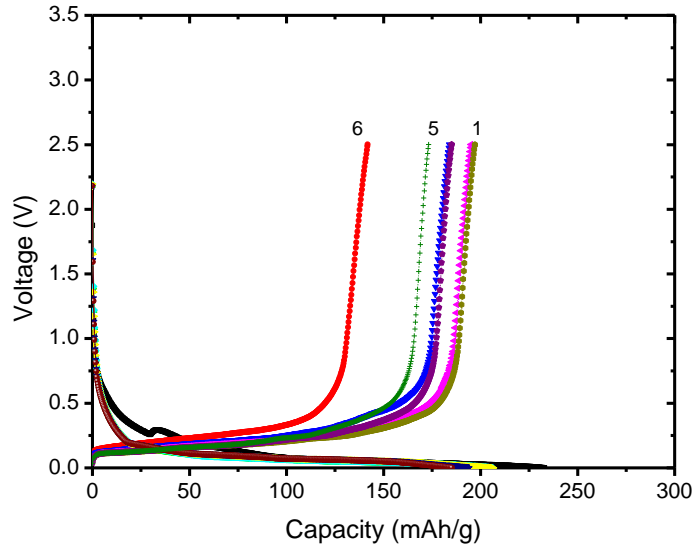


Figure 4.5 Discharge - charge profiles of GO thermally treated at 400°C (GO400)

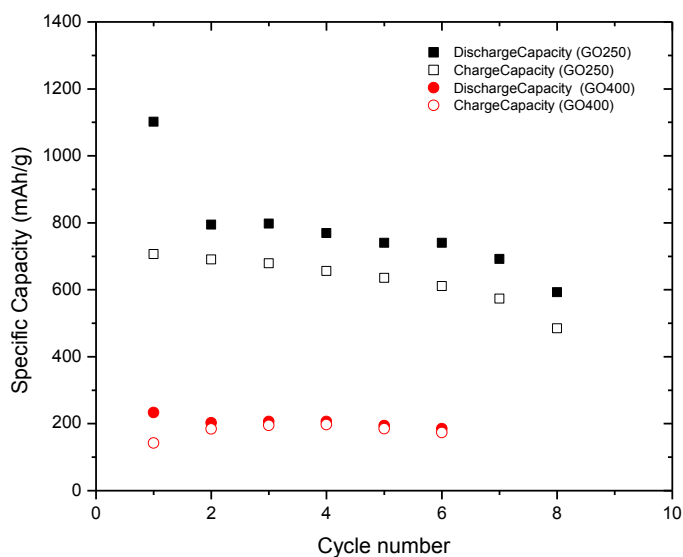


Figure 4.6 Cycle performance of Graphene Oxide synthesized at 400°C (GO400) and 250°C (GO250)

Figure 4.6 shows the capacity cycle graph of graphene oxide synthesized at 250°C and 400°C. It can be observed clearly that the charge and discharge capacities of graphene oxide synthesized at 400°C are much smaller than those of graphene oxide synthesized at 250°C.

4.2.4 NGP

The pristine NGPs were fabricated via low-cost wet intercalation followed by thermal shock, provided by Angstrom Materials [7, 64]. The extent of intercalation with a liquid agent was well-controlled to obtain large-batch NGPs with a narrow thickness distribution. A controlled-atmosphere furnace was used for thermal shock exfoliation and reduction at 900°C. The physical properties of the pristine NGPs such as particle distribution and BET surface area were quantized. NGPs had an in-plane dimension of up

to 300 nm and vertical dimension of 1-2 nm. Figure 4.7 exhibited Atomic Force Microscope (AFM) image of NGP, prepared by thermal shock followed by high-temperature hydrogen reduction. One folding monolayer graphene sheet was clearly visualized. The step height was measured approximately 0.39 nm. The slightly larger step height than the theoretically monolayer thickness 0.335 nm might have resulted from the gap between the top and bottom folded area.

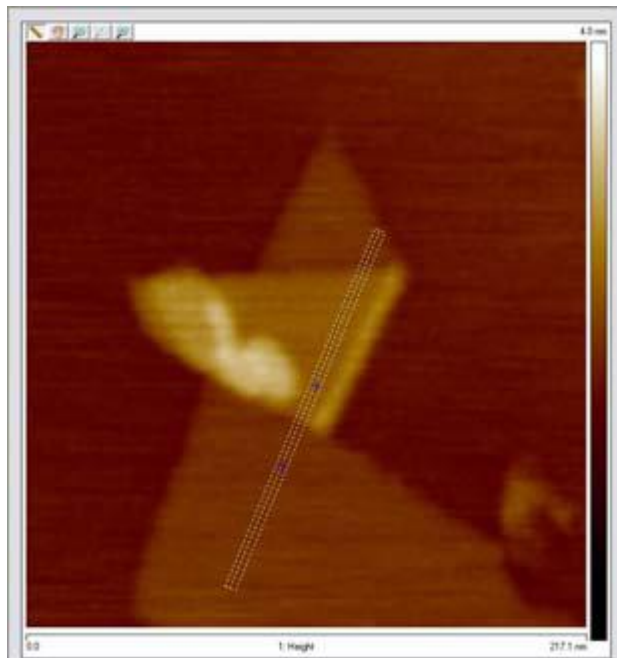


Figure 4.7 AFM image of the specimen NGP

Figure 4.8 showed the first discharge and charge (d/c) profile obtained on the pristine NGPs at a galvanostatic intermittent discharge/charge mode. The current density was $50 \mu\text{A}/\text{cm}^2$ and the current loading as well as intermittent rest time was 10 minutes. The first discharge capacity was 890 mAh/g and the charge capacity 560 mAh/g in average. Hence, the first charge/discharge columbic efficiency was 62%. Two

distinguished potential regions were observable in the d/c profile. The high potential region above 0.2V showed similar characteristics of lithium storage in the short single-wall nanotube. The low potential region below 0.2 V showed the typical characteristics of lithium intercalation in graphite. The electrochemical characteristic profile, together with AFM observations, indicates that NGP specimen was made up of mono layered and multilayered graphene nanosheets.

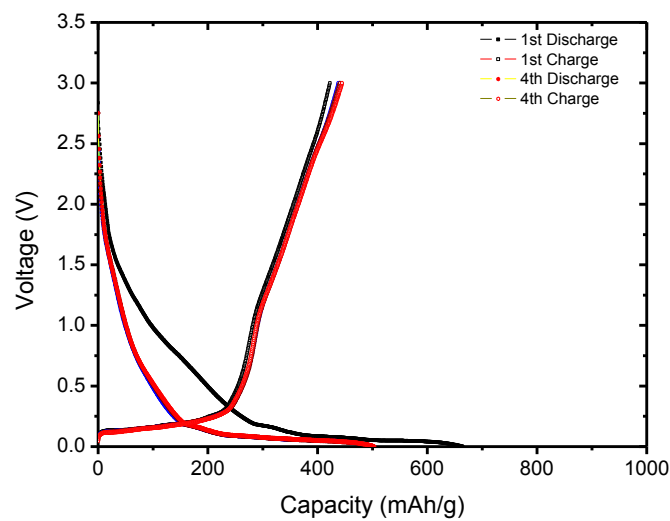


Figure 4.8 Discharge - charge profiles of Nano Graphene Platelets (NGP)

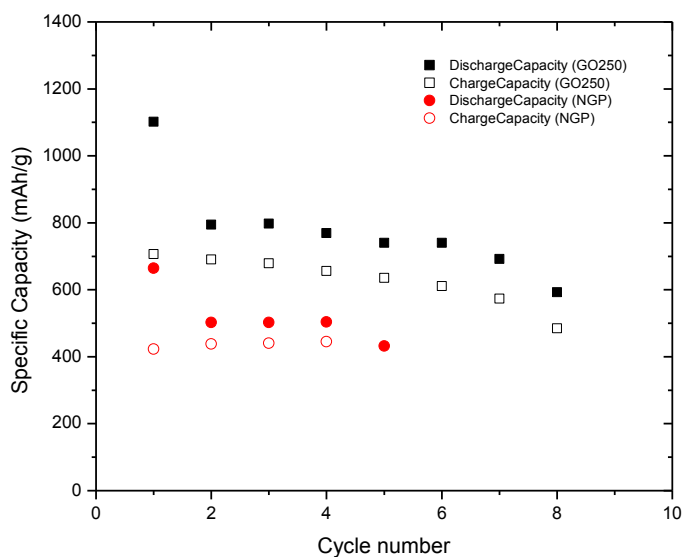


Figure 4.9 Capacity cycle performances of NGP and GO250

The NGP specimen was estimated to contain approximately 40 - 50% monolayer graphene based on the reversible capacity data, as well as the assumptions that lithium storage capacities in mono layered and multilayered graphene were 700 - 740 mAh/g and 320-360 mAh/g, respectively.

Figure 4.9 shows the capacity cycle graph of graphene oxide synthesized at 250°C and NGP. It can be observed clearly that the charge and discharge capacities of graphene oxide synthesized at 250°C are larger than those of NGPs. Annealing of NGPs at a high temperature of 900°C may have resulted in crystallization and reducing the surface area. This resulted in lower charge capacities when compared to GO250 sample.

4.3 Summary

Graphene oxide is chemically synthesized using modified hummers method. Several graphene oxide anode samples namely GO250, RGO, GO400, NGP are studied for their electrochemical performances. The electrochemical results of the anode samples are summarized in Table 4.2 below. Figure 4.10 shows the combined 2nd discharge and 1st charge profiles of all graphene oxide anode samples. Similarly, Figure 4.11 shows combined charge capacity cycle performances of all graphene oxide anode samples. It can be concluded that GO250 exhibited a relatively high reversible capacity of 706 mAh/g and fine cycle performance when compared to other anode samples, though there is large irreversible capacity during the first cycle due the formation of SEI layer. Also, all anode samples exhibited a large voltage hysteresis between the charge and discharge cycles which are characteristic of graphene based anodes.

In RGO anode sample, lithium is absorbed on each side of the reduced graphene oxide sheet but not in the cavities and hydrogen terminated edges of the graphene fragments resulting in reduced capacities. The low discharge capacities of GO400 is believed to be associated with the graphene layers stacked on top of each other into 3D structure as a consequence of heat treatment at 400°C. This resulted in less surface area for lithium intercalation. Similarly, low charge capacities of NGPs is due to annealing at a high temperature of 900°C may have resulted in crystallization and reducing the surface area. This resulted in lower charge capacities when compared to GO250 sample. From these studies, it can be suggested that graphene oxide heat treated at 250°C (GO250)

possess the intensive potential as a candidate of anode materials with high reversible capacity and fine cycle performance.

Table 4.2 Summary of Graphene Oxide Results

Anode Sample	Initial Discharge Capacity(mAh/g)	Initial Reversible Charge Capacity (mAh/g)	Second Discharge Capacity(mAh/g)	Second Reversible Charge Capacity (mAh/g)	1st Cycle Columbic Efficiency (1st charge/discharge)	2nd Cycle Columbic Efficiency (2nd charge/discharge)	Capacity Fade Per Cycle	nth Cycle Charge Capacity	No of Cycles
GO250	1102	706	794	690	64%	87%	3.9%	485	8
RGO	708	397	489	426	56%	87%	3.2%	267	10
GO400	232.9	142	202.4	184	60.5%	90.4%	-3.7%	173	6
NGP	664	422	502	438	63.5%	87.2%	-0.1%	445	4

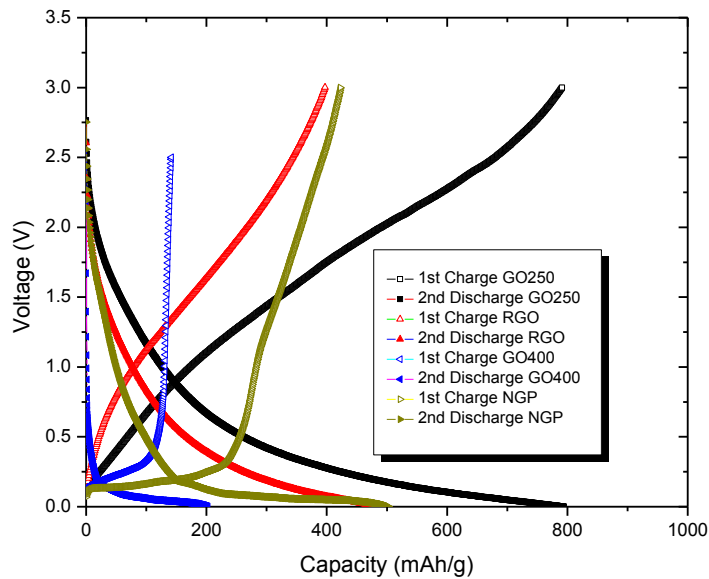


Figure 4.10 Combined discharge charge profiles of graphene oxide samples (GO250, RGO, GO400 and NGP)

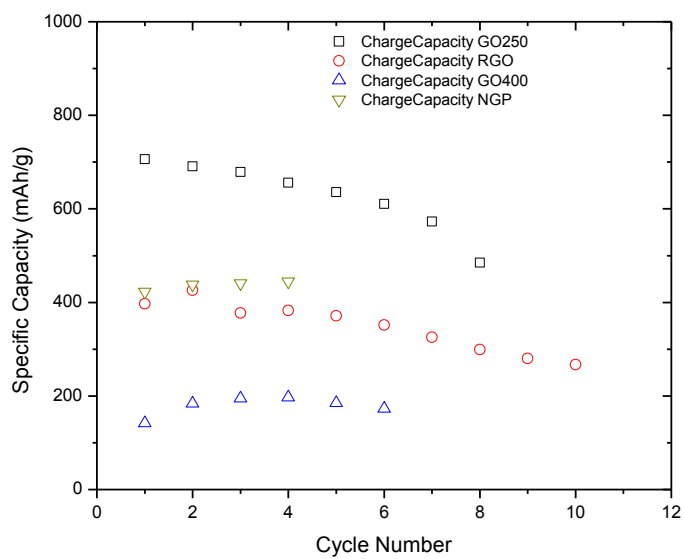


Figure 4.11 Combined charge capacity cycle performances of graphene oxide samples (GO250, RGO, GO400 and NGP)

5. Synthesis and Li Storage Characteristics of GO/MnAc

5.1 *Chemical Synthesis of GO/MnAc Composites*

In this research study, graphene oxide (GO250) and manganese acetate (MnAc) composites synthesized in different ways are studied for their electrochemical properties. The GO/MnAc composites are chemically synthesized in three different ways as described below.

Simple Method (SM): 50 mg of Graphene oxide and 50mg of Manganese acetate are mixed thoroughly and battery cells are prepared as defined in section 3.2. In addition, the battery cells are also prepared from the mixture heat treated at 400°C.

Liquid Method (LM): 50mg of manganese acetate is dissolved in water. To this, 50 mg of graphene oxide is added and mixed thoroughly. The mixture is heat treated in oven at 400°C for 6 hours. The residual powder is used in preparing the battery cells as defined in section 3.2

Solid Method (SDM): 150mg of manganese acetate is mixed in water. The mixture is heated on a hot plate at 150°C for 2hrs. The residual powder obtained is assumed to be in the form of MnO_x . 50mg of MnO_x is taken and mixed with 50mg of graphene oxide and heat treated at 500°C for 6hrs. The residual powder is used in preparing the battery cells as defined in section 3.2.

The different graphene oxide and manganese acetate composite anode samples with acronyms and description provided in the Table 5.1 are studied for their electrochemical performances.

Table 5.1 Graphene Oxide and Manganese Acetate Composite Anode Samples

S.No	Acronym	Anode Sample
1	GO/MnAc	Graphene oxide and Manganese acetate composite prepared through simple method
2	GO/MnAc-400	Graphene oxide and Manganese acetate composite prepared through simple method and heat treated at 400°C
	GO/MnAc-SM	
3	GO/MnAc-LM	Graphene oxide and Manganese acetate composite prepared through liquid method and heat treated at 400°C
4	GO/MnO _x -5050	Graphene oxide and Manganese acetate is mixed in ratio of 50:50, prepared through solid method and heat treated at 500°C.
5	GO/MnO _x -7525	Graphene oxide and Manganese acetate is mixed in ratio of 75:25, prepared through solid method and heat treated at 500°C.

5.2 Effect of Heat Treatment on Charge Capacities

The effect of heat treatment on the electrochemical charge capacities and cycle life of graphene oxide and manganese acetate composites has been studied. Two composite samples prepared through simple method are compared for their charge capacities at room temperature and at 400°C. Figure 5.1 shows charge-discharge curves of GO/MnAc composite electrodes synthesized at room temperature at a current density

of 50 mA/cm² between 0 and 3.0 V vs Li⁺/Li. The shape of the profiles is not significantly altered from 2 cycle onwards, indicating the stability of the composite as anode. There are no plateaus observed expect for the first cycle discharge curve. In discharge, the capacity over 0.5 V corresponds to the formation of Li₂O accompanying the reduction of transition metal particles. In addition, the capacity below 0.5 V can be attributed to lithiation of graphene [26] and/or a reversible polymerization of the electrolyte. Initial discharge capacity and charge capacity of 1104 mAh/g and 533 mAh/g with a coulombic efficiency of 48% is achieved. The large irreversible capacity during first cycle could be caused by the formation of the solid electrolyte interphase (SEI). However, after the first cycle, the GO/MnAc anode shows highly reversible behavior. The anode can retain a reversible capacity of 463 mAh/g with capacity fade per cycle of 1.8% after 7 cycles. However, large voltage hysteresis is observed between the charge and discharge cycles similar to graphene based anodes.

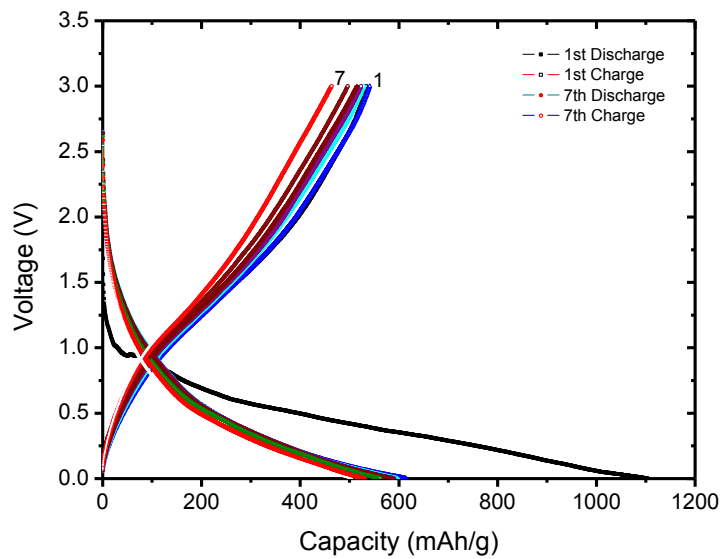


Figure 5.1 Discharge - charge profiles of GO and MnAc composite anode synthesized at room temperature through simple method (GO/MnAc)

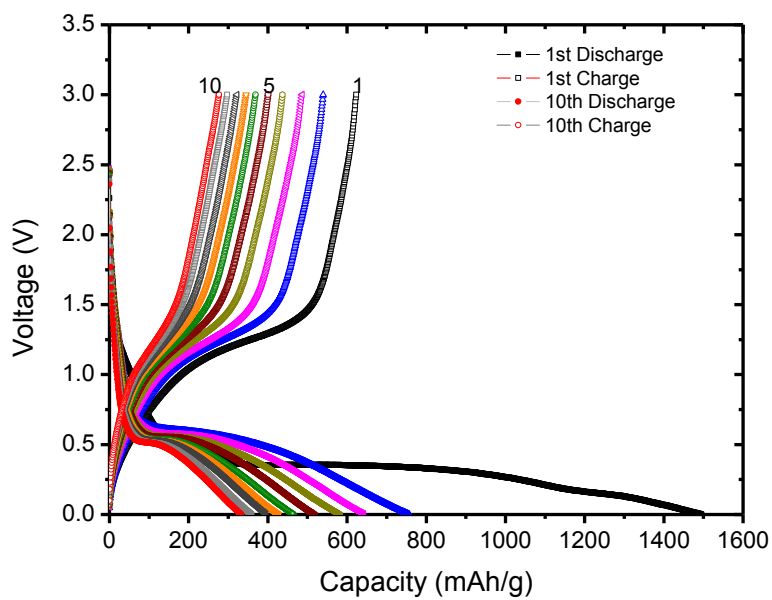


Figure 5.2 Discharge - charge profiles of GO and MnAc composite synthesized at 400°C temperature through simple method (GO/MnAc-400)

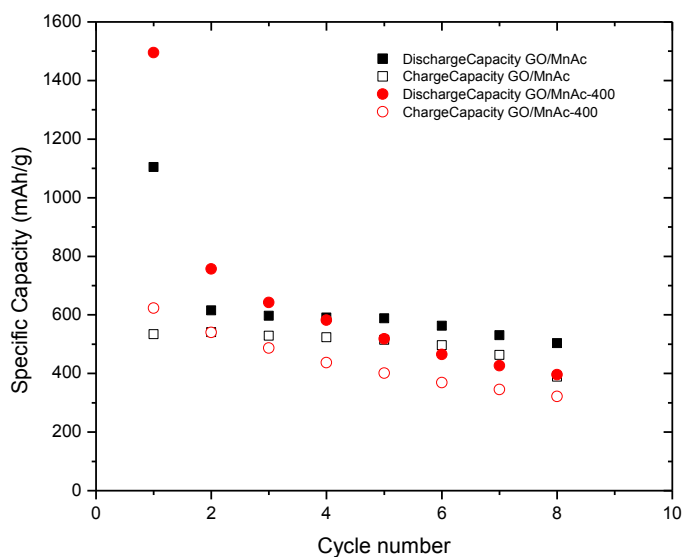


Figure 5.3 Capacity cycle performances of GO/MnAc and GO/MnAc-400

Figure 5.2 shows charge-discharge curves of GO/MnAc-400 composite electrodes synthesized at 400°C at a current density of 50 mA/cm² between 0 and 3.0 V vs Li⁺/Li. In discharge, plateau at 0.5V corresponds to the formation of Li₂O accompanying the reduction of transition metal particles. Initial discharge capacity and charge capacity of 1496 mAh/g and 622 mAh/g with a coulombic efficiency of 42% is achieved. The large irreversible capacity during first cycle could be caused by the formation of the solid electrolyte interphase (SEI). The voltage hysteresis between charge discharge cycles is less than the GO/MnAc anode sample, but the capacity fade per cycle is 5.56% which is higher than the 1.8% for GO/MnAc anode sample.

Figure 5.3 shows the capacity cycle graph of GO/MnAc and GO/MnAc-400 anode samples. As can be observed from the graph, the initial discharge capacity of 1496 mAh/g for GO/MnAc-400 is larger than the 1104 mAh/g for GO/MnAc, but GO/MnAc-

400 shows larger capacity fade per cycle. This may be due to the particles are swollen due to heat treatment and particle strength is reduced during repeated lithiation and delithiation process, thereby increasing the capacity fade per cycle. On the other side, GO/MnAc maintains the charge capacities with very little capacity fade of 1.8 % per cycle.

5.3 Effect of Mixing Methods on Charge Capacities

The effect of mixing method followed in the chemical synthesis of GO/MnAc composite anodes on the electrochemical charge capacities and cycle life has been studied. Composite samples of GO/MnAc-SM synthesized through simple method heat treated at 400°C and GO/MnAc-LM synthesized through liquid method heat treated at 400°C are compared.

Figure 5.4 for charge- discharge curves of GO/MnAc-SM composite electrodes synthesized through simple method heat treated at 400°C at a current density of 50 mA/cm² between 0 and 3.0 V vs Li⁺/Li. In discharge, plateau at 0.5V corresponds to the formation of Li₂O accompanying the reduction of transition metal particles. Initial discharge capacity and charge capacity of 1496 mAh/g and 622 mAh/g with an initial cycle coulombic efficiency of 42% is achieved. The large irreversible capacity during first cycle could be caused by the formation of the solid electrolyte interphase (SEI). The capacity fade per cycle is high which is 5.56 % up to 10 cycles.

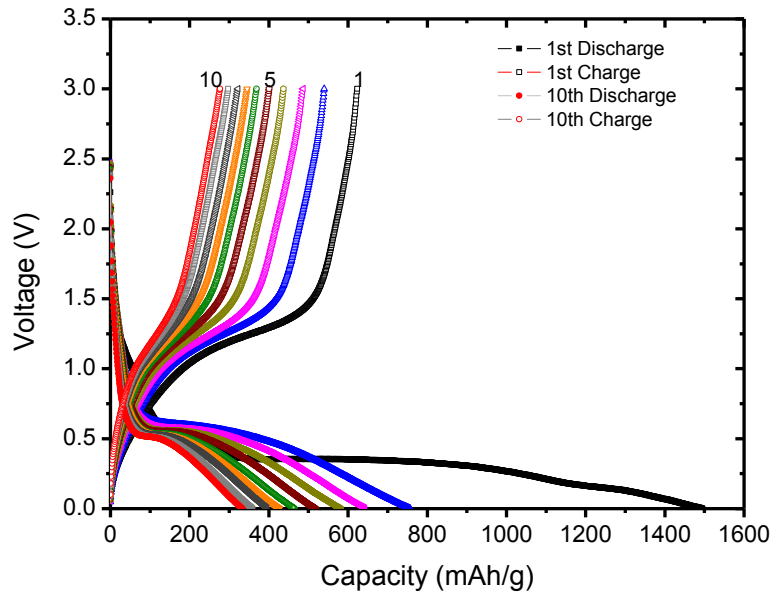


Figure 5.4 Discharge - charge profiles of GO/MnAc-SM composite synthesized at 400°C through simple method

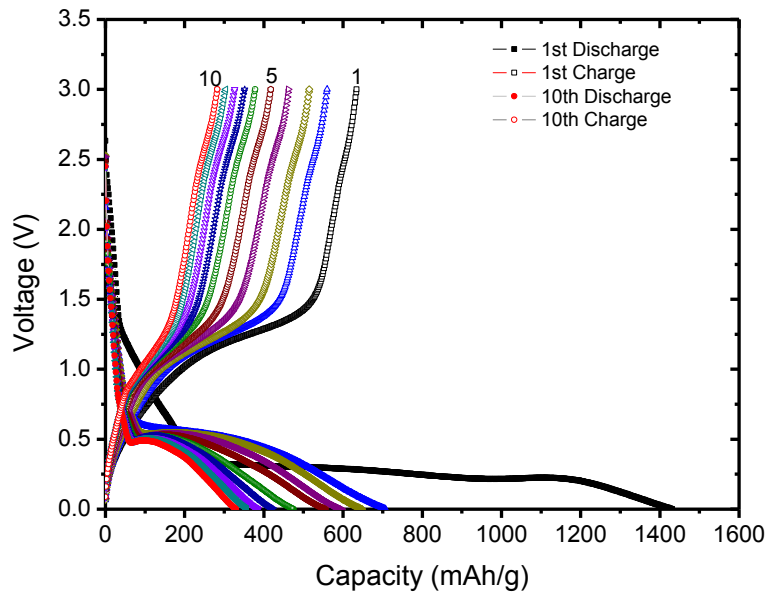


Figure 5.5 Discharge - charge profiles of GO/MnAc-LM composite synthesized at 400°C through liquid method

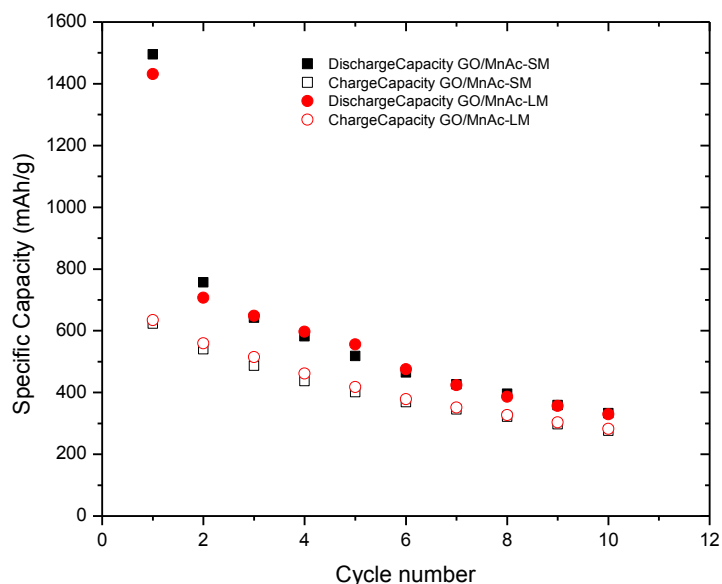


Figure 5.6 Capacity cycle performances of GO/MnAc-SM and GO/MnAc-LM

Figure 5.5 shows charge-discharge curves of GO/MnAc-LM composite electrodes synthesized through liquid method heat treated at 400°C at a current density of 50 mA/cm² between 0 and 3.0 V vs Li⁺/Li. In discharge, plateau at 0.5V corresponds to the formation of Li₂O accompanying the reduction of transition metal particles. In addition, the capacity below 0.5 V can be attributed to lithiation of graphene. Initial discharge capacity and charge capacity of 1431 mAh/g and 634 mAh/g with a coulombic efficiency of 45% almost same as that of GO/MnAc-SM are achieved. Similarly, there is large capacity fade per cycle of 4.46% which is almost same as that of the GO/MnAc-SM composite sample. Figure 5.6 shows the capacity cycle graph of GO/MnAc-SM and GO/MnAc-LM anode samples. As can be observed from the graph, the initial charge and discharge capacities are almost same for both the composite anodes. Also, both the

composite anode samples show large capacity fade per cycle. This shows there is no effect of the chemical synthesis method on the electrochemical behavior of GO/MnAc composite anodes at 400°C.

5.4 Effect of GO and MnO_x Composition Ratio on Charge Capacities

The effect of composition of GO/MnO_x composite anodes on the electrochemical charge capacities and cycle life has been studied. In this research study, composite samples of GO/MnO_x-5050 synthesized through solid method heat treated at 500°C and GO/MnO_x-7525 synthesized through solid method heat treated at 500°C are compared.

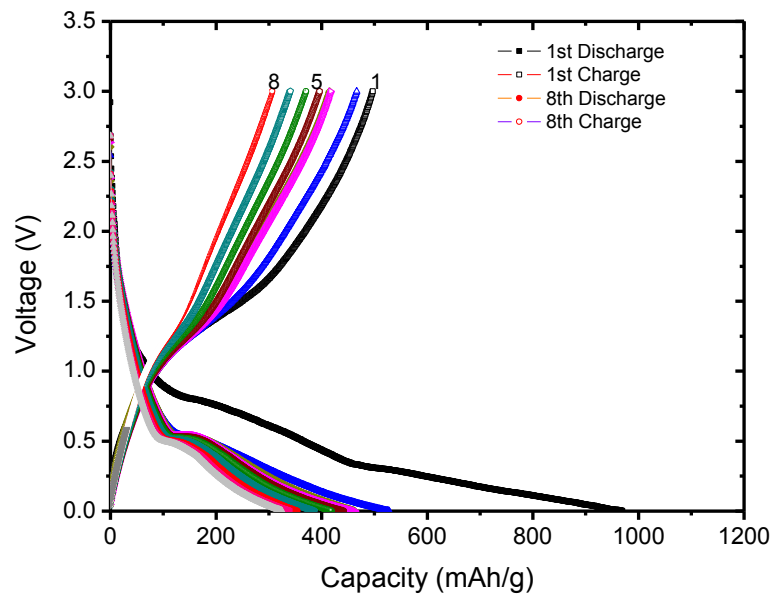


Figure 5.7 Discharge - charge profiles of GO/MnO_x-5050 composite synthesized at 500°C through solid method

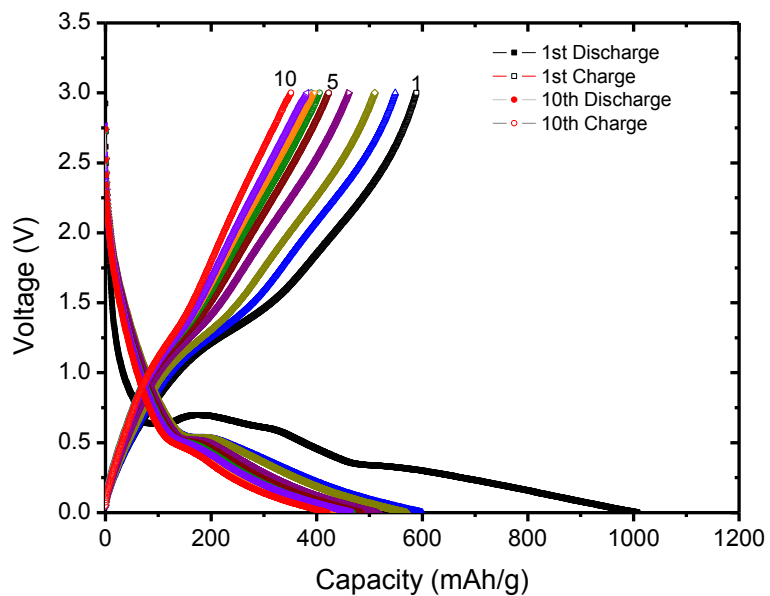


Figure 5.8 Discharge - charge profiles of GO/MnOx-7525 composite synthesized at 500°C through solid method

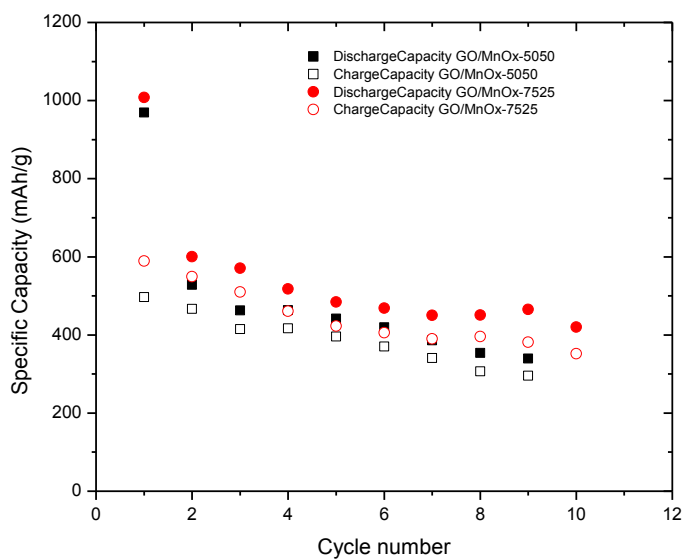


Figure 5.9 Capacity cycle performances of GO/MnOx-5050 and GO/MnOx-7525

Figure 5.7 shows charge-discharge curves of GO/MnO_x-5050 composite electrodes synthesized through solid method heat treated at 500°C at a current density of 50 mA/cm² between 0 and 3.0 V vs Li⁺/Li. In discharge, the plateau observed at 0.5 V corresponds to the formation of Li₂O accompanying the reduction of transition metal particles. The plateaus are clearly visible when water is used during chemical synthesis of the composite anode. In addition, the capacity below 0.5 V can be attributed to lithiation of graphene [26] and/or a reversible polymerization of the electrolyte. Initial discharge capacity and charge capacity of 970 mAh/g and 497 mAh/g with a coulombic efficiency of 52% is achieved. The large irreversible capacity during first cycle could be caused by the formation of the solid electrolyte interphase (SEI). However, after the first cycle, the GO/MnO_x-5050 anode shows highly reversible behavior. The anode can retain a reversible capacity of 295 mAh/g after 9 cycles and shows large capacity fade per cycle of 4.51%. And also, large voltage hysteresis is observed between the charge and discharge cycles similar to graphene based anodes.

Figure 5.8 shows charge-discharge curves of GO/MnO_x-7525 composite electrodes synthesized through solid method heat treated at 500°C at a current density of 50 mA/cm² between 0 and 3.0 V Vs Li⁺/Li. In discharge, the similar plateau is observed at 0.5 V corresponds to the formation of Li₂O accompanying the reduction of transition metal particles. Initial discharge capacity and charge capacity of 1008 mAh/g and 600 mAh/g with a coulombic efficiency of 58% is achieved. The large irreversible capacity during first cycle could be caused by the formation of the solid electrolyte interphase (SEI). The anode can retain a reversible capacity of 351 mAh/g after 10 cycles and shows

large capacity fade per cycle of 4.03%. And also, large voltage hysteresis is observed between the charge and discharge cycles similar to graphene based anodes.

Figure 5.9 shows the capacity cycle graph of GO/MnO_x-5050 and GO/MnO_x-7525 anode samples. As can be observed from the graph, the initial charge/discharge capacities, coulombic efficiency and capacity fade per cycle of GO/MnO_x-7525 composite are slightly better than GO/MnO_x-5050 composite anodes. This improved performance may be due to higher composition of graphene oxide leading to higher lithium intercalation and better charge capacities. This show with increase in graphene oxide content, the anode electrode shows better electrochemical performance. Even though anode electrodes consists of transition metal oxides(MnO_x), the contribution to charge capacities from Li-alloying process, involving the formation and decomposition of Li₂O is limited due to the large particle size of the transition metals. The use of transition-metal nanoparticles might enhance surface electrochemical reactivity and will lead to further improvements in the performance of lithium-ion batteries. In the following chapter, graphene oxide and manganese oxide nano composite is chemically synthesized and studied for their electrochemical performance.

5.5 Summary

Graphene oxide and manganese acetate composite anode samples are synthesized using simple, liquid and solid method. Several composite anode samples namely GO/MnAc, GO/MnAc-400, GO/MnAc-SM, GO/MnAc-LM, GO/MnO_x-5050 and GO/MnO_x-7525 are studied for their electrochemical performances. The electrochemical results of the composite anode samples are summarized in Table 5.2 below. Figure 5.10

shows the combined 2nd discharge and 1st charge profiles of all graphene oxide and manganese acetate composite anode samples. Similarly, Figure 5.11 shows combined charge capacity cycle performances of all graphene oxide and manganese acetate composite anode samples.

Though the initial discharge capacities of 1496 mAh/g for GO/MnAc-400 and 1431 mAh/g for GO/MnAc-LM anode samples heat treated at 400°C is larger than the 1104 mAh/g observed for GO/MnAc, but the heat treated samples shows larger capacity fade per cycle. This may be due to the particles are swollen due to heat treatment and particle strength is reduced during repeated lithiation and de-lithiation process, thereby increasing the capacity fade per cycle. The composite anode samples heat treated at 500°C (GO/MnO_x-5050 and GO/MnO_x-7525) also show large capacity fade per cycle. This confirms that the heat treatment at higher temperature degrades the capacity cycle life of the composite anode. On the other side, GO/MnAc maintains the charge capacities with very little capacity fade of 1.8 % per cycle.

The initial charge and discharge capacities, capacity cycle behavior of GO/MnAc-SM and GO/MnAc-LM are almost same for both the composite anodes. Also, both the composite anode samples show large capacity fade per cycle. This shows there is no effect of the chemical synthesis method on the electrochemical behavior of GO/MnAc-SM and GO/MnAc-LM composite anodes heat treated at 400°C.

The effect of composition of graphene oxide to manganese oxide on electrochemical performance is studied using GO/MnO_x-5050 and GO/MnO_x-7525 anode samples. GO/MnO_x-7525 shows an initial reversible capacity of 589 mAh/g, larger than

497 mAh/g observed for GO/MnO_x-5050. Similarly, GO/MnO_x-7525 exhibited a better capacity cycle behavior when compared to GO/MnO_x-5050. This improved performance may be due to higher composition of graphene oxide leading to higher lithium intercalation and better charge capacities. This show with increase in graphene oxide content, the anode electrode shows better electrochemical performance.

From these studies, it can be observed that the graphene oxide and manganese acetate composite anode (GO/MnAc) showed better capacity cycle behavior than other anode samples. It can be suggested that GO/MnAc composite anode possess the intensive potential as a candidate of anode materials with high reversible capacity and fine cycle performance

Table 5.2 Summary of Graphene Oxide and Manganese Acetate Composite Results

Anode Sample	Heat Treatment at °C	Initial Discharge Capacity(mAh/g)	Initial Reversible Charge Capacity (mAh/g)	Second Discharge Capacity(mAh/g)	Second Reversible Charge Capacity (mAh/g)	1st Cycle Columbic Efficiency (1st charge/discharge)	2nd Cycle Columbic Efficiency (2nd charge/discharge)	Capacity Fade Per Cycle	nth Cycle Charge Capacity	No of Cycles
GO/MnAc		1104	533	615	540	48%	88%	1.8%	463	7
GO/MnAc-400	400	1496	622	756.7	539.6	41.6%	71.3%	5.6%	276	10
GO/MnAc-SM	400									
GO/MnAc-LM	400	1431	634.4	707	559.6	44.3%	79.2%	5.5%	283	10
GO/MnO _x -5050	500	969.5	496.7	528	466.4	51.2%	88.3%	4.51%	295	9
GO/MnO _x -7525	500	1008	588.9	600	549	58.4%	91.5%	4.03%	351	10

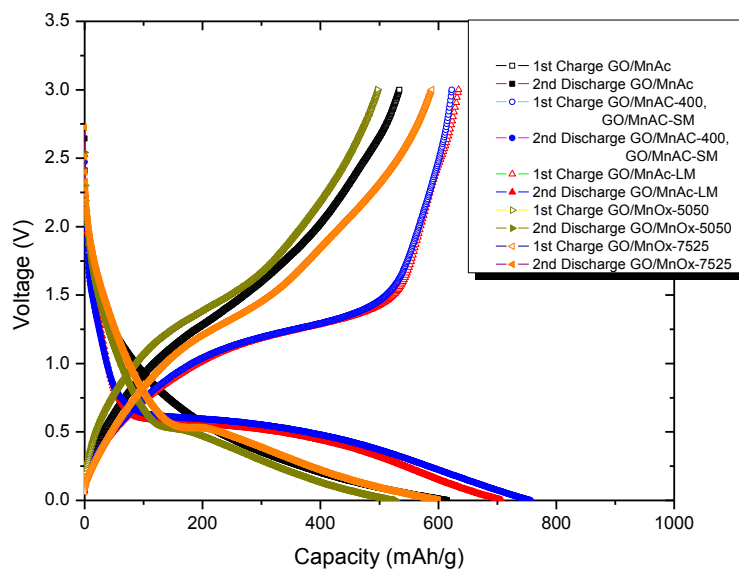


Figure 5.10 Combined discharge charge profiles of graphene oxide and manganese acetate composite samples (GO/MnAc, GO/MnAc-400, GO/MnAc-SM, GO/MnAc-LM, GO/MnO_x--5050 and GO/MnO_x--7525)

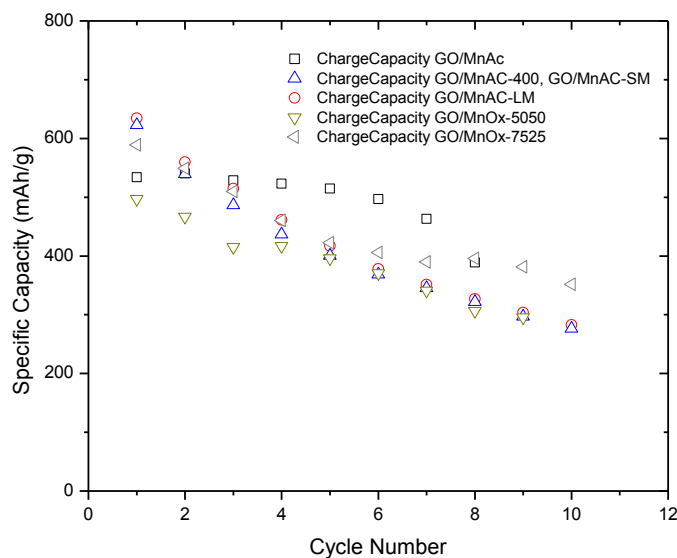


Figure 5.11 Combined charge capacity cycle performances of graphene oxide and manganese acetate composite samples (GO/MnAc, GO/MnAc-400, GO/MnAc-SM, GO/MnAc-LM, GO/MnO_x-5050 and GO/MnO_x-7525)

6. Synthesis and Li Storage Characteristics of GO/MnO_x

6.1 Chemical Synthesis of GO/MnO_x - Nano Composites

GO/MnO_x nanocomposite was prepared in the following procedure. Manganese acetate (Aldrich) and graphene oxide was taken in the weight ratio of 72:28, resulting in the hybrid of MnO_x and GO in the weight ratio of 58 over 42. Firstly, graphene oxide was kept in water under ultrasonication and manganese acetate solution was added and stirred for 2 hours. Secondly, ammonium hydroxide and hydrazine were added to the mixture and stirring was continued for 3 hours at the 100°C. Thirdly, the mixture was filtered and dried at 150°C [65]. The residual powder is used in preparing the battery cells as defined in section 3.2. In this research study, the electrochemical performance of GO/MnO_x nano composite is studied. The different GO/MnO_x nano composite anode samples with acronyms and description provided in the Table 6.1 are studied for their electrochemical performances.

Table 6.1 Graphene Oxide and Manganese Acetate Composite Anode Samples

S.No	Acronym	Anode Sample
1	GO/MnO _x	Nano composite
2	GO/MnAc	Graphene oxide and Manganese acetate composite prepared through simple method as defined in chapter 5
3	GO/MnO _x -250	Nano composite heat treated at 250°C in air.
4	GO/MnO _x -400	Nano composite heat treated at 400°C in air.
	GO/MnO _x -Air	
5	GO/MnO _x -Inert	Nano composite heat treated at 400°C in inert atmosphere.

6.2 GO/MnO_x Nano Composite vs. GO/MnAc Composite

Figure 6.1 exhibited the charge-discharge profiles of prepared graphene oxide and manganese oxide nano composite anode -GO/MnO_x. The first discharge capacity is 1325 mAh/g based on the total mass of the active materials. The capacity in the voltage range above 0.5 V was mostly correlated to the irreversible reaction between Li and GO as well as decomposition of the electrolyte forming the solid electrolyte interphase (SEI).

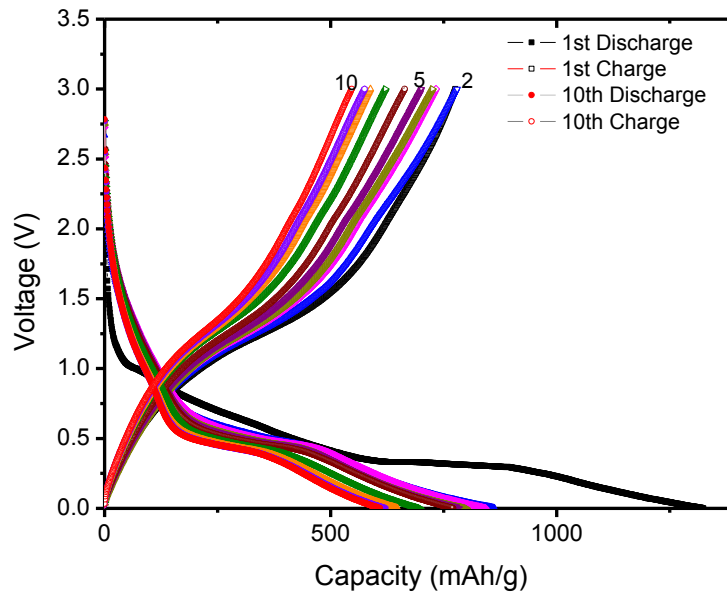


Figure 6.1 Discharge - charge profiles of GO/MnO_x

It is interesting to observe a long plateau at around 0.4V in the GO/MnO_x in the discharge profile, distinguished from that in GO. The plateau reflected the displacement reaction between Li and manganese oxide, which can be expressed in the following general reaction:



Accordingly, one mole of MnO reacts with 2 moles of Li resulting MnO can theoretically deliver charge capacity of 756 mAh/g. Increase the valency of manganese in the oxide, e.g. Mn₃O₄ and MnO₂, can theoretically increase capacity of 936 mAh/g and 1232 mAh/g, respectively. Capacity below the 0.4 V plateau is the sum lithium storage in graphene oxide and reduction from manganese (II) and Mn (0) [27]. The reverse reaction corresponding to Mn oxidation occurs mainly in the range of 1.0 to 1.5V. These characteristics corroborated well with what was observed by Pasero et al in Co-doped Mn₃O₄ (Mn_{2.6}Co_{0.4}O₄) prepared by solid state synthesis. It is also interesting to note that from the second discharge cycle the discharge reduction plateau shift upwards to ~ 0.6 V, also consistence to the value observed in Mn_{2.6}Co_{0.4}O₄. This reversible lithium storage potential value vs. Li is advantageous over other common anode materials, i.e. carbon (less than 0.2V), Si composite (average 0.35V), and Li₄Ti₅O₁₂ (1.6V). The operating voltage is suitable to prevent the possibility of metallic lithium resulting from over discharge and high-rate discharge, as occurred in carbon or Si-base anode, without no significant sacrifice of the voltage and hence, energy, as observed in titanate anode.

The reversible discharge capacities after the first discharge is 863 mAh per total mass of active materials, i.e. GO and Mn₃O₄. The composition of GO/ Mn₃O₄ composite is 58 weight percent of Mn₃O₄ to 42 weight percent of GO. Based on the GO capacity in the second discharge is 800mAh/g (see Figure 4.1), it is calculated the reversible capacity of lithium storage in Mn₃O₄ is 900mAh/g. This value is two-three times higher than that reported in Mn₃O₄ and Mn_{2.6}Co_{0.4}O₄, close to the theoretical value of 936mAh/g. It was stated that the electronic conduction was enhanced due to the presence of mixed valence Co and Mn, thereby facilitating the redox reactions involved. In the prepared GO/ Mn₃O₄,

the electronic conductance is significantly enhanced by the GO sheet supporter in comparison to the cobalt doping. The enhanced electronic conductance also significantly increased the kinetics of Mn_3O_4 reduction leading to the dramatic increase of reversible capacity. After the first cycle, the GO/ MnO_x specimen showed highly reversible behavior with average coulombic efficiency of 95% in the following cycles.

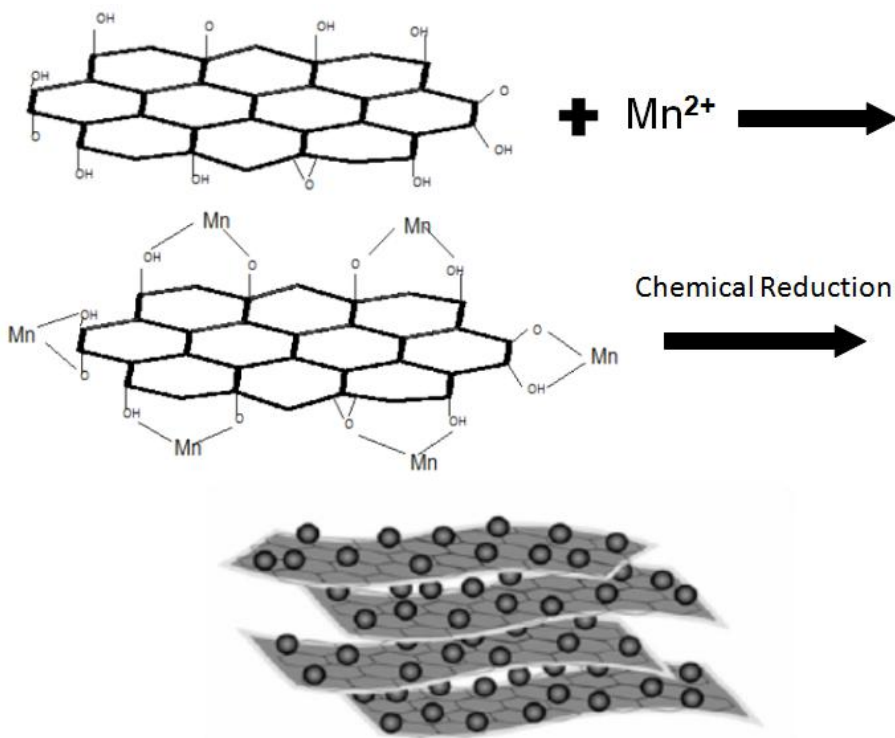


Figure 6.2 Schematic diagram of the synthesis of the Graphene oxide/ MnO_x nanocomposite with a 3D architecture

It is believed that the high reversibility of the GO/ MnO_x nanocomposite is due to its unique 3D nanostructure where manganese oxide nanoparticles are supported and separated by the graphene oxide layers. Figure 6.2 is a schematic diagram of the nanocomposite, showing the homogeneous distribution of the Mn nanoparticles on the graphene oxide nanosheets. Graphene oxide layers act as buffer to mitigate the large

volume change of manganese oxide in the charge/discharge process. The use of manganese oxide nanoparticles can also contribute to a reduction of the large volume changes during the reaction and also enable electrochemical reduction of Li_2O during charge process. The stability of the electrode is further improved by manganese oxide nanoparticles being prevented from aggregation by graphene oxide layers. The manganese oxide nano-particles are bound to graphene oxide layers in cavities formed due its crumpled and corrugated structure and also aggregation of manganese oxide nano particles is prevented by the graphene layer during the charge/discharge process. Similarly, the graphitization of graphene is prohibited by the nano particles present between the graphene layers. The 3D nano structure of graphene oxide layers separated by manganese oxide nano particles greatly enhance the electrochemical performance of the electrode, especially the conversion reaction materials that generally suffer from large volume change and low electronic conductivity [65]. The nanostructure using a graphene framework can be more widely applied to other promising conversion reaction electrodes to enhance their electrochemical activities.

Figure 6.3 shows charge-discharge curves of GO/MnAc composite electrodes synthesized at room temperature at a current density of 50 mA/cm^2 between 0 and 3.0 V vs Li^+/Li . The shape of the profiles is not significantly altered from 2 cycle onwards, indicating the stability of the composite as anode. There are no plateaus observed expect for the first cycle discharge curve. In discharge, the capacity over 0.5 V corresponds to the formation of Li_2O accompanying the reduction of transition metal particles. In addition, the capacity below 0.5 V can be attributed to lithiation of graphene [26] and/or a reversible polymerization of the electrolyte. Initial discharge capacity and charge

capacity of 1104 mAh/g and 533 mAh/g with a coulombic efficiency of 48% is achieved. The large irreversible capacity during first cycle could be caused by the formation of the solid electrolyte interphase (SEI). However, after the first cycle, the GO/MnAc anode shows highly reversible behavior. The anode can retain a reversible capacity of 463 mAh/g with capacity fade per cycle of 1.8% after 7 cycles. However, large voltage hysteresis is observed between the charge and discharge cycles similar to graphene based anodes.

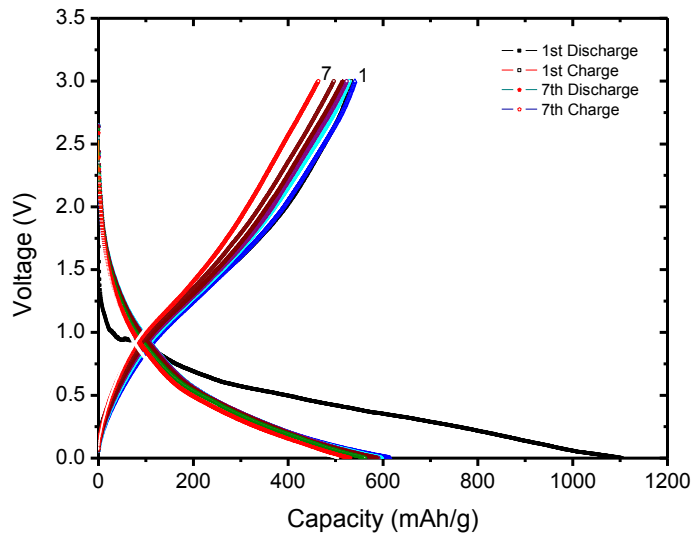


Figure 6.3 Discharge - charge profiles of GO/MnAc composite synthesized at room temperature

Figure 6.4 shows the capacity cycle graph of GO/MnO_x and GO/MnAc composite anode samples. The initial discharge and charge capacities of 1325 mAh/g and 776 mAh/g are observed for GO/MnO_x respectively, which are larger than the initial discharge and charge capacities of 1104 mAh/g and 533 mAh/g observed for GO/MnAc. The first cycle coulombic efficiency of 59% is achieved for GO/MnO_x nano composite

anode sample which is better than the first cycle coulombic efficiency of 48% achieved for GO/MnAc anode sample. These large capacities observed in GO/MnO_x nano composite anode sample is due to the chemical synthesis treatment resulting in uniform distribution of manganese oxide particles between the graphene layers as shown in figure 6.2. The particle sizes obtained is also comparatively smaller than using the normal mixing method used for GO/MnAc anode sample. During lithium insertion and extraction, the particle sizes in GO/MnO_x nano composite anode sample are further reduced leading to higher charge capacities. This explains why the second charge capacity of 780 mAh/g is higher than the first charge capacity of 776 mAh/g. The charge capacities in GO/MnO_x nano composite anode sample are contributed via lithium insertion in graphene layers and lithium displacement of MnO_x particles in the ratio of its composition of graphene oxide and manganese oxide as shown in the below equation. The MnO_x particles are considered to be in amorphous form in the nano composite sample. In order to estimate the contribution of MnO_x to the charge capacity of GO/MnO_x nano composite anode, the charge capacity of GO is subtracted from the charge capacity of GO/MnO_x. GO (theoretical capacity 744mAh/g) with 22% ratio in nano composite contributed a capacity of 164mAhg. GO/MnO_x nano composite delivered a total charge capacity of 776mAh/g. So it can be concluded that MnO_x delivered a charge capacity of 612mAh/g. GO/MnAc maintains the charge capacities with very little capacity fade of 1.8 % per cycle when compared to 2.9 % capacity fade per cycle for GO/MnO_x anode sample. In further analysis, GO/MnO_x anode samples heat treated at 250° and 400° are studied.

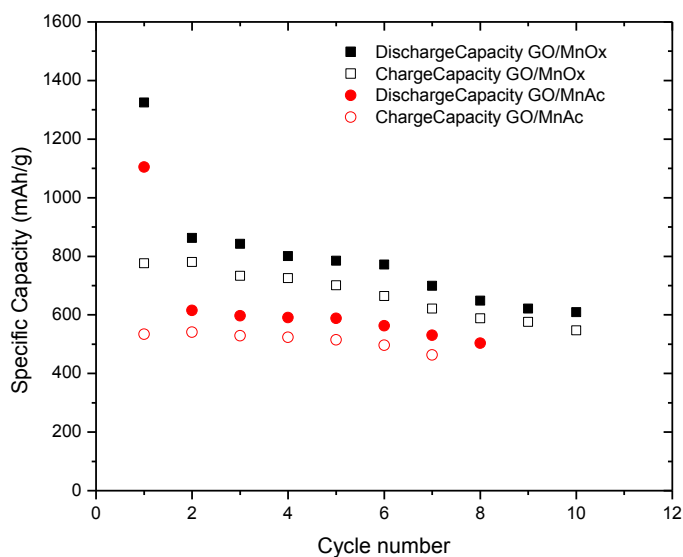


Figure 6.4 Capacity cycle performance of GO/MnO_x nano composite and GO/MnAc composite

6.3 Effect of Heat Treatment on Charge Capacities

6.3.1 At Different Temperatures

The effect of heat treatment on the electrochemical charge capacities and cycle life of graphene oxide and manganese oxide nano composites has been studied. Two nano composite samples prepared through chemical synthesis are compared for their charge capacities at 250°C and at 400°C. The aim of the heat treatment is to crystallize the anode samples and study the effect of crystallization on the electrochemical behavior of the anode samples.

Figure 6.5 shows charge-discharge curves of GO/MnO_x-250 nano composite electrodes synthesized at 250°C at a current density of 50 mA/cm² between 0 and 3.0 V

vs. Li^+/Li and tested up to 5 cycles. There is weight reduction in the anode sample due to heat treatment at 250°C . The weight of the sample used before the heat treatment is 150mg and sample weight after the heat treatment is 110mg showing a weight reduction of 27%. This shows that considerable amount of graphene oxide and to certain extent manganese oxide is combusted. The shape of the profiles is not significantly altered from 2 cycles onwards, indicating the stability of the composite as anode. In discharge, the plateau observed at 1.4V corresponds to the formation of $\text{Li}_\delta\text{MnO}_x$ compound and the plateau observed at 0.4 V corresponds to the formation of Li_2O , both the reactions accompanying the reduction of transition metal particles. In addition, the capacity below 0.4 V can be attributed to lithiation of graphene [26] and/or a reversible polymerization of the electrolyte. In charge cycle, the plateau observed at 1.5V corresponds to reduction of Li_2O accompanying the oxidation of transition metal particles. Initial discharge capacity and charge capacity of 1765 mAh/g and 718mAh/g with a coulombic efficiency of 41% is achieved. The large irreversible capacity during first cycle could be caused by the formation of the solid electrolyte interphase (SEI). However, after the first cycle, the GO/MnO_x-250 anode shows reversible behavior with an average columbic efficiency of 81%. The anode can retain a reversible capacity of 431mAh/g with capacity fade per cycle of 7.9% after 5 cycles. However, large voltage hysteresis is observed between the charge and discharge cycles which are characteristic of graphene based anodes.

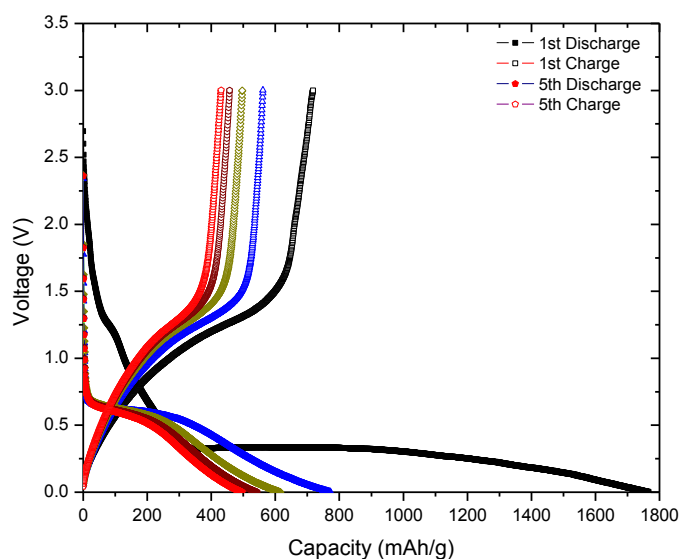


Figure 6.5 Discharge – charge profiles of GO/ MnO_x nano composite synthesized at 250°C (GO/ MnO_x-250)

Figure 6.6 shows charge-discharge curves of GO/MnO_x-400 nano composite electrodes synthesized at 400°C at a current density of 50 mA/cm² between 0 and 3.0 V vs. Li⁺/Li and tested up to 10 cycles. The anode sample is heat treated at 400°C to crystallize it to Mn₃O₄. Here too, considerable weight reduction is observed in the anode sample due to heat treatment at 400°C. The weight of the sample used before the heat treatment is 250mg and sample weight after the heat treatment is 75mg showing a weight reduction of 70%. This shows that complete graphene oxide and to a considerable certain extent manganese oxide is combusted. The left over material after the heat treatment is assumed to be in the form of Mn₃O₄. In discharge, the plateau observed at 0.4 V corresponds to the formation of Li₂O accompanying the reduction of transition metal particles. In addition, the capacity below 0.4 V can be attributed to lithiation of graphene

and/or a reversible polymerization of the electrolyte. In charge cycle, the plateau observed at 1.4V corresponds to reduction of Li_2O accompanying the oxidation of transition metal particles. Initial discharge capacity and charge capacity of 1655 mAh/g and 778mAh/g with a coulombic efficiency of 35% is achieved. The large irreversible capacity during first cycle could be caused by the formation of the solid electrolyte interphase (SEI). However, after the first cycle, the $\text{GO}/\text{MnO}_x\text{-400}$ anode shows reversible behavior with an average coulombic efficiency of 82%. The anode can retain a reversible capacity of 233mAh/g with a large capacity fade per cycle of 5.9% after 10 cycles.

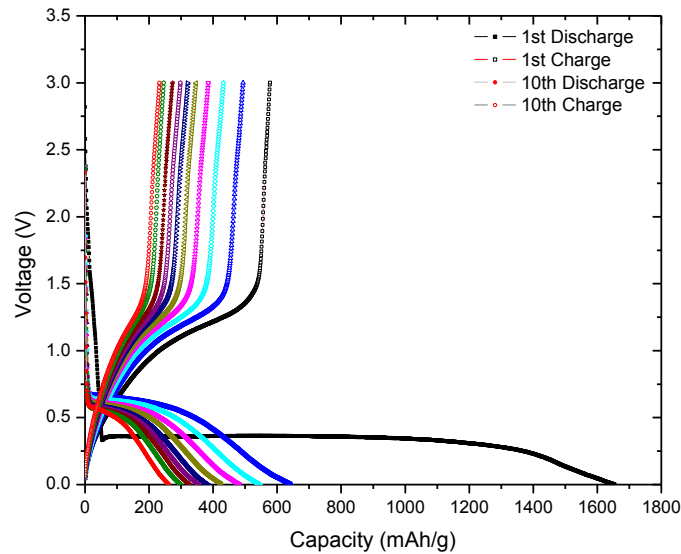


Figure 6.6 Discharge - charge profiles of $\text{GO}/\text{Mn}_3\text{O}_4$ nano composite synthesized at 400°C ($\text{GO}/\text{MnO}_x\text{-400}$)

Figure 6.7 shows the capacity cycle graph of $\text{GO}/\text{MnO}_x\text{-250}$ and $\text{GO}/\text{Mn}_3\text{O}_4\text{-400}$ nano composite anode samples. The initial discharge and charge capacities of 1765

mAh/g and 718mAh/g with coulombic efficiency of 41% are observed for GO/MnO_x-250 anode sample heat treated at 250°C. The initial discharge and charge capacities of 1655 mAh/g and 778mAh/g coulombic efficiency of 35% are observed for GO/Mn₃O₄-400 anode sample heat treated at 400°C. Average coulombic efficiency of 82 % is maintained for both the anode samples after 2 cycles onwards. This show at higher heat treatment temperatures, lower charge capacities and reduced cycle life are observed. The anode sample heat treated at 400°C showed larger capacity fade per cycle of 5.9%, whereas the anode sample heat treated at 250°C showed a capacity fade per cycle of 7.9%. In addition, there is huge weight reduction of 70% due to heat treatment of the anode sample at 400°C when compared to weight reduction of 27% due to heat treatment of the anode sample at 250°C. This shows combustion of graphene oxide and to a certain extent manganese oxide takes place due to heat treatment in air. In further work, the heat treatment of the anode sample is carried out in inert atmosphere, so that the anode material crystallizes without any combustion.

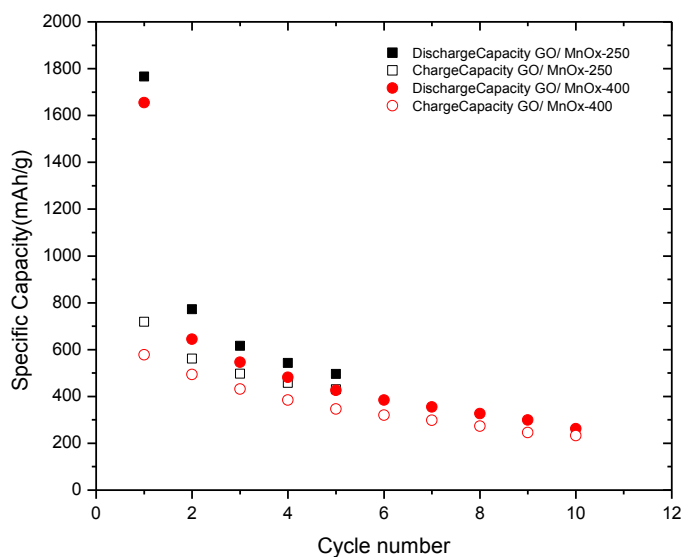


Figure 6.7 Capacity cycle performance of GO/ MnO_x-250 and GO/ Mn₃O₄-400 in air

6.3.2 Thermal Treatment Environment

The effect of atmosphere during chemical synthesis of GO/MnO_x nano composite anode on the electrochemical charge capacities and cycle life has been studied. In this research study, nano composite samples of GO/MnO_x-Air heat treated at 400°C in air and GO/MnO_x-Inert heat treated at 400°C in inert atmosphere are compared. The aim of the heat treatment of the anode sample in inert atmosphere is to crystallize the material without any combustion and compare its electrochemical performance with the anode sample heat treated in air.

Figure 6.8 shows charge-discharge curves of GO/MnO_x-Inert nano composite electrodes synthesized at 400°C in inert atmosphere at a current density of 50 mA/cm² between 0 and 3.0 V vs. Li⁺/Li and tested up to 10 cycles. Here too, there is a slight

weight reduction in the anode sample due to heat treatment at 400°C in inert atmosphere. The weight of the sample used before the heat treatment is 150mg and sample weight after the heat treatment is 112mg showing a weight reduction of 25%. The weight loss percentage of 25% is comparatively lesser when compared to weight loss of 70% for anode sample heat treated at 400°C in air. The shape of the profiles is not significantly altered from 2 cycles onwards, indicating the stability of the composite as anode. In discharge, the plateau observed at 1.4V corresponds to the formation of $Li_{\delta}MnO_x$ compound and the plateau observed at 0.4 V corresponds to the formation of Li_2O , both the reactions accompanying the reduction of transition metal particles. The plateau observed at 1.0V corresponds to the formation of SEI layer. In addition, the capacity below 0.4 V can be attributed to lithiation of graphene and/or a reversible polymerization of the electrolyte. In charge cycle, the plateau observed at 1.5V corresponds to reduction of Li_2O accompanying the oxidation of transition metal particles. Initial discharge capacity and charge capacity of 1343 mAh/g and 798mAh/g with a coulombic efficiency of 60% is achieved. The large irreversible capacity during first cycle could be caused by the formation of the solid electrolyte interphase (SEI). However, after the first cycle, the GO/ MnO_x -Inert anode shows reversible behavior with an average coulombic efficiency of 95%. The anode can retain a reversible capacity of 653mAh/g with capacity fade per cycle of 1.8% after 10 cycles. However, large voltage hysteresis is observed between the charge and discharge cycles which are characteristic of graphene based anodes.

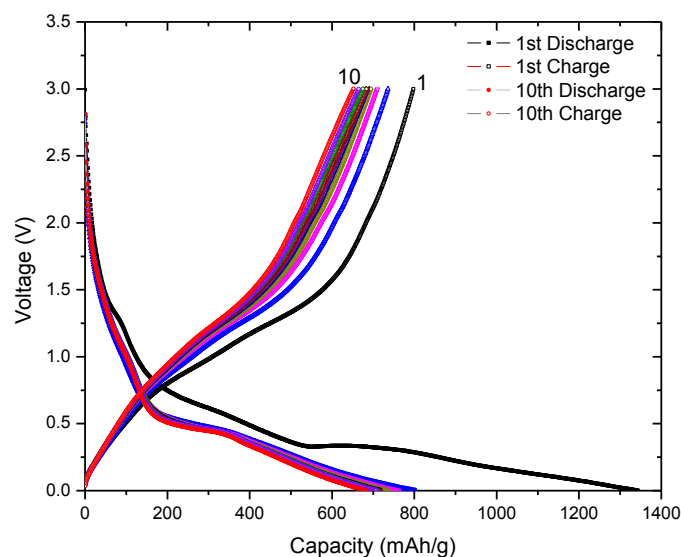


Figure 6.8 Discharge - charge profiles of GO/ MnO_x-Inert nano composite synthesized at 400°C in inert atmosphere

Figure 6.9 shows charge-discharge curves of GO/MnO_x-Air nano composite electrodes synthesized at 400°C at a current density of 50 mA/cm² between 0 and 3.0 V vs. Li⁺/Li and tested up to 10 cycles. The anode sample is heat treated at 400°C to crystallize it to Mn₃O₄. Here too, considerable weight reduction is observed in the anode sample due to heat treatment at 400°C. The weight of the sample used before the heat treatment is 250mg and sample weight after the heat treatment is 75mg showing a weight reduction of 70%. This shows that complete graphene oxide and to a considerable certain extent manganese oxide is combusted. The left over material after the heat treatment is assumed to be in the form of Mn₃O₄. In discharge, the plateau observed at 0.4 V corresponds to the formation of Li₂O accompanying the reduction of transition metal particles. In addition, the capacity below 0.4 V can be attributed to lithiation of graphene

and/or a reversible polymerization of the electrolyte. In charge cycle, the plateau observed at 1.4V corresponds to reduction of Li_2O accompanying the oxidation of transition metal particles. Initial discharge capacity and charge capacity of 1655 mAh/g and 778mAh/g with a coulombic efficiency of 35% is achieved. The large irreversible capacity during first cycle could be caused by the formation of the solid electrolyte interphase (SEI). However, after the first cycle, the GO/ MnO_x -Air anode shows reversible behavior with an average coulombic efficiency of 82%. The anode can retain a reversible capacity of 233mAh/g with a large capacity fade per cycle of 5.9% after 10 cycles.

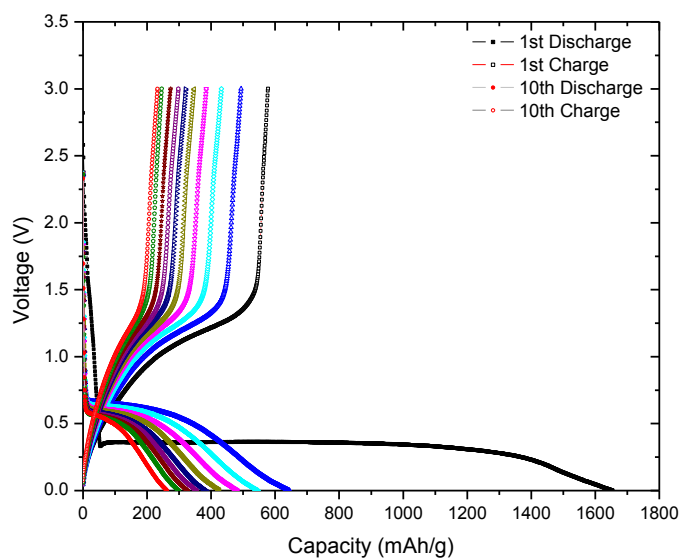


Figure 6.9 Discharge - charge profiles of GO/ MnO_x -Air nano composite synthesized at 400°C in air

Figure 6.10 shows the capacity cycle graph of GO/ MnO_x -Air and GO/ Mn_3O_4 -Inert nano composite anode samples. Though GO/ MnO_x -Air anode sample showed

higher initial discharge capacity of 1655mAh/g than the GO/MnO_x-Inert sample which showed initial discharge capacity of 1343mAh/g, the GO/MnO_x-Inert sample showed higher average columbic efficiency of 95 % than the GO/MnO_x-Air sample which showed only 82% average columbic efficiency up to 10 cycles. Also the GO/MnO_x-Inert sample can retain a capacity of 653mAh/g with less capacity fade per cycle of 1.8% for 10 cycles when compared to GO/MnO_x-Air sample with a capacity fade per cycle of 5.9% for 10 cycles retaining a charge capacity of 233mAh/g for 10th cycle. Heat treatment in inert atmosphere resulted in less combustion of graphene oxide and crystallization of the manganese oxide. The presence of graphene oxide in the GO/MnO_x-Inert sample improved the conductivity by maintaining electrical contact with copper foil and the crystallization of manganese oxide resulted in higher charge capacities with good cycle life. Also graphene oxide layers act as buffer to mitigate the large volume change of manganese oxide in the charge/discharge process. This shows heat treatment of GO/MnO_x-Inert anode sample in inert atmosphere results in higher charge capacities with very good cycle life.

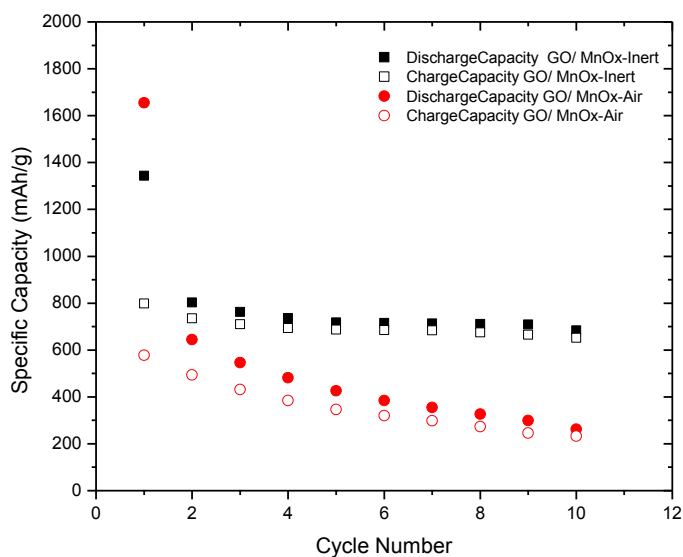


Figure 6.10 Capacity cycle performance of GO/ MnO_x-Air and GO/ Mn₃O₄-Inert samples

6.4 Summary

GO/MnO_x nano composite anode samples are chemically synthesized. Several nano composite anode samples namely GO/MnO_x, GO/MnO_x-250, GO/MnO_x-400, GO/MnO_x-Air, GO/MnO_x-Inert along with GO/MnAc composite anodes are studied for their electrochemical performances. The electrochemical results of the nano composite anode samples are summarized in Table 6.2. Figure 6.11 shows the combined 2nd discharge and 1st charge profiles of all nano composite anode samples. Similarly, Figure 6.12 shows combined charge capacity cycle performances of all nano composite anode samples.

GO/MnO_x nanocomposite delivered an initial discharge capacity of 1325 mAh/g and charge capacity of 776 mAh/g. It is believed that the large capacities and high reversibility of the GO/MnO_x nanocomposite is due to its unique 3D nanostructure where

manganese oxide nanoparticles are supported and separated by the graphene oxide layers. The charge capacities in GO/MnO_x nano composite anode sample are contributed via lithium insertion in graphene layers and lithium displacement of MnO_x particles in the ratio of its composition of graphene oxide and manganese oxide. The initial discharge and charge capacities of 1104 mAh/g and 533 mAh/g are observed for GO/MnAc anode sample. The large capacities observed in GO/MnO_x nano composite anode sample is due to the chemical synthesis treatment resulting in uniform distribution of manganese oxide particles between the graphene layers. The particle sizes obtained is also comparatively smaller than using the normal mixing method used for GO/MnAc anode sample. During lithium insertion and extraction, the particle sizes in GO/MnO_x nano composite anode sample are further reduced leading to higher charge capacities.

Effect of crystallization on the electrochemical behavior of the anode samples GO/MnO_x-250 and GO/MnO_x-400 are studied. The initial discharge and charge capacities of 1765 mAh/g and 718mAh/g are observed for GO/MnO_x-250 anode sample heat treated at 250°C. The initial discharge and charge capacities of 1655 mAh/g and 778mAh/g are observed for GO/MnO_x-400 anode sample heat treated at 400°C. Both the anode samples show large capacity fade per cycle. This show with increase in heat treatment temperatures of anode samples, decrease in charge capacities and cycle life are observed. But there is huge weight reduction of 70% due to heat treatment of the anode sample at 400°C when compared to weight reduction of 27% due to heat treatment of the anode sample at 250°C. This shows combustion of graphene oxide and to a certain extent manganese oxide takes place due to heat treatment in air at higher temperatures and also the amount of combustion increases with increase in heat treatment temperature.

Effect of crystallization can be studied by heat treating the anode samples in inert atmosphere. GO/MnO_x-Air heat treated in air at 400°C and GO/Mn₃O₄-Inert heat treated in inert atmosphere at 400°C are studied. Though GO/MnO_x-Air anode sample showed higher initial discharge capacity of 1655mAh/g than the GO/MnO_x-Inert sample which showed initial discharge capacity of 1343mAh/g, the GO/MnO_x-Inert sample showed higher average columbic efficiency of 95 % than the GO/MnO_x-Air sample which showed only 82 % average columbic efficiency up to 10 cycles. Also the GO/MnO_x-Inert sample can retain a capacity of 653mAh/g with less capacity fade per cycle of 1.8% for 10 cycles when compared to GO/MnO_x-Air sample with a capacity fade per cycle of 5.9% for 10 cycles retaining a charge capacity of 233mAh/g for 10th cycle. Heat treatment in inert atmosphere resulted in less combustion of graphene oxide and crystallization of the manganese oxide. The presence of graphene oxide in the GO/MnO_x-Inert sample improved the conductivity by maintaining electrical contact with copper foil and the crystallization of manganese oxide resulted in higher charge capacities with good cycle life. Also graphene oxide layers act as buffer to mitigate the large volume change of manganese oxide in the charge/discharge process. This shows heat treatment of GO/MnO_x-Inert anode sample in inert atmosphere results in higher charge capacities with very good cycle life.

Overall GO/MnO_x-Inert nano composite anode sample showed high reversibility and good cycle performance when compared to other anode samples. This suggests that GO/MnO_x-Inert anode sample can be considered as a potential candidate for anode materials with good cycle life and large capacities.

Table 6.2 Summary of Graphene Oxide and Manganese Oxide Nano Composite Results

Anode Sample	Heat Treatment at °C	Initial Discharge Capacity(mAh/g)	Initial Reversible Charge Capacity (mAh/g)	Second Discharge Capacity(mAh/g)	Second Reversible Charge Capacity (mAh/g)	1st Cycle Columbic Efficiency (1st charge/discharge)	2nd Cycle Columbic Efficiency (2nd charge/discharge)	Capacity Fade Per Cycle	nth Cycle Charge Capacity	No of Cycles
GO/MnOx		1325	776	862.7	780	58.6%	90.4%	2.95%	547	10
GO/MnAc		1104	533	615	540	48%	88%	1.8%	463	7
GO/MnOx-250	250	1766	718	772	561	40.6%	73%	7.9%	431	5
GO/MnOx-400	400	1655	578	645	494	35%	77%	5.9%	233	10
GO/MnOx-Air	400									
GO/MnOx-Inert	400	1344	798	803	736	59%	92%	1.8%	652	10

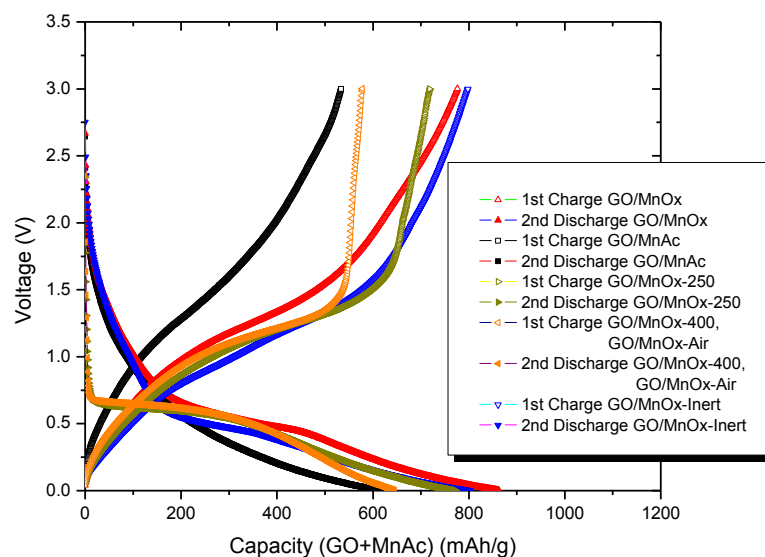


Figure 6.11 Combined discharge charge profiles of graphene oxide and manganese oxide nano composite samples (GO/MnOx, GO/MnOx-250, GO/MnOx-400, GO/MnOx-Air, GO/MnOx-Inert and GO/MnAc)

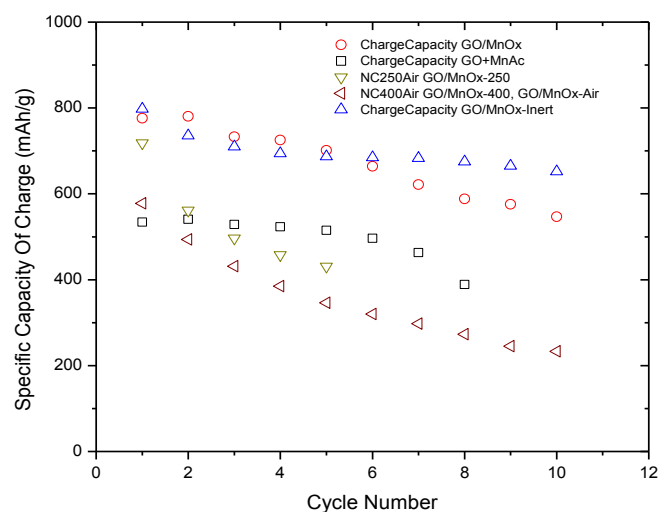


Figure 6.12 Combined charge capacity cycle performances of graphene oxide and manganese oxide nano composite samples (GO/MnOx, GO/MnOx-250, GO/MnOx-400, GO/MnOx-Air, GO/MnOx-Inert and GO/MnAc)

7. Electrochemical Impedance Results

7.1 Graphene Oxide

To investigate the kinetics evolution of electrode process of graphene oxide (GO) electrode, electrochemical impedance spectroscopy was utilized to analyze the electrode impedance at the different stage of lithium storage. The EIS spectra recorded for both discharge and charge profiles are presented.

Discharge: The EIS spectra were recorded at every 222.5 mAh/g interval during discharge. The selected Nyquist complex plots at 0, 222mAh/g, 445mAh/g, 890mAh/g, 1112mAh/g, 1333mAh/g and 1444mAh/g are presented in Figure 7.1(a). The voltages corresponding to each discharge capacity stop points are OCV, 1.385V, 0.8754V, 0.484V, 0.2977V, 0.1618 and 0.1055V respectively. During discharge, the presence of long tails showed diffusion inside the bulk and/or surface of the active materials, surface double layer capacitance. Gradually at higher discharge capacities the tails were not observed, this is due to the dominance of electrode charge transfer.

From the Figure 7.1 (b), it is apparent from the $R_{\text{electrolyte}}$ plot, the electrolyte resistance changed insignificantly indicating the stability of the cell and electrolyte. From $R_{\text{electrode}}$ plot, it can be seen that the total electrode impedance is 321 ohms at the open circuit voltage. As voltage decreased to 0.8754V, the impedance increased to 602 ohms. The increase in electrode resistance clearly associated with the formation of SEI. The $R_{\text{electrode}}$ started to decrease gradually till the end of discharge due to the increase of

electrical conductance as the lithium absorption together with electron injection on the graphene surfaces.

Charge: The EIS spectra were recorded at every 111.1 mAh/g interval during charge. The selected Nyquist complex plots at 0, 111.1mAh/g, 222.2mAh/g, 333.3mAh/g, 444.4mAh/g, 555.6mAh/g, 666.7mAh/g, 778mAh/g, 887mAh/g and 1000mAh/g are presented in Figure 7.1(c). The voltages corresponding to each charge capacity stop points are 0.5971, 0.9294V, 1.22V, 1.473V, 1.783V, 1.99, 2.208, 2.451 and 2.526V respectively. Initially short tails are observed due to diffusion limitation. As the lithium is taken out, the length of the tails starts increasing. This is due to increase in diffusion. During the lithium take out, it is not only due to desorption but also due to diffusion of lithium. Diffusion continues to increase with the increase in lithium take out. When all the lithium is taken out, the deviation seen is actually due to the dominance of double layer processing.

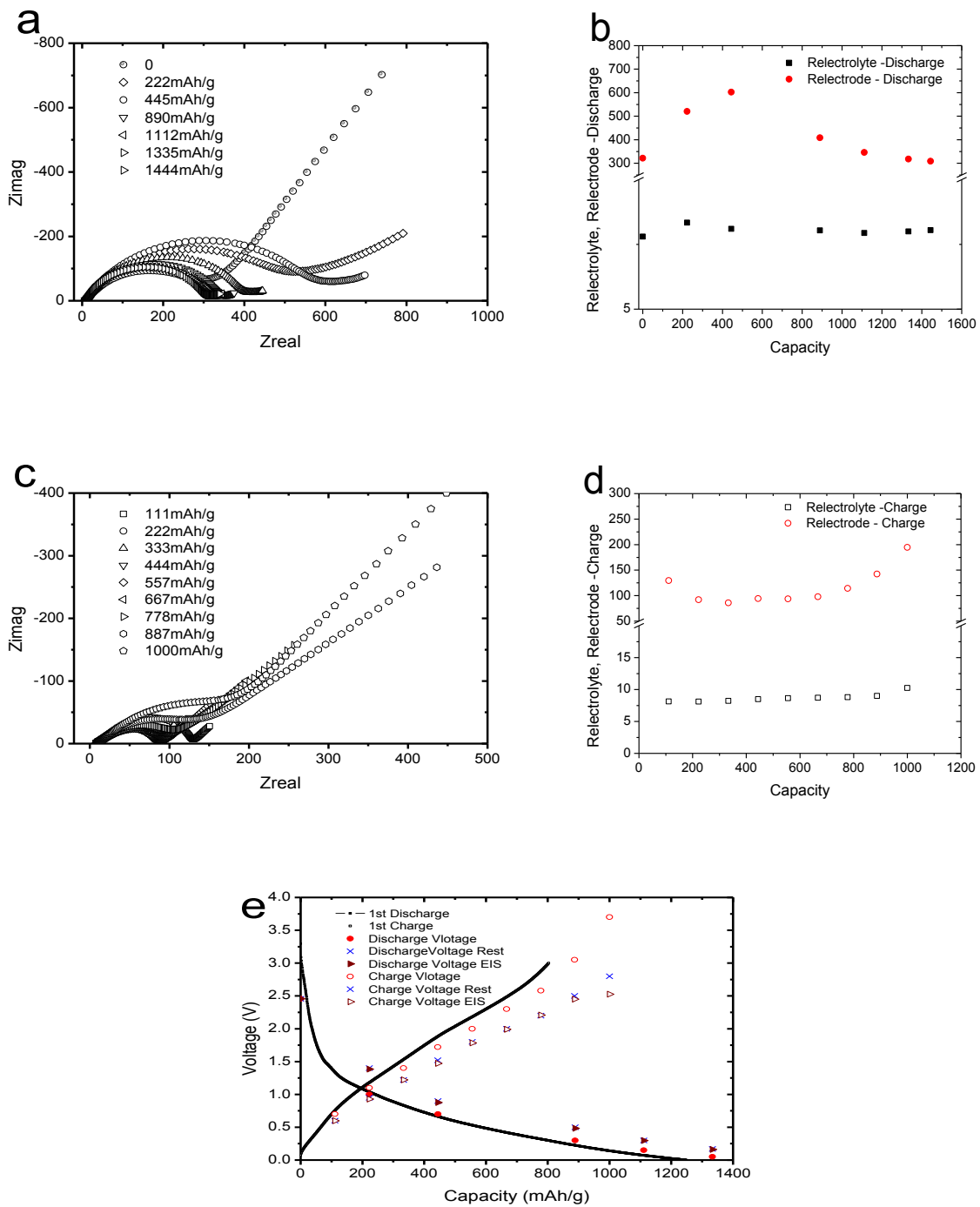


Figure 7.1 a) Nyquist plots of GO at different discharge stages b) $R_{\text{electrolyte}}$ and $R_{\text{electrode}}$ plots at different discharge stages c) Nyquist plots of GO at different charge stages d) $R_{\text{electrolyte}}$ and $R_{\text{electrode}}$ plots at different charge stages e) Discharge charge profile with different voltage points.

From the Figure 7.1 (d) it is apparent from the $R_{\text{electrolyte}}$ plot, the electrolyte resistance changed insignificantly indicating the stability of the cell and electrolyte. From the $R_{\text{electrode}}$ charge plot, it can be seen that the total electrode impedance is 129 ohms and showed a slight decrease till 93 ohms and gradually increases until 194 ohms. Resistance started increasing from 2.2 volts. This shows during initial charge the conduction is high and gradually the conduction is decreased as lithium is restored back into the lithium metal. Desorption in lithium is faster in charge than in discharge. Therefore the $R_{\text{electrode}}$ of charge is less when compared with $R_{\text{electrode}}$ of discharge. The charge resistance is less than discharge resistance shows that the lithium extraction is faster than lithium insertion. For the convenience of comparison, the complete discharge and charge profiles obtained at the constant current, and each voltage points obtained after the interrupted discharge steps were included in the figure 7.1 (e).

7.2 GO/MnO_x Nano Composite

The EIS spectra were recorded for both discharge and charge profiles to analyze the electrode impedance of graphene oxide manganese oxide nano composite anode (GO/MnO_x).

Discharge: The EIS spectra were recorded at every 204 mAh/g except the final EIS spectra which is recorded at a difference of 102mAh/g with the previous interval (i.e. 1224.5mAh/g) during discharge. The selected Nyquist complex plots at 0, 204mAh/g, 408mAh/g, 612mAh/g, 816mAh/g, 1020mAh/g, 1224.5mAh/g and 1327mAh/g are presented in Figure 7.2(a). The voltages corresponding to each capacity stop points are

OCV (3V), 1.142V, 0.7381V, 0.5937V, 0.4995V, 0.3438V, 0.2072V and 0.1508V respectively.

Figure 7.2(b) plotted the $R_{\text{electrolyte}}$ and $R_{\text{electrode}}$ of discharge as function of the discharge capacity at each stage of lithium storage. It is apparent from the $R_{\text{electrolyte}}$ discharge plot, the electrolyte resistance changed insignificantly indicating the stability of the cell and electrolyte. Nano composite has low conductivity that is because the ratios used in the preparation of nano composite are graphene oxide ratio is 22% and manganese oxide ratio is 78%. Therefore the impedance is high due to the significant amount of MnO_x . From the $R_{\text{electrode}}$ discharge plot, it can be seen that the total electrode impedance is 800 ohms at the open circuit voltage. Due to high resistance from MnO_x has overshadowed the SEI formation. Therefore the impedance started with 800 ohms at OCV and showed decrease to 600ohms, 410 ohms in the region of reducing Mn_3O_4 to Mn (II), $R_{\text{electrode}}$ remained constant at around 350 ohms. (Note: The nano composite particles are assumed to be amorphous and the obtained impedance points are not accurate). Upon completion of the Mn_3O_4 reduction process, the $R_{\text{electrode}}$ started to decrease gradually till the end of discharge due to the increase of electrical conductance resulting from Mn(0) formation and lithium absorption together with electron injection on the graphene surfaces. During discharge, the tails have some diffusion effect, surface double layer capacitance. Gradually the tails were not observed, this is due to electrode charge transfer dominance. This tails observed are related to double layer capacitance.

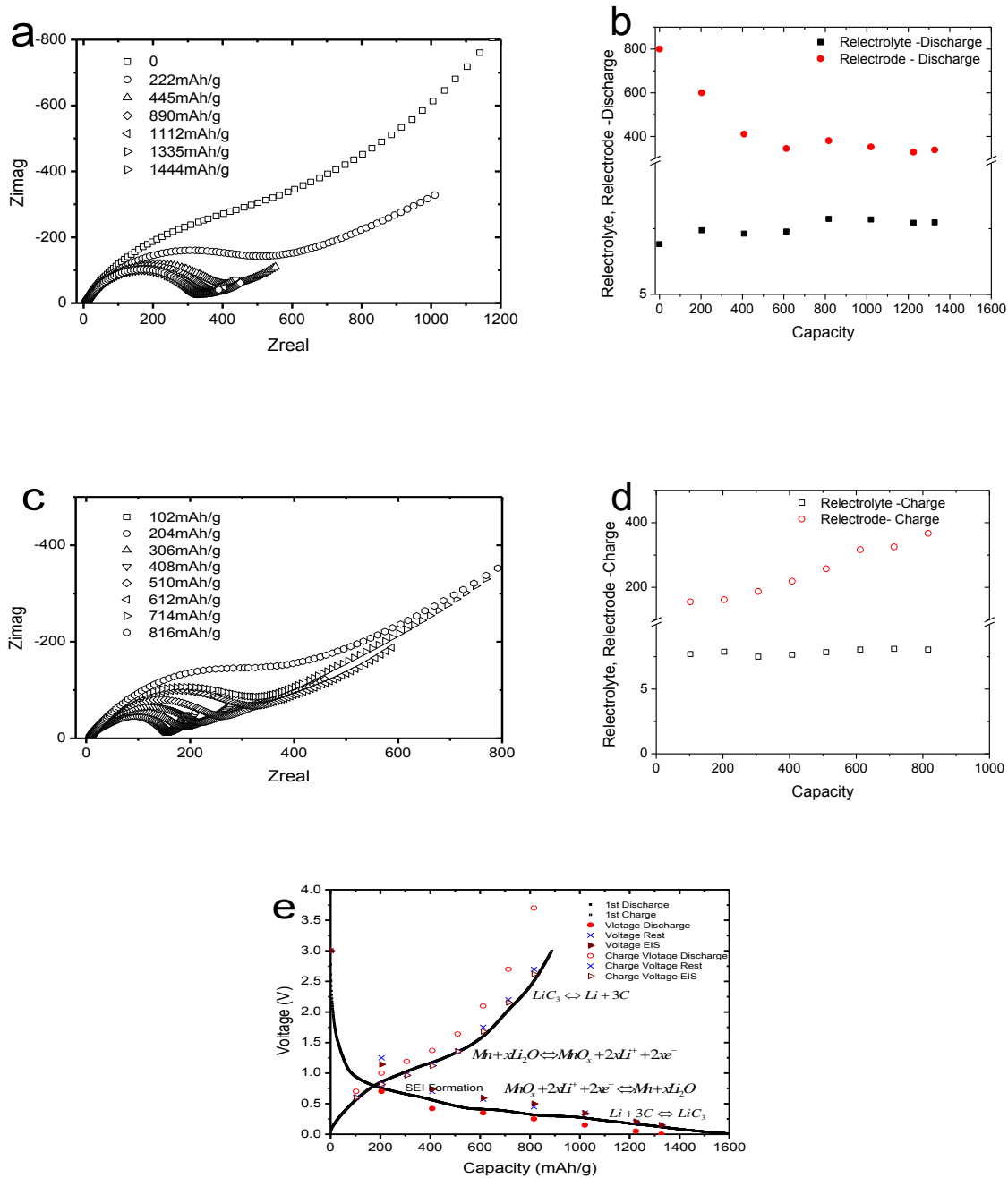


Figure 7.2 a) Nyquist plots of GO/MnOx at different discharge stages b) $R_{\text{electrolyte}}$ and $R_{\text{electrode}}$ plots at different discharge stages c) Nyquist plots of GO/MnOx at different charge stages d) $R_{\text{electrolyte}}$ and $R_{\text{electrode}}$ plots at different charge stages e) Discharge charge profile with different voltage points.

Charge: The EIS spectra were recorded at every 102 mAh/g interval during charge. The selected Nyquist complex plots at 102mAh/g, 204mAh/g, 306mAh/g, 408mAh/g, 510mAh/g, 612mAh/g, 714mah/g, and 816mAh/g are presented in Figure 7.2(c). The voltages corresponding to each capacity stop points are 0.6027V, 0.8156V, 0.9648V, 1.12V, 1.355V, 1.681V, 2.154 and 2.617V respectively. Initially short tails are observed due to diffusion limitation. As the lithium is taken out, the length of the tails starts increasing. This is due to increase in diffusion. During the lithium take out, it is not only due to desorption but also due to diffusion of lithium. Diffusion continues to increase with the increase in lithium take out. When all the lithium is taken out, the deviation seen is actually due to the dominance of double layer processing.

From the Figure 7.2 (d) it is apparent from the $R_{\text{electrolyte}}$ charge plot, the electrolyte resistance changed insignificantly indicating the stability of the cell and electrolyte. From the $R_{\text{electrode}}$ charge plot, it can be seen that the total electrode impedance is 155 ohms and showed gradual increase in resistance until 366 ohms. This is due to the lithium extraction during charge, forms the MnO_x compound and thereby increases the resistance. As lithium is taken out, the resistance of charge keeps on increasing and the impedance of charge touched 366 ohms. For the convenience of comparison, the complete charge and discharge profiles obtained at the constant current, and each voltage points obtained after the interrupted discharge steps were included in the figure 7.2 (e).

7.3 *GO/MnO_x Nano Composite – HT in Air at 400°C*

The EIS spectra were recorded for both discharge and charge profiles to analyze the electrode impedance of graphene oxide and manganese oxide nano composite anode heat treated in air at 400°C (GO/MnO_x-Air).

Discharge: The EIS spectra were recorded at every 222 mAh/g during discharge. The selected Nyquist complex plots at 0, 222mAh/g, 444mAh/g, 666.7mAh/g, 888.8mAh/g, 1111mAh/g, 1333mAh/g and 1444mAh/g are presented in Figure 7.3(a). The voltages corresponding to each capacity stop points are OCV (3.345V), 1.065V, 0.8849V, 0.6468V, 0.5496V, 0.4375V, 0.1925V and 0.0088V respectively.

Figure 7.3(b) plotted the $R_{\text{electrolyte}}$ and $R_{\text{electrode}}$ of discharge as a function of the discharge capacity at each stage of lithium storage. It is apparent from the $R_{\text{electrolyte}}$ discharge plot, the electrolyte resistance changed insignificantly indicating the stability of the cell and electrolyte. The impedance is high due to the significant amount of MnO_x in the nano composite due to combustion of graphene oxide. From the $R_{\text{electrode}}$ discharge plot, it can be seen that the total electrode impedance is 1000 ohms at the open circuit voltage. Due to high resistance from MnO_x has overshadowed the SEI formation. Therefore the impedance started with 1000 ohms at OCV and decreased gradually. (Note: The nano composite particles are assumed to be crystalline and the obtained impedance points are not accurate). Upon completion of the Mn₃O₄ reduction process, the $R_{\text{electrode}}$ started to decrease gradually till the end of discharge due to the increase of electrical conductance resulting from Mn(0) formation and lithium absorption together with electron injection on the graphene surfaces. During discharge, the tails have some diffusion effect, surface double layer capacitance. Gradually the tails were not observed,

this is due to electrode charge transfer dominance. This tails observed are related to double layer capacitance.

Charge: The EIS spectra were recorded at every 111 mAh/g interval during charge. The selected Nyquist complex plots at 111mAh/g, 222mAh/g, 333mAh/g, and 444mAh/g are presented in Figure 7.3(c). The voltages corresponding to each capacity stop points are 0.556V, 0.894V, 1.043V, and 1.132V respectively. Initially short tails are observed due to diffusion limitation. As the lithium is taken out, the length of the tails starts increasing. This is due to increase in diffusion. During the lithium take out, it is not only due to desorption but also due to diffusion of lithium. Diffusion continues to increase with the increase in lithium take out. When all the lithium is taken out, the deviation seen is actually due to the dominance of double layer processing.

From the Figure 7.3 (d) it is apparent from the $R_{\text{electrolyte}}$ charge plot, the electrolyte resistance changed insignificantly indicating the stability of the cell and electrolyte. From the $R_{\text{electrode}}$ charge plot, it can be seen that the total electrode impedance is 188.3 ohms and showed gradual increase in resistance until 543.3 ohms. This is due to the lithium extraction during charge, forms the MnO_x compound and thereby increases the resistance. As lithium is taken out, the resistance of charge keeps on increasing and the impedance of charge touched 543.3 ohms. For the convenience of comparison, the complete charge and discharge profiles obtained at the constant current, and each voltage points obtained after the interrupted discharge steps were included in the figure 7.3 (e).

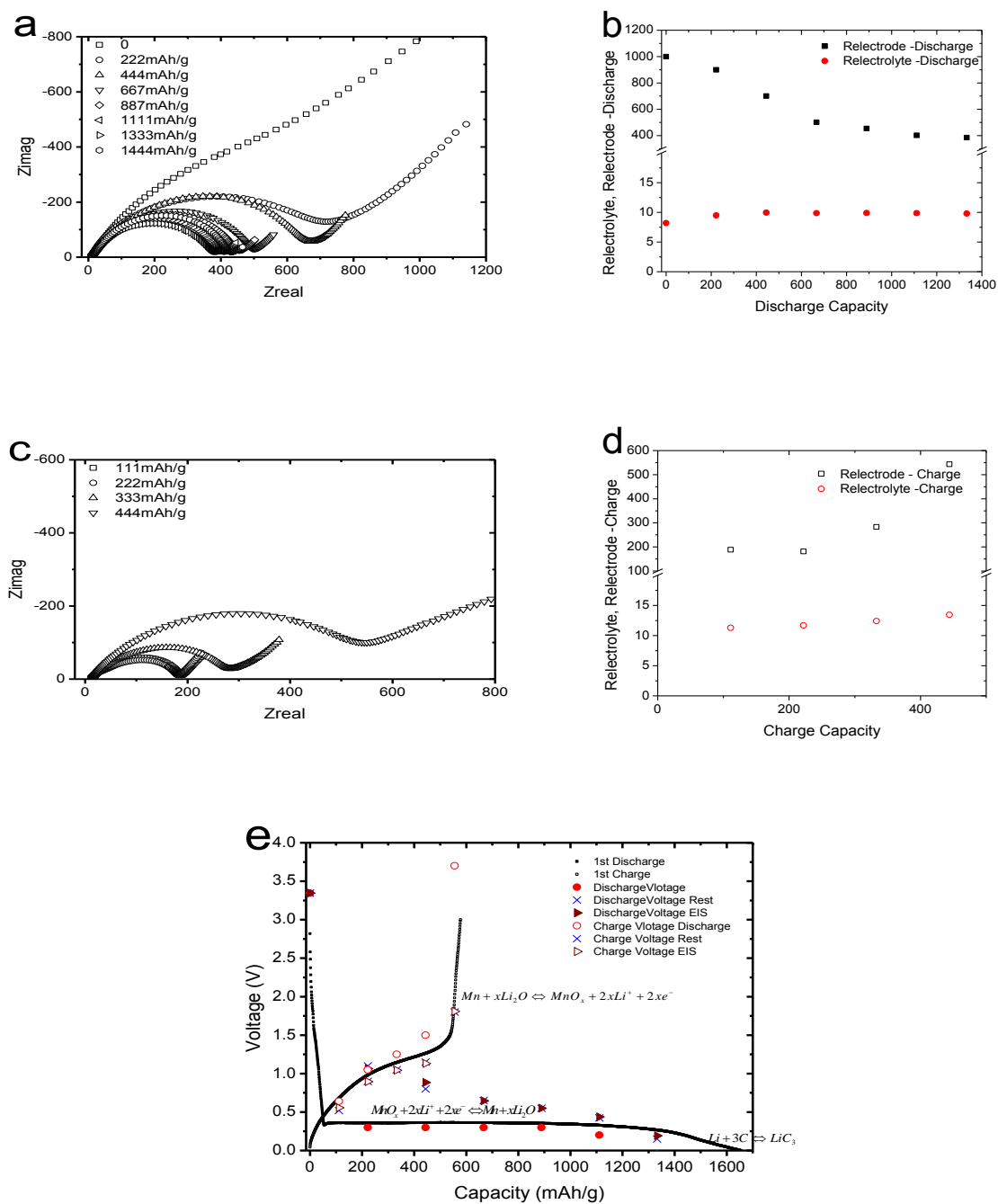


Figure 7.3 a) Nyquist plots of GO/MnO_x-Air heat treated at 400°C at different discharge stages b) R_{electrolyte} and R_{electrode} plots at different discharge stages c) Nyquist plots of GO/MnO_x-Air heat treated at 400°C in air at different charge stages d) R_{electrolyte} and R_{electrode} plots at different charge stages e) Discharge charge profile with different voltage points.

7.4 GO/MnO_x Nano Composite – HT in Inert Atmosphere at 400°C

The EIS spectra were recorded for both discharge and charge profiles to analyze the electrode impedance of graphene oxide and manganese oxide nano composite anode heat treated in inert atmosphere at 400°C (GO/MnO_x-Inert).

Discharge: The EIS spectra were recorded at every 111 mAh/g during discharge. The selected Nyquist complex plots at 0, 111mAh/g, 222mAh/g, 333mAh/g, 333mAh/g, 444mAh/g, 555mAh/g, 666mAh/g, 777.7mAh/g, 888.8mAh/g, 1000mAh/g, 1111mAh/g and 1222mAh/g are presented in Figure 7.4(a). The voltages corresponding to each capacity stop points are OCV (3.292V), 1.781V, 1.105V, 0.9021V, 0.6726V, 0.525V, 0.5087V, 0.4468V, 0.3668V, 0.2238V, 0.1571V and 0.0699V respectively.

Figure 7.4(b) plotted the $R_{\text{electrolyte}}$ and $R_{\text{electrode}}$ of discharge as function of the discharge capacity at each stage of lithium storage. It is apparent from the $R_{\text{electrolyte}}$ discharge plot, the electrolyte resistance changed insignificantly indicating the stability of the cell and electrolyte. From the $R_{\text{electrode}}$ discharge plot, it can be seen that the total electrode impedance is 900 ohms at the open circuit voltage. Due to high resistance from MnO_x has overshadowed the SEI formation. Therefore the impedance started with 900 ohms at OCV and gradually decreased. (Note: The nano composite particles are assumed to be crystalline form MnO, MnO₂ and Mn₃O₄ and the obtained impedance points are not accurate). Upon completion of the Mn₃O₄ reduction process, the $R_{\text{electrode}}$ started to decrease gradually till the end of discharge due to the increase of electrical conductance resulting from Mn(0) formation and lithium absorption together with electron injection on the graphene surfaces. During discharge, the tails have some diffusion effect, surface

double layer capacitance. Gradually the tails were not observed, this is due to electrode charge transfer dominance.

Charge: The EIS spectra were recorded at every 111 mAh/g interval during charge. The selected Nyquist complex plots at 111mAh/g, 222mAh/g, 333mAh/g, 333mAh/g, 444mAh/g, 555mAh/g, 666mAh/g, 777.7mAh/g and 888.8mAh/g are presented in Figure 7.4(c). The voltages corresponding to each capacity stop points are 0.4834V, 0.7299V, 0.895V, 1.035V, 1.212V, 1.509V, 1.97V and 2.471V respectively. Initially short tails are observed due to diffusion limitation. As the lithium is taken out, the length of the tails starts increasing. This is due to increase in diffusion. During the lithium take out, it is not only due to desorption but also due to diffusion of lithium. Diffusion continues to increase with the increase in lithium take out. When all the lithium is taken out, the deviation seen is actually due to the dominance of double layer processing.

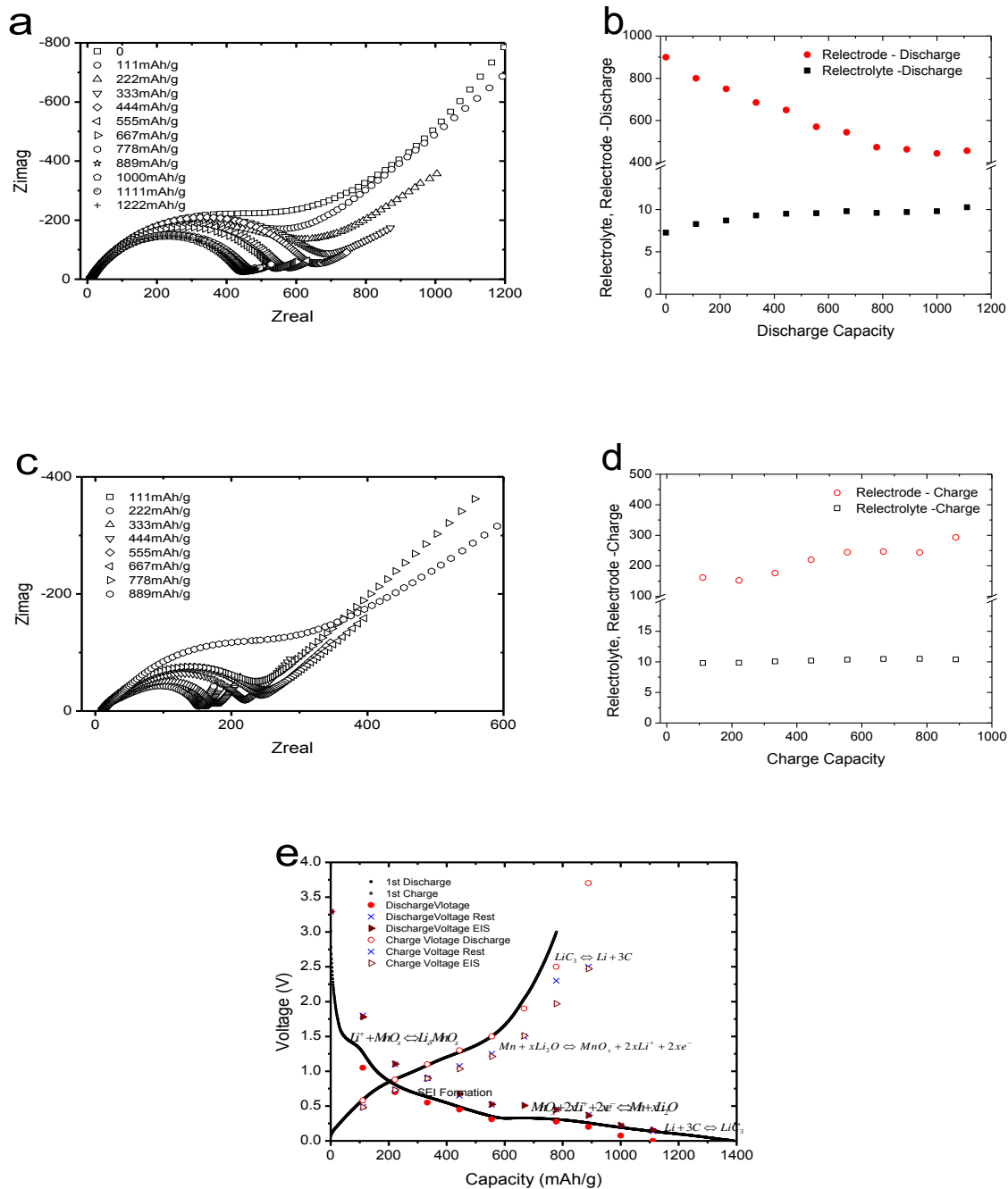


Figure 7.4 a) Nyquist plots of GO/MnO_x-Inert heat treated at 400°C in inert atmosphere at different discharge stages b) R_{electrolyte} and R_{electrode} plots at different discharge stages c) Nyquist plots of GO/MnO_x-Inert heat treated at 400°C in inert atmosphere at different charge stages d) R_{electrolyte} and R_{electrode} plots at different charge stages e) Discharge charge profile with different voltage points.

From the Figure 7.4 (d) it is apparent from the $R_{\text{electrolyte}}$ charge plot, the electrolyte resistance changed insignificantly indicating the stability of the cell and electrolyte. From the $R_{\text{electrode}}$ charge plot, it can be seen that the total electrode impedance is 161 ohms and showed gradual increase in resistance until 292 ohms. This is due to the lithium extraction during charge, forms the MnO_x compound and thereby increases the resistance. As lithium is taken out, the resistance of charge keeps on increasing and the impedance of charge touched 292 ohms. For the convenience of comparison, the complete charge and discharge profiles obtained at the constant current, and each voltage points obtained after the interrupted discharge steps were included in the figure 7.4 (e).

7.5 Summary

Graphene oxide and manganese oxide nano composite anode (GO/MnO_x) showed higher resistance when compared to graphene oxide anode(GO). This is because MnO_x is electronic insulator and the content of graphene oxide in nano composite is 22%. In graphene oxide (GO) $R_{\text{electrode}}$ discharge plot, SEI formation can be clearly observed as the resistance increases initially and then reduces gradually. In GO/MnO_x nano composite $R_{\text{electrode}}$ discharge plot, both the SEI formation and lithium storage in MnO_x are over shadowed by already high resistance in nano composite. Therefore the SEI formation is not observed in the GO/MnO_x nano composite $R_{\text{electrode}}$ discharge plot. In the nano composite, lithium is stored in 2 ways. 1) Lithium intercalation with graphene oxide 2) Lithium oxidized with MnO_x . Desorption in lithium is faster in charge than discharge in the graphene oxide. Therefore the $R_{\text{electrode}}$ of charge is less when compared with

$R_{\text{electrode}}$ of discharge in graphene oxide(GO). In GO/MnO_x nano composite, initially the resistance of charge is less than discharge. But gradually resistance increases during charge up to 400 ohms.

Initially graphene oxide and manganese oxide nano composite is in amorphous form, after the heat treatment at 400°C, the nano composite is assumed to be in crystallized form. In the nano composite heat treated in inert atmosphere at 400°C (GO/MnO_x-Inert), the manganese is assumed to be in MnO_x form and also contains significant amount of graphene oxide after heat treatment, whereas the nano composite heat treated at 400°C in air (GO/MnO_x-Air) contains Mn₃O₄ with insignificant amount of graphene oxide left in it. MnO_x obtained in GO/MnO_x-Inert anode is not the same as in GO/MnO_x-Air. In GO/MnO_x-Inert, an extra plateau observed at 1.5V in the discharge profile may be related to MnO₂, Mn₃O₄ and MnO and plateau at 0.3V corresponds to Mn₃O₄ and as the voltage dropped the plateau corresponds to graphene oxide. In GO/MnO_x-Air, a flat plateau observed at 0.3V is related to Mn₃O₄ and no observable plateaus are found at lower voltages as very small amount of graphene oxide is present after the heat treatment. Similarly in the charge profile, no plateaus are observed that are related to graphene oxide in GO/MnO_x-Air. The charge capacities observed in the GO/MnO_x-Inert are higher when compared to GO/MnO_x-Air as there is no contribution to charge capacities from graphene oxide. Due to insignificant amount of graphene oxide GO/MnO_x-Air the resistance is higher for the charge capacities when compared with the charge capacities in the GO/MnO_x-Inert.

8. Conclusion and Future Work

8.1 Conclusion

Lithium storage characteristics of graphene-based anode materials have found great potentials in alternative energy technologies. Electrochemical characteristics of graphene-based anode materials Graphene oxide (GO), Reduced graphene oxide (RGO) and Nano Graphene Platelets (NGPs), GO/Manganese acetate (GO/MnAc) composites and GO/manganese oxide (GO/MnO_x) composites, were studied. Graphene oxide synthesized using modified hummers method and heat treated at 250°C (GO250) showed a reversible capacity of 706 mAh/g with an average columbic efficiency of 87%. Graphene oxide sheets heat treated at elevated temperatures, e.g. 400°C (GO400), may stack into 3D structure, rendering dramatic reduction of lithium storage capacity. NGPs delivered a reversible charge capacity of 422 mAh/g. The comparatively low charge capacity of NGPs is due to annealing at a high temperature of 900°C may have resulted in crystallization and reduction of surface area. Also in RGO anode sample, lithium is absorbed on each side of the reduced graphene oxide sheet but not in the cavities and hydrogen terminated edges of the graphene fragments resulting in reduced capacities.

GO/MnAc composite delivered reversible charge capacities of 533 mAh/g with an average columbic efficiency of 88% and low capacity fade per cycle of 1.8%. GO/MnAc-400 composite thermally annealed at temperatures higher than 400°C delivered a reversible charge capacity of 622mAh/g, but showed a larger capacity fade per cycle indicating reduced particle strength during lithiation and de-lithiation process.

The charge and discharge capacities, capacity cycle behavior of GO/MnAc-SM (synthesized using simple method) and GO/MnAc-LM (synthesized using liquid method) are observed same. Both the anode samples are heat treated at 400°C. This shows no considerable effect of the synthesis method followed on the lithium storage characteristics on both the anode materials. GO/MnO_x-7525 (GO:MnO_x is mixed in ratio of 75:25) composite anode delivered an initial reversible charge capacity of 589 mAh/g, larger than 497 mAh/g observed for GO/MnO_x-5050 (GO:MnO_x is mixed in ratio of 50:50). Both the anode samples are heat treated at 500°C and synthesized through solid method. The improved performance of GO/MnO_x-7525 is due to higher composition of graphene oxide leading to higher lithium intercalation and better charge capacities.

GO/MnO_x composites anodes delivered a reversible charge capacity of 776 mAh/g with an average columbic efficiency of 92%. The large capacities observed in GO/MnO_x nano composite anode sample is due to the chemical synthesis treatment resulting in uniform distribution of manganese oxide particles between the graphene layers and forming a unique 3D nanostructure. The particle sizes obtained is also comparatively smaller than using the normal mixing method used for GO/MnAc anode sample. During lithium insertion and extraction, the particle sizes in GO/MnO_x nano composite anode sample are further reduced leading to higher charge capacities than the GO/MnAc anode sample. Effect of crystallization on the electrochemical behavior is studied on anode samples annealed at different temperatures in air and inert atmosphere. GO/MnO_x-250 heat treated at 250°C and GO/MnO_x-400 heat treated at 400°C delivered reversible charge capacity of 718mAh /g and 578mAh /g respectively. Large capacity fade per cycle is observed for both the anode samples indicating poor cycle life. Also

combustion of graphene oxide and to a certain extent manganese oxide occurred due to heat treatment of anode samples in air and the amount of material combusted increases with increase in heat treatment temperature. Two anode samples GO/MnO_x-Air heat treated in air at 400°C and GO/Mn₃O₄-Inert heat treated in inert atmosphere at 400°C are studied. GO/MnO_x-Inert and GO/MnO_x-Air anode samples delivered reversible charge capacity of 798 mAh/g and 578mAh/g respectively. GO/MnO_x-Inert sample showed higher average columbic efficiency of 95 % and less capacity fade per cycle of 1.8% than the GO/MnO_x-Air sample which showed only 82 % average columbic efficiency and a large capacity fade per cycle of 5.9%. This confirms heat treatment in inert atmosphere resulted in less combustion of graphene oxide and crystallization of the manganese oxide. The presence of graphene oxide in the GO/MnO_x-Inert sample improved the conductivity and also acts as a buffer to mitigate the large volume changes of manganese oxide during charge/discharge process resulting in large reversible capacities with fine cycle life.

The EIS spectra of discharge and charge profiles of GO and GO/MnO_x composites were analyzed to investigate the kinetics evolution of electrode process and impedance at different stages of lithium storage. Graphene oxide and manganese oxide nano composite (GO/MnO_x) showed higher resistance when compared to graphene oxide (GO). This is because the GO/MnO_x composite contains only 22% of graphene oxide. GO/MnO_x composite is in amorphous form. GO/MnO_x-Inert heat treated in inert atmosphere at 400°C and GO/MnO_x-Air heat treated in air at 400°C are assumed to be in crystallized state. In GO/MnO_x-Inert composite, the manganese is assumed to be in MnO_x (MnO₂, Mn₃O₄ and MnO) form and also contains significant amount of graphene oxide after heat treatment, whereas in GO/MnO_x-Air composite contains Mn₃O₄ with

insignificant amount of graphene oxide left in it after the heat treatment. Due to insignificant amount of graphene oxide in GO/MnO_x-Air, the resistance is higher for the charge capacities when compared with the charge capacities in the GO/MnO_x-Inert

In this research, GO/MnO_x-Inert, GO/MnAc and GO250 exhibited large reversible capacities of 798 mAh/g, 533mAh/g and 706 mAh/g respectively and also have good cycle life. It can be concluded that GO/MnO_x-Inert nano composite possess the intensive potential as a candidate of anode materials with high reversible capacity and fine cycle performance.

8.2 Future Work

The lithium-ion batteries have been widely used in portable electronic devices and viewed as a promising device in the application of electric vehicle. There is much research being carried out to enhance the lithium-ion batteries properties on higher specific capacity and more durable cycling performance. Graphene-based anodes for lithium-ion batteries are under extensive development to improve the storage capacity and cycle life. In this research work, charge capacities of up 800 mAh/g are achieved. Further effort must be made to improve the charge capacities through varying the composition of anode material and heat treatment at different temperatures in air and inert atmospheres. Along with high reversible capacity, further research needs to be carried to improve the cycle life of the anode materials.

In this current research, GO/MnO_x nano composite gave very promising results. Further research work needs to be continued on the nano composite with varying

compositions and heat treated in inert atmosphere at different temperatures to find the right composition and heat treatment that gives best results. Also there should be more elaborate electrochemical impedance studies on the anode materials to understand the chemical reactions and kinetics of electrode process occurring at the plateaus with 0.5V. Develop an equivalent circuit for accurate measurement of the resistance of electrode ($R_{\text{electrode}}$) to study the resistance vs. capacity plots. Also more analysis needs to be carried on the tail sections of the Nyquist plots to understand the diffusion and the charge transfer process during electrochemical reactions.

Different lithium alloying materials like silicon and tin needs to be investigated. Silicon has highest theoretical capacity and also has large volume changes during alloying and de-alloying. Further studies needs to be carried to find out ways to decrease the large volume changes and prolong the cycle life. Further, metal oxides like Iron oxalate needs to be studied for their lithium storage characteristics as they known to deliver high energy density.

Finally extensive research on other graphene based anode materials like Graphene-Iron Oxalate composite and Graphene-Silicon composite might give good results and needs to be investigated. Electrochemical studies can be conducted on anode materials with varying composition, chemical synthesis and heat treatments to understand lithium storage characteristics.

These studies may provide a greater insight into the lithium storage characteristics of graphene based anode materials and find anode materials with high specific capacities and fine cycle performance.

REFERENCES

1. **Martin Winter, Ralph J. Brodd.** What Are Batteries, Fuel Cells, and Supercapacitors? *Chem. Rev.* 2004, Vol. 104, 4245-4269.
2. **Gholam-Abbas Nazari, Gianfranco Pistoia.** *Lithium Batteries Science and Technology.* s.l. : Springer, 2009.
3. **A. K. Shukla, T. Prem Kumar.** Materials for next-generation lithium batteries. *CURRENT SCIENCE.* 2008, Vol. 94, 3.
4. **Kim, John B. Goodenough and Youngsik.** Challenges for Rechargeable Li Batteries. *Chemistry of Materials.* 2010, Vol. 22, 587-603.
5. **D.A.J. Rand, P.T. Moseley.** SECONDARY BATTERIES - LEAD- ACID SYSTEMS Overview. *Encyclopedia of Electrochemical Power Sources 2009.* 2009, 550-575.
6. **A.K. Shukla, S. Venugopalan, B. Hariprakash.** SECONDARY BATTERIES - NICKEL SYSTEMS Nickel–Cadmium: Overview. *Encyclopedia of Electrochemical Power Sources.* 2009, 452-458.
7. **B. Hariprakash, A.K. Shukla, S. Venugoplan.** SECONDARY BATTERIES - NICKEL SYSTEMS Nickel–Metal Hydride: Overview. *Encyclopedia of Electrochemical Power Sources, 2009.* 2009, 494-501.
8. **Yan Geng, Shu Jun Wang, Jang-Kyo Kim.** Preparation of graphite nanoplatelets and graphene sheets. *Journal of Colloid and Interface Science.* 2009, Vol. 336, 592-598.

9. **Uday Kasavajjula, Chunsheng Wang, A. John Appleby.** Nano- and bulk-silicon-based insertion anodes for lithium-ion secondary cells. *Journal of Power Sources*. 2007, Vol. 163, 1003-1039.
10. **Jane Yao, Xiaoping Shen, Bei Wang, Huakun Liu, Guoxiu Wang.** In situ chemical synthesis of SnO₂-graphene nanocomposite as anode materials for lithium-ion batteries. *Electrochemistry Communications*. 2009, Vol. 11, 1849-1852.
11. **S. Stankovich, D. A. Dikin, G. Dommett, K. Kohlhaas, E. J. Zimney, E. Stach, R. Piner, S. T.** Graphene-based Composite Materials. *Nature*. 2006, Vol. 442, 282-286.
12. **P. Poizot, S. Laruelle, S. Grugeon, L. Dupont and J-M. Tarascon.** Nano-sized transition-metal oxides as negative-electrode materials for lithium-ion batteries. *NATURE*. 2000, Vol. 407, 496-499.
13. **Guoxiu Wang, Bei Wang, Xianlong Wang, Jinsoo Park, Shixue Dou, Hyojun Ahn and Kiwon Kim.** Sn/graphene nanocomposite with 3D architecture for enhanced reversible lithium storage in lithium ion batteries. *Journal of Materials Chemistry*. 2009, Vol. 19, 8378-8384.
14. **Hongfa Xiang, Kai Zhang, Ge Ji, Jim Yang Lee, Changji Zou, Xiaodong Chen, Jishan Wu.** Graphene/nanosized silicon composites for lithium battery anodes with improved cycling stability. *Carbon*. 2011, Vol. 49, 1787-1796.
15. **Tetsuya Kawamura, Shigeto Okada, Jun-ichi Yamaki.** Decomposition reaction of LiPF₆-based electrolytes for lithium ion cells. *Journal of Power Sources*. 2006, Vol. 156, 547-554.

16. **Guoxiu Wang, Xiaoping Shen, Jane Yao, Jinsoo Park.** Graphene nanosheets for enhanced lithium storage in lithium ion batteries. *Carbon*. 2009, Vol. 47, 2049 -2053.
17. **Guoxiu Wang, Bei Wang, Jinsoo Park, Ying Wang, Bing Sun, Jane Yao.** Highly efficient and large-scale synthesis of graphene by electrolytic exfoliation. *Carbon*. 2009, Vol. 47, 3242-3246.
18. **Peng Guo, Huaihe Song, Xiaohong Chen.** Electrochemical performance of graphene nanosheets as anode material for lithium-ion batteries . *Electrochemistry Communications*. 2009, Vol. 11, 1320-1324.
19. **Xuyang Wang, Xufeng Zhou, Ke Yao, Jiangang Zhang, Zhaoping Liu.** A SnO₂/graphene composite as a high stability electrode for lithium ion batteries. *Carbon*. 2011, Vol. 49, 133-139.
20. **Qin Si, K. Hanai, N. Imanishi, M. Kubo, A. Hirano, Y. Takeda, O. Yamamoto.** Highly reversible carbon–nano-silicon composite anodes for lithium rechargeable batteries. *Journal of Power Sources*. 2009, Vol. 189, 761-765.
21. **Shu-Lei Chou, Jia-Zhao Wang, Mohammad Choucair, Hua-Kun Liu, John A. Stride.** Enhanced reversible lithium storage in a nanosize silicon/graphene composite. *Electrochemistry Communications*. 2010, Vol. 12, 303-306.
22. **Guangmin Zhou, Da-Wei Wang, Feng Li, Lili Zhang, Na Li, Zhong-Shuai Wu, Lei Wen, Gao Qing (Max) Lu, and Hui-Ming Cheng.** Graphene-Wrapped Fe₃O₄ Anode Material with Improved Reversible Capacity and Cyclic Stability for Lithium Ion Batteries. *Chemistry of Materials*. 2010, Vol. 22, 5306-5313.

23. **Hailiang Wang, Li-Feng Cui, Yuan Yang, Hernan Sanchez Casalongue, Joshua Tucker Robinson, Yongye Liang, Yi Cui, and Hongjie Dai.** Mn₃O₄-Graphene Hybrid as a High-Capacity Anode Material for Lithium Ion Batteries. *J. AM. CHEM. SOC.* 2010, Vol. 132, 13978–13980.
24. **Y.J. Mai, X.L. Wang, J.Y. Xiang, Y.Q. Qiao, D. Zhang, C.D. Gu, J.P. Tu.** CuO/graphene composite as anode materials for lithium-ion batteries. *Electrochimica Acta.* 2011, Vol. 56, 2306-2311.
25. **Haegyeom Kim, Dong-Hwa Seo, Sung-Wook Kim, Jongsoon Kim, Kisuk Kang.** Highly reversible Co₃O₄/graphene hybrid anode for lithium rechargeable batteries. *Carbon.* 2011, Vol. 49, 326-332.
26. **Peichao Lian, Xuefeng Zhu, Shuzhao Liang, Zhong Li, Weishen Yang, Haihui Wang.** Large reversible capacity of high quality graphene sheets as an anode material for lithium-ion batteries. 2010, Vol. 55, 3909-3914.
27. **D. Pasero, N. Reeves, A.R. West.** Co-doped Mn₃O₄: a possible anode material for lithium batteries . *Journal of Power Sources.* 2005, Vol. 141, 156-158.
28. **Masayuki Itagaki, Nao Kobari, Sachiko Yotsuda, Kunihiro Watanabe, Shinichi Kinoshita, Makoto Ue.** In situ electrochemical impedance spectroscopy to investigate negative electrode of lithium-ion rechargeable batteries. *Journal of Power Sources.* 2004, Vol. 135, 255-261.

29. **Peichao Lian, Xuefeng Zhu, Shuzhao Liang, Zhong Li, Weishen Yang, Haihui Wang.** Large reversible capacity of high quality graphene sheets as an anode material for lithium-ion batteries. *Electrochimica Acta*. 2010, Vol. 55, 3909-3914.
30. **Yuping Wu, Changyin Jiang, Chunrong Wan, Eishun Tsuchida.** Effects of catalytic oxidation on the electrochemical performance of common natural graphite as an anode material for lithium ion batteries . *Electrochemistry Communications*. 2000, Vol. 2, 272-275.
31. **T.L. Wang, W.T. Huang, W.C. Wang, B.X. Liu.** Ion beam mixing to study the metallic glass formation of the Cu–Zr system . *Materials Letters*. 2010, Vol. 64, 96-98.
32. **A. Concheso, R. Santamaría, R. Menéndez, J.M. Jiménez-Mateos, R. Alcántara, P. Lavela, J.L. Tirado.** Electrochemical improvement of low-temperature petroleum cokes by chemical oxidation with H₂O₂ for their use as anodes in lithium ion batteries. *Electrochimica Acta*. 2006, Vol. 52, 1281-1289.
33. **A. Concheso, R. Santamaría, R. Menéndez, R. Alcántara, P. Lavela, J.L. Tirado.** Influence of the oxidative stabilisation treatment time on the electrochemical performance of anthracene oils cokes as electrode materials for lithium batteries. *Journal of Power Sources*. 2006, Vol. 161, 1324-1334.
34. **Xuyang Wang, Xufeng Zhou, Ke Yao, Jiangang Zhang, Zhaoping Liu.** A SnO₂/graphene composite as a high stability electrode for lithium ion batteries. *Carbon*. 2011, Vol. 49, 133-139.

35. **Novoselov KS, Geim AK, Morozov SV, Jiang D, Zhang Y, Dubonos SV.** Electric field effect in atomically thin carbon films. . *Science*. 2004, Vol. 306, 666-669.
36. **Miao F, Wijeratne S, Zhang Y, Coskun UC, Bao W, Lau CN.** Phase-coherent transport in graphene quantum billiards. *Science*. 2007, Vol. 317, 1530-1533.
37. **Peres NMR, CastroNeto AH, Guinea F.** Conductance quantization in mesoscopic graphene. *Physical Review B*. 2006, Vol. 73, 195411–195419.
38. **Paek SM, Yoo EJ, Honma I.** Enhanced Cyclic Performance and Lithium Storage Capacity of SnO₂/Graphene Nanoporous Electrodes with Three-Dimensionally Delaminated Flexible Structure. *Nano Letters*. 2009, Vol. 9, 72-75.
39. **Li FH, Song JF, Yang HF, Gan SY, Zhang QX, Han DX.** One-step synthesis of graphene/SnO₂ nanocomposite and its application electrochemical supercapacitors. *Nanotechnology*. 2009, Vol. 20, 455602–8.
40. **Wang DH, Kou R, Choi D, Yang ZG, Nie ZM, Li J.** Ternary self-assembly of ordered metal oxide-graphene nanocomposites for electrochemical energy storage. *ACS Nano*. 2010, Vol. 4, 1587-1595.
41. **Xu C, Wang X, Zhu JW, Yang XJ, Lu LD.** Deposition of Co₃O₄ nanoparticles onto exfoliated graphite oxide sheets. *Journal of Materials Chemistry*. 2008, Vol. 18, 5625-5629.
42. **Chen S, Zhu JW, Wu XD, Han QF, Wang X.** Graphene oxide-MnO₂ nanocomposites for supercapacitors. *ACS Nano*. 2010, Vol. 4, 2822-2830.

43. **Hongfa Xiang, Kai Zhang, Ge Ji, Jim Yang Lee, Changji Zou, Xiaodong Chen, Jishan Wu.** Graphene/nanosized silicon composites for lithium battery anodes with improved cycling stability. *Carbon*. 2011, Vol. 49, 1787-1796.
44. **Beaulieu LY, Hatchard TD, Bonakdarpour A, Fleischauer MD, Dahn JR.** Reaction of Li with alloy thin films studied by in situ AFM. *Journal of The Electrochemical Society*. 2003, Vol. 150, 1457-1464.
45. **Geim AK, Novoselov KS.** The rise of graphene. *Nature Materials*. 2007, Vol. 6, 183–191.
46. **Wu J, Pisula W, Mullen K.** Graphenes as potential material for electronics. . *Chemical Reviews*. 2007, Vol. 107, 718-747.
47. **Bunch JS, van der Zande AM, Verbridge SS, Frank IW, Tanenbaum DM, Parpia JM.** Electromechanical resonators from graphene sheets. *Science*. 2007, Vol. 315, 490-493.
48. **Dikin DA, Stankovich S, Zimney EJ, Piner RD, Dommett GHB, Evmnenko G.** Preparation and characterization of graphene oxide paper. *Nature*. 2007, Vol. 448, 457-460.
49. **McAllister MJ, Li JL, Adamson DH, Schniepp HC, Abdala AA, Liu J.** Single sheet functionalized graphene by oxidation and thermal expansion of graphite. *Chemistry of Materials*. 2007, Vol. 19, 4396–4404.

50. **Li XL, Wang XR, Zhang L, Lee S, Dai HJ.** Chemically derived, ultrasmooth graphene nanoribbon semiconductors. *Science*. 2008, Vol. 319, 1229-1232.
51. **Novoselov KS, Geim AK, Morozov SV, Jiang D, Zhang Y, Dubonos SV.** Electric field effect in atomically thin carbon films. *Science*. 2004, Vol. 306, 666-669.
52. **Lu J, Yang JX, Wang JZ, Lim AL, Wang S, Loh KP.** One-pot synthesis of fluorescent carbon nanoribbons, nanoparticles and graphene by the exfoliation of graphite in ionic liquids. *ACS Nano*. 2009, Vol. 3, 2367-2375.
53. **Sutter W, Flege JI, Sutter EA.** Epitaxial graphene on ruthenium. *Nature Materials*. 2008, Vol. 7, 406-411.
54. **Coraux J, N'Diaye AT, Busse C, Michely T.** Structural coherency of graphene on Ir(1 1 1). *Nano Letters*. 2008, Vol. 8, 565-570.
55. **Berger C, Song ZM, Li XB, Wu XS, Brown N, Naud C.** Electronic confinement and coherence in patterned epitaxial graphene. *Science*. 2006, Vol. 312, 1191-1196.
56. **Dato A, Radmilovic V, Lee Z, Phillips J, Frenklach M.** Substrate-free gas-phase synthesis of graphene sheets. *Nano Letters*. 2008, Vol. 8, 2012-2016.
57. **Kim KS, Zhao Y, Jang H, Lee SY, Kim JM, Kim KS.** Largescale pattern growth of graphene films for stretchable transparent electrodes. *Nature*. 2009, Vol. 457, 706-710.
58. **Reina A, Jia X, Ho J, Nezich D, Son H, Bulovic V.** Large area, few-layer graphene films on arbitrary substrates by chemical vapor deposition. *Nano Letters*. 2009, Vol. 9, 30-35.

59. **Li X, Zhang G, Bai X, Sun X, Wang X, Wang E.** Highly conducting graphene sheets and Langmuir–Blodgett films. *Nature Nanotechnology*. 2008, Vol. 3, 538-542.
60. **Hernandez Y, Nicolosi V, Lotya M, Blighe FM, Sun Z, De S.** High-yield production of graphene by liquid-phase exfoliation of graphite. *Nature Nanotechnology*. 2008, Vol. 3, 563-568.
61. **Y.J. Mai, X.L. Wang, J.Y. Xiang, Y.Q. Qiao, D. Zhang, C.D. Gu, J.P. Tu.** CuO/graphene composite as anode materials for lithium-ion batteries. *Electrochimica Acta*. 2011, Vol. 56, 2306-2311.
62. **Peichao Lian, Xuefeng Zhu, Hongfa Xiang, Zhong Li, Weishen Yang, Haihui Wang.** Enhanced cycling performance of Fe₃O₄–graphene nanocomposite as an anode material for lithium-ion batteries. *Electrochimica Acta*. 2010, Vol. 56, 834-840.
63. **Yang He, Ling Huang, Jin-Shu Cai, Xiao-Mei Zheng, Shi-Gang Sun.** Structure and electrochemical performance of nanostructured Fe₃O₄/carbon nanotube composites as anodes for lithium ion batteries. *Electrochimica Acta*. 2010, Vol. 55, 1140-1144.
64. **S. L. Cheekati, Y. Xing, Y. Zhuang, and H. Huang.** Lithium Storage Characteristics in Nano-Graphene Platelets. *Materials Challenges in Alternative and Renewable Energy*. 2010, Vol. 224, 117-127.
65. **S. L. Cheekati, Y. Xing, Y. Zhuang, and H. Huang.** Graphene Platelets and Their Manganese Composites for Lithium Ion Batteries. *ECS Transactions - Las Vegas, NV*. 2011, Vol. 33.